INTERFACIAL TENSION AND CONTACT ANGLE MEASUREMENTS OF CO_2/BRINES/SURFACTANTS/OIL SYSTEMS WITH DOLOMITE ROCK

BY

AHMAD MAHBOOB

A Thesis Presented to the
DEANSHIP OF GRADUATE STUDIES

KING FAHD UNIVERSITY OF PETROLEUM & MINERALS

DHAHRAN, SAUDI ARABIA

In Partial Fulfillment of the
Requirements for the Degree of

MASTER OF SCIENCE

In

PETROLEUM ENGINEERING

DECEMBER 2016

KING FAHD UNIVERSITY OF PETROLEUM & MINERALS

DHAHRAN- 31261, SAUDI ARABIA

DEANSHIP OF GRADUATE STUDIES

This thesis, written by **AHMAD MAHBOOB** under the direction his thesis advisor and approved by his thesis committee, has been presented and accepted by the Dean of Graduate Studies, in partial fulfillment of the requirements for the degree of **MASTER OF SCIENCE IN PETROLEUM ENGINEERING.**

Dr. ABDULLAH S. SULTAN
(Advisor)

Dr. ABDULLAH S. SULTAN
Department Chairman

Dr. SIDQI ABU-KHAMSIN
(Member)

Dr. Salam A. Zummo
Dean of Graduate Studies

Dr. MOHAMED KANDIL
(Member)

22/12/16

Date

Dedication

I dedicate this effort to my mother; the reason of my success in every step of my life.

ACKNOWLEDGMENTS

All praise to the Almighty for his countless blessings bestowed upon me and giving me the strength to complete this work. Without his help, nothing is possible. No words of thanks are enough to express my gratitude towards him.

I am proud to have been awarded scholarship by King Fahd University of Petroleum & Minerals throughout my Master's program, for which I am extremely thankful to the University.

I am grateful to my thesis advisor, Dr. Abdullah Sultan who allowed me the opportunity to work in my area of interest and mentored and guided me throughout the research. His contribution to this work is immense.

I would like to thank my thesis committee members, Dr. Abu-Khamsin and Dr. Mohamed Kandil for their valuable input and suggestions throughout my work and I am honored to have them in my thesis committee.

I would also like to express my thanks to the Center of Integrative Petroleum Research (CIPR) at The Research Institute (RI) of KFUPM for providing me the funding to conduct my research project and for providing access to conduct experimental work at Fluid Characterization Lab and Multi-purpose core-flood lab. A special acknowledgment to Engr. Abdussamad who helped, facilitated, supported and guided me greatly throughout the research conducted. In addition, Engr. Aziz Khan and Engr. Ali Khalid helped me a lot in core preparation and polishing disks for CA experiments.

I would also like to thank Engr. Zaid Zafar for his continuous help, guidance and support in conducting the IFT experiments and measuring high pressure densities for my thesis. I am thankful to Muzammil Shakeel and Wasef Nofel for providing the oil data. I shall be grateful to Zeeshan Sheikh and Shams Kalam for helping me with ANN techniques.

I also thank all my friends at KFUPM especially Sarmad Zafar Khan and Mobeen Murtaza, who have been my support system during this entire time I spent at KFUPM. Osama Yousef has been a brother to me who provided conveyance every time I needed, Muhammad Mansoor Alam helped me in shopping and I will always be grateful to Muzammil H. Rammay and Danish Hashmat for their unconditional care and immense help. Special thanks to Aneeq Nasir, Owais Ahmad, Ahmad Sadeed and Hassan Sheikh.

TABLE OF CONTENTS

LIST OF TABLES

LIST OF FIGURES

LIST OF ABBREVIATIONS

EOR	:	Enhanced Oil Recovery
IFT	:	Interfacial Tension
CA	:	Contact Angle
BRINE1	:	Brine with 67708 ppm salinity
BRINE2	:	Brine with 33854 ppm salinity
BRINE3	:	Brine with 16927 ppm salinity
BRINE4	:	Brine with 8464 ppm salinity
BSS1	:	Brine4 containing 0.1% Alfoterra L167-4S 90
BSS2	:	Brine4 containing 0.1% Armovis EHS
BSS3	:	Brine4 containing 0.15% FS-50
CO_2	:	Carbon dioxide

ABSTRACT (ENGLISH)

Full Name : Ahmad Mahboob

Thesis Title : Interfacial Tension and Contact Angle Measurements of CO_2/Brine/Surfactant/Oil Systems with Dolomite Rock

Major Field : Petroleum Engineering

Date of Degree : December,2016

In this work the effects of different parameters such as surfactant type, salinity, temperature, pressure, and oil type have been studied experimentally in the presence of CO_2 at temperatures of up to 90^oC and pressures as high as 5500 psi for changes in interfacial tension and wettability with dolomite rock.

EOR techniques are the main source of increase in recovery factor for most wells of today. Surfactants and Water-alternating-gas (WAG) are modern EOR techniques that are more focused and strategic and define a new way of increasing oil recovery. Most of the experimental studies on IFT and Contact angle have been conducted on either Gas (CO_2)-with-brine or Brine-with-Surfactants. No work has been done previously for measuring interfacial tension and contact angle of CO_2/Brine/Surfactant/Oil/Dolomite co-existing. If a seawater containing a surfactant is injected into the reservoir followed by CO_2 injection, the former will reduce the interfacial tension of the oil and CO_2 will cause a decrease in viscosity and cause a better displacement of hydrocarbon. Therefore, their combination will cause a relatively high hydrocarbon recovery.

In the 1st step, IFT of four multicomponent brines of different salinities were compared and the brine showing lowest IFT with CO_2 was used in the 2nd step for comparison of three different brine-surfactant solutions (BSS). The BSS with lowest IFT was then used

to study the IFT behavior of three different oils with CO_2. Last step consists of contact angle (CA) measurements of oil with dolomite rock in the presence of CO_2 and BSS. Brines are multicomponent with salinities ranging from 8,464 to 67,708ppm. Comparison of surfactants is among solutions of an alcohol-propoxysulfate surfactant, a viscoelastic surfactant and a fluorosurfactant.

IFT of brines increases with increase in salinity and temperature and decreases with increase in pressure. This is due to solubility of CO_2 in brine. IFT increases linearly till density difference of 0.2 g/ml and forms a plateau (or a region of less increase) at certain region of density difference and as the density difference increases further, the IFT slope changes again making it almost linear. The drop volume increases with pressure and decreases with temperature. IFT decreases with increase in pressure for brine-surfactant solutions (BSS) also. Out of the three surfactants, most soluble solution is a fluorosurfactant and gives ultra-low IFT with CO_2. This BSS of fluorosurfactant when used with oil, forms pressure-sensitive micro emulsions in CO_2 causing the IFT of the oil to decrease. CA of oils with dolomite rock increase with pressure in the presence of fluorosurfactant and CO_2. Effect of micro-emulsions on CA has also been reported and a correlation has been constructed using ANN that depends on IFT, density and pressure for CA prediction in these systems.

In the literature, comparison of IFTs of different surfactants in CO_2-Brine systems, Brine-Oil systems, Surfactant-CO_2 systems, and surfactant-oil systems have been reported but this work reports on all CO_2/Brine/Surfactant/Oil/Dolomite co-existing which can help in planning a Surfactant-Alternating-Gas(SAG) or Water-Alternating-Gas(WAG) process accurately.

ABSTRACT (ARABIC)

ملخص الرسالة

الاسم الكامل: أحمد محبوب

عنوان الرسالة: قياسات التوتر السطحي وزاوية التماس لأنظمة ثاني أكسيد الكربون/المحلول الملحي/خافض التوتر السطحي/الزيت مع صخر الدولومايت.

التخصص: هندسة البترول.

تاريخ الدرجة العلمية: أبريل 2016.

تقنيات الاستخلاص المعزز للنفط هي المصدر الرئيسي لزيادة معامل الاستخلاص لمعظم الآبار. تقنيات الاستخلاص المعزز باستخدام خافض التوتر السطحي و عملية تبادل الماء والغاز تعتبر تقنيات حديثة لزيادة استخلاص الزيت. خوافض التوتر السطحي تعمل على إنقاص تشبع الزيت المتبقي وتغيير درجة التبلل بهدف زيادة استخلاص الزيت. هناك حالات في عملية تبادل الماء والغاز عندما تتواجد موائع مختلفة من تقنيات الاستخلاص المعزز للنفط مع موائع المكمن. معظم الدراسات المعملية على التوتر السطحي وزاوية التماس تم إجراؤها على غاز (ثاني أكسيد الكربون) مع محلول ملحي أو محلول ملحي مع خافض التوتر السطحي. لا يوجد عمل أجري لقياس التوتر السطحي وزاوية التماس لأنظمة ثاني أكسيد الكربون/المحلول الملحي/خافض التوتر السطحي/النفط/صخر الدولومايت.

إذا تم ضخ ماء البحر المحتوي على خافض التوتر السطحي داخل المكمن متبوعاً بغاز ثاني أكسيد الكربون، فإن محلول ماء البحر يعمل على إنقاص التوتر السطحي للزيت، كما أن الغاز يسبب خفضاً للزوجة مما يؤدي إلى أزاحة أفضل للهيدروكربون. بالتالي، اندماج هذه الوائع يسبب استخلاص أفضل للهيدروكربون.

في هذا العمل يتم إجراء دراسة معملية لتأثير عوامل مختلفة مثل نوع خافض التوتر السطحي ودرجة الملوحة ودرجة الحرارة والضغط ونوع الزيت في حضور غاز ثاني اكسيد الكربون على درجة حرارة أكثر من 90 درجة مئوية وضغط عالي عند 5500 بي إس آي، ومدى تغير التوتر السطحي ودرجة التبلل مع صخر الدولومايت.

الخطوة الأولى يتم فيها مقارنة التوتر السطحي لأربعة محاليل ملحية مختلفة التكوين ودرجة الملوحة، والمحلول الملحي المحتوي على أقل توتر سطحي مع غاز ثاني أكسيد الكربون يتم استخدامه في الخطوة الثاني ليتم مقارنته مع ثلاثة محاليل ملحية مع خافض التوتر. محاليل الملح مع خافض التوتر ذات التوتر السطحي الأقل تستخدم فيما بعد لدراسة سلوك التوتر السطحي لثلاثة زيوت مختلفة مع غاز ثاني اكسيد الكربون. الخطوة الأخيرة تتكون من قياسات زاوية التماس للزيت مع صخر الدولومايت في حضور ثاني أكسيد الكربون ومحاليل الملح مع خافض التوتر.محاليل الملح عبارة عن مكونات متعددة مع درجات ملوحة تتراوح بين 8464 إلى 67708 جزء بالمليون. مقارنة خوافض التوتر هي بين خافض التوتر (alcohol-propoxysulfate) وخافض التوتر ذو اللزوجة المرنة و (fluorosurfactant).

التوتر السطحي للمحاليل الملحية يزيد مع زيادة درجة الملوحة ودرجة الحرارة وينقص مع الزيادة في الضغط. هذا بسبب ذوبانية غاز ثاني أكسيد الكربون في المحلول الملحي. الترت السطحي يزيد بصورة خطية حتى التغير في الكثافة يصل إلى 0.2 غم/مل، وتقل هذه الزيادة عند حد معين من تغير الكثافة، وعند زيادتها فإن منحنى التوتر السطحي يتغير مجدداً بصورة خطية. من الثلاثة خوافض التوتر، خافض التوتر الأكثر ذوبانية هو (fluorosurfactant) ويعطي توتراً سطحياً مع غاز ثاني أكسيد الكربون بقيمة قليلة جداً. محلول الملح وخافض التوتر هذا يستخدم لاحقاً مع الزيت لتكوين مستحلب دقيق يتأثر بالضغط مع غاز ثاني أكسيد الكربون، مسبباً إنقاص التوتر السطحي للزيت.

في الكتابات العلمية، مقارنة التوتر السطحي لخوافض التوتر المنخفضة في أنظمة ثاني أكسيد الكربون/المحلول الملحي، وأنظمة المحلول الملحي/الزيت، وأنظمة خافض التوتر/ثاني أكسيد الكربون، وأنظمة خافض التوتر/ الزيت قد أشير إليها،

ولكن هذا العمل يشير إلى ثاني أكسيد الكربون والمحلول الملحي وخافض التوتر والزيت وصخر الولومايت كلها مجتمعة. هذا العمل قد يساعد في التخطيط لعمليات تبادل خافض التوتر والغاز أو تبادل الماء والغاز بصورة دقيقة.

.

CHAPTER 1

INTRODUCTION

1.1 Introduction to EOR and Interfacial phenomenon

Enhanced Oil recovery (EOR) is used to increase oil recovery from oil reservoirs beyond their natural production capability. One of the famous EOR processes is CO_2 injection which is being used as a tertiary EOR in more than 70 operations in USA [1]. The main reason for successful development of this process is the availability of low cost CO_2**.**

1.1.1 CO_2 EOR:

Injection of CO_2 at supercritical pressure to displace the immobile oil to producing zone can also serve as a means of reducing the amount of CO_2 in the atmosphere by capturing and sequestering in the mature reservoirs. CO_2 has been closely linked to global climate change hence there are incentives to sequester it. It is a good solvent for light crudes as well as miscible with oil at moderate reservoir pressures. The number of projects injecting CO_2 has been steadily rising and anticipated to increase further in the foreseeable future. CO_2 can easily be in a supercritical fluid state at relatively low temperature and pressure conditions. From phase diagram, Figure 8, critical point of CO_2 is at 1070 psi and 32°C.

Application of CO_2 flooding as means of enhanced recovery has its challenges which various investigators have tried to solve over the decades. The common challenges being

faced are gravity segregation, reservoir heterogeneity and high mobility ratio of CO_2 [2]. These cause a reduction in macroscopic sweep efficiency even though the microscopic efficiency sweep efficiency may be high.

1.1.2 Water-Alternating-Gas (WAG):

The WAG process, patented by Parrish in 1966, was initially proposed as a method to increase the sweep effiiciency during gas injection. In WAG processes, water and gas are injected as alternate slugs either in cycles or simultaneously in order to improve the sweep efficiency of waterflooding and miscible/immiscible gas flood. Because of their low viscosities, miscible gases generally have poor flood perforrmance than water does in a waterflood. Almost all-commercial miscible floods today employ the WAG method. In addition to improving sweep efficiency, WAG injection was found to imporve the displacement efficiency in heavy oil reservoirs by oil phase swelling and viscosity reduction [3]. This oil phase swelling is goverened by capillary pressure reduction.

1.1.3 Surfactant Alternating Gas (SAG):

An improved form of WAG process is Surfactant-Alternating-Gas (SAG) in which a surfactant solution in injected alternating with CO_2 or N_2. Surfactant serves the purpose of generating foam with CO_2 which helps in further reduction of CO_2 mobility and improves CO_2 diplacement efficiency as reported in both field and laboratory studies by several investigators [4]–[9].

There are many carbonate reservoirs in US below their minimum miscibility pressure that are naturally fractured [10]. For water wet formations, waterflooding is very effective but many fractured carbonate reservoirs are mixed wet and recoveries with conventional

methods are low (less than 10%). Thermal and miscible tertiary recovery techniques are not effective in these reservoirs[10]. Therefore use of surfactants for flooding is the only hope [11], although in the past it was developed for sandstone reservoirs [12].

SAG provides higher oil recovery because foam has better viscosity and also increases the trapped gas saturation. The first observation of trapped gas influence on residual oil saturation was reported by Holmgren and Morse (1951). Trapped gas has been found to lower residual oil in several experimental studies [13]. Another benefit is the cost. For SAG process, 85 to 95% of gas is used and therefore saves water consumption as compared to WAG [2]. Surfactant also serves to decrease the interfacial tension of the fluids.

Surfactants (surface active agents) are compounds whose molecular structures contain both hydrophobic (water repelling)/lipophobicity (lipid/fat/oil repelling) and hydrophilic/CO_2-phillic (water or CO_2 attracting) groups. Most surfactants consist of a hydrophobic tail group and a hydrophilic head group. When added to an aqueous fluid, surfactant molecules combine to form structures known as “micelles”. Surfactants reduce IFT and aid in the solubilization of hydrophilic compounds into hydrophobic solvents or vice versa due to their amphiphilic nature [14]. The hydrophilic heads surrounds the core that is formed by association of hydrophobic tails of the micelles. This isolates the tails from contact with water. Micelles are typically spherical in shape.

In this work supercritical CO_2 will be used that has a major drawback. It is a poor solvent because of extremely low polarizability/volume ratio and many lipophilic and hydrophilic

compounds are not soluble. In order to render CO_2 a better solvent for these compounds, surfactants are necessary.

The interfacial tension, γ, of CO_2 with mixtures representative of the fluids in underground formations is an important thermophysical property for the design of SAG EOR process. It has been long recognized that interfacial interactions (interfacial tension, wettability, capillarity and interfacial mass transfer) govern fluid distribution and behavior in porous media. This work focuses on interfacial tension and wettability measurements.

1.1.4 Interfacial Tension:

The interfacial tension (IFT) is the free energy per unit surface area that is required for creating an interface between two condensed phases. The IFT is an important factor in a number of applications related to surfactant injection for improved oil recovery, emulsion stability, transport of organic contaminants through soil, and ensuring water quality in aquifers, which includes the ability to predict the behavior of dense nonaqueous phase liquids such as chlorinated solvents. The IFT influences the capillary pressure between two nonmiscible fluids, which in turn impacts how fluids flow in porous media. Other applications where IFT plays a major role include micelle formation and other self-assembly processes of nanoparticles or colloidal particles at liquid/liquid interfaces. Self-assembly at liquid/liquid interfaces is an important process in materials science and technology, which is highly relevant to food supplements and cosmetics. The IFT also plays an important role in pharmaceutical applications such as drug delivery, where surfactants help to form microemulsions, which improves the bioavailability of lipophilic

or amphiphilic drugs [15]. Lowest interfacial tension is always desireable since low IFT corresponds to high mobility and stable foam [2].

1.1.5 Wettability:

Wetting phenomenon plays an important role in our everyday lives. The behavior and properties of materials such as paints, adhesives, detergents, and lubricants are all manifestations of wetting phenomena. Furthermore, wetting is an essential element in the behavior of biological systems. For examples, studies of wetting properties of plant leaves has helped to develop insecticides that repel insects and protect the leaves from diseases. Investigation of cell adhesion to biological membrane, and the tear film which wets the eyeball facilitating vision are other phenomenon studied because of wetting phenomenon. Very often contact angle studies are used to gain insight into the fundamentals of wetting many systems. Contact angle is defined as the angle between the tangents to the planes of two intersecting interfaces at their intersecting line; of the two possible angles according to the convention, contact angle is the angle measured through the denser phase. Although it seems conceptually easy to measure contact angles for many systems, contact angle phenomena are by no means a simple subject matter. Contact angle depends on many factors such as heterogeneity of the system, presence of surfactants, smoothness of the surface, line tension [16], density and the size of the drop. All of these factors need to be understood to better understand and predict the wettability of a fluid. However studying all of the participating factors at once can be very complex; the present thesis will focus on the contact angle get better understandings of the subject. The interfacial formation wettability is considered as one of the controlling parameters

for residual oil recovery from carbonate reservoirs. It has a significant impact on relative permeability, capillary pressures and on oil displacement in porous media [17].

In either cases of co-injetion of Surfactant solution and gas or surfactant alternating gas, the CO_2, water, oil and surfactant will co-exist in the reservoir. In the current literature, separate systems have been used by several authors, mentioned in Chapter 2, such as CO_2 with Water/Brine, CO_2 with surfactants, Surfactants with Oil, and CO_2 with Oil. There has been a gap in literature for co-existance of IFT data for CO_2, Brine, Oil and Surfactant. Also not a lot of work has been done on dolomite rock with Oil and CO_2 systems.

1.2 Problem Statement and Thesis Objectives:

Current understanding of the interfacial properties for reservoir when there is a coexistence of EOR fluids in the reservoir needs to be revised because of the following reasons:

1- There is a need to study methods for decrease is IFT and wettability for SAG injection
2- Current literature does not cover the combinations of CO_2, brine, Oil and surfactants co-existing.
3- Florosurfactant with CO_2 and oil has not been used before.
4- Very less work has been done on Contact Angle with carbonate rocks especially high purity dolomite.

Owning the above shortcomings, the main objective of the thesis are as follows:

i- Study the interfacial properties of CO_2, Brines containing surfactants and oil coexisting.

ii- Study the effect of:

a. Change in brine salinity
b. Change in temperature
c. Change in pressure
d. Type of surfactant
e. Type of oil (model oil and crude oil)

on interfacial properties (Interfacial tension and wettability) of the various combination of systems.

CHAPTER 2

LITERATURE REVIEW

Main focus of this work is interfacial tension and contact angle measurements of CO_2, Brine, Oil and Surfactant systems. This chapter covers all the studies that have already been published related to these systems.

2.1 Interfacial Tension Measurements

Bachu and Bennion (2009) studied the effect of pressure, temperature and brine salinities on interfacial tension of CO_2 – water [18]. They performed 378 IFT measurements between CO_2 and water/brine at 20 to 125 °C temperatures and for pressures from 2 to 27 MPa. Five multi-component brines with salinities ranging from 0 to 334 010 $mg \cdot L^{-1}$ were used. The laboratory experiments were conducted using the pendant drop method for the profile of the brine drop in the CO_2-brine equilibrium environment. They showed that at constant salinity and temperature, IFT decreases steeply with increasing pressure when pressure is less than critical pressure and mildly decreases when pressure is greater than critical pressure with an asymptotic trend toward a constant value at high pressures. If the temperature and pressure are kept constant, IFT increases with increasing salinity, which means CO_2 solubility in brine decreases with increase in salinity. For temperature, less than critical temperature, IFT increases with increasing temperature, and close to the critical point ($T \approx T_c$), IFT significantly decreases, probably because at T_c the IFT between CO_2 liquid and vapor phases tends to zero, and then increases again with

increasing temperature for temperature greater than T_c with an asymptotic trend toward a constant value for higher temperatures. The dependence of IFT on salinity, pressure and temperature for CO_2-water/brine systems can be, according to the author, approximated by a power function of pressure whose coefficient and exponent depend on salinity and temperature.

Saraji et al. (2014) in their study used axisymmetric drop shape analysis (ADSA) and no-Apex (ADSA-NA) method to measure density, IFTs, contact angles of CO_2/brine/quartz systems at high pressures and temperatures [19]. Measurements were performed at 50^oC to 100^oC temperature and 2000 to 4000 psig pressures and brine salinities from 0.2 to 5 gm/L which is relevant to carbon sequestration in deep saline aquifers. The effect of SO2 as a co-contaminant was also investigated in this work. Contact angle hysteresis and its implications of the results on some mechanisms of CO_2 trapping was examined. Density of the brine increased with temperature but it remained unaffected by pressure. However density of supercritical CO_2 increased with increasing pressure and decreased with increasing temperature. Variations in pressure did not have a significant effect on the IFT of between equilibrated CO_2-rich and aqueous phases, but temperature increase caused slight reduction of the IFT. The relative insensitivity of IFT to P and T in the supercritical region of CO_2 may stem from the fact that the solubility of CO_2 in brine does not drastically change in the P and T ranges studied in this work. Similar to the IFT data, the dynamic contact angles also did not change significantly with P and T. There was only a slight increase in the contact angles and contact angle hysteresis by the increase in pressure. However, due to the lack of enough temperature overlap in the presented data, a general trend cannot be deducted. The density of CO_2 was insensitive to the changes in

salt concentration, however brines with the higher ionic strength had larger densities. There was a significant increase in IFT by an increase in the ionic strength. For example, IFT between equilibrated sc- CO_2 and brine at 3000 psig and 60°C increased from 26 to 39 mN/m by changing the ionic strength from 0.2 to 5 M. According to the authors, this behavior was partly due to the decrease in CO_2 solubility in brine at higher salinities and partly because of hydration of ions that leads to an ion-free layer at the water interface.

Kim and Santamarina (2014) studied the manipulation of Capillary factor to attain improved sweep efficiency [20]. It was found through experimentation that surfactants that have hydrophilic heads and CO_2-philic tails lower the IFT between CO_2 and water. The long- chain nonionic surfactant used in these experiments (weight percent wt. ≈ 0.4%) lowered the CO_2–water interfacial tension from γ_{fl}~ 50 mN/m to γ_{fl}~ 4 mN/m at a pressure of $P \geq 7$ MPa. The parallelism in surface tension-vs-pressure trends for tests conducted with and without surfactant suggests a pressure-independent concentration of surfactants at the interface. The contact angle formed by a water-surfactant droplet resting on a glass substrate and surrounded by CO_2 increases from θ~ 20° at P = 0.1 MPa to $\theta \sim 70°$ at P = 10 MPa. Reduced interfacial tension γ_{fl} and larger contact angle θ combine to produce a marked decrease in the capillary factor $\gamma_{fl} \cos \theta$.

Iglauer et al. (2014) studied contact angle and wettability measurement on a quartz surface after applying different cleaning methods and demonstrated clearly that the main factor which leads to a broad data in different researches is due to surface contamination [21]. It is clear that typically inappropriate cleaning methods were used which resulted in artificially high contact angle measurements. Cleaning methods described in surface

chemistry community were used and it was found that the water contact angle θ on a clean quartz substrate is low, 0–30°, and that θ increases with pressure. They concluded that quartz is strongly water-wet at high pressure conditions.

Chalbaud et al., (2010) performed interfacial tension and contact angle experiments using ADSA technique between CO_2 and brine at conditions of geological storage [22]. Experiments were performed at 4.5 MPa to 25.5 MPa and at temperatures 27, 71 and 100°C and for single component (NaCl) brine with salinity ranging from 5000 to 150 000 ppm. Based on the results authors developed a correlation using the Parachor model, using the sensitivity of salinity and applying a regression fit of more than one hundred IFT experimental values.

$$\gamma_{b,CO_2} = \gamma_{W_{plateau}} + \lambda * x_{NaCl} + \left[\frac{P}{M}(\Delta\rho)\right]^{\eta} * T_r^{\beta}$$

where λ, β and η are regression coefficients. Remaining parameters have been explained in the paper. Also in this paper, Glass micromodels were used to study the fluid distribution in the case of different thermodynamic conditions and wettability.

Lun et al. (2012) used axisymmetric drop shape analysis (ADSA) for the pendant drop case to measure IFT between CO_2 and reservoir brine at high temperatures and pressures [23]. Measurements were taken for multi-component brines of three salinities (0 mg/L, 14224.2 mg/L and 21460.6 mg/L) at pressures till 35 MPa and at two temperatures 45°C and 97.53°C. It was found that the equilibrium IFT decreases as the pressure increases but increases as the salinity increases. Also, the wettability of the reservoir brine and CO_2

system changes from the hydrophilic case to the hydrophobic case as the pressure increases, and the same phenomenon decreases as the brine salinity increases.

Shariat et al (2012) used pendant drop method to measure interfacial tension between CO2 and water between 7 MPa to 124 MPa and on temperatures up to 204^{o}C [24]. They also measured water-vapor-saturated CO_2 as well as CO_2- saturated-water densities at each pressure and temperature. They showed that IFT of CO_2 and Water decrease with increasing temperature however quite independent of pressure with values between 10 to 23 dynes/cm. Complete miscibility between CO_2 and H_2O at any pressure and temperature was never observed. CO_2-saturated water densities showed a strong dependence on pressure and temperature, while water-vapor-saturated CO_2 densities showed little change from the CO_2 density with no vapor content.

Georgiadis et al. (2011) used pendant drop method, at high pressure and temperature, to evaluate the interfacial tension between water and [(1 - x)n-decane + x CO_2] for three different compositions of CO_2 in the alkane-rich phase, of mole fractions x = (0.0, 0.2, and 0.5), along several isotherms at temperatures up to 170^{o}C and pressures ranging from the miscibility state points for (n-decane + CO_2) up to 50 MPa. Bulk phase was [n-decane + CO_2] and drop phase was water [25]. On comparison with literature, the results of binary system were in complete agreement at ambient pressure whereas for high pressures, the literature values were lower than the work of this study. It was found that IFT of the system (H_2O + [n-decane + CO_2]) system decreases by increasing concentration of CO2. Also n-alkane and CO2 become miscible at high temperatures and pressure and the IFT curve vanishes. The reported results have a relative average standard deviation of 1.7 %.

Sun and Chen (2005) used pendant drop method to study IFT between CO2 injected crude oil and reservoir water at 66°C and 11.7 MPa [26]. This study was conducted to observe the effect of CO_2 molar composition (x_{CO_2}) on the IFT of CO_2 injected crude oil and reservoir water (salinity 2695.58 ppm, Multi-component brine). x_{CO_2} was ranging from (0, 10.0, 34.1, 44.7, 48.9, 57.8, to 65.0) mol %. The bubble point pressure for these CO_2 injected oil systems was also determined using a PVT device. The experimental data showed that when x_{CO_2} changed from (0 to 65.0) mol %, the interfacial tension value decreased by about one-third. The pressure had a slight effect on the interfacial tension. When x_{CO_2} was 65.0 mol %, the CO_2 injected oil system approached complete miscibility and the interfacial tension data of CO_2 injected crude oil with reservoir water changed a little with an increase of pressure.

Yang et al. (2005) used ADSA pendant drop technique to measure IFTs of CO_2 with Brine, Brine with Crude Oil, CO_2 with Crude oil and Crude Oil with CO_2-saturated-brine at pressures ranging from 0.1 MPa to 31.4 MPa and at two temperatures 27°C and 58°C [27]. For both systems the IFT decreases with increase in pressure and increases with increase in pressure. For CO_2-Brine systems, at pressure higher than 12.238 MPA at 58°C, the drop was not formed therefore the data is not available. However, for CO_2-Crude oil system, the IFT remains unaffected at pressures higher than 8.879 MPa at 27°C and 13.362 MPa at 58°C. For Crude oil with Brine systems, IFT is independent of both pressure and temperature. Also IFTs of Crude Oil, CO_2, and reservoir brine were measured by bubbling CO_2 in the cell containing brine and generating a drop of oil in the CO_2-saturated-brine. IFT slightly decreased with increase in both pressure and temperature.

Xing et al. (2013) presented a review on the research progress of the interfacial tension in supercritical CO_2-water/ oil system [28]. He found that according to many researchers that IFT decreases with increasing pressure for both CO_2-reservoir and CO_2-crude oil systems. For CO_2-water system, the quasi-static pendant drop method was utilized to measure IFT at temperatures ranging from 278 to 335 K and pressures from 0.1 to 20 MPa, the IFT showed a pronounced dependence on pressure and temperature. Furthermore for the Crude oil-brine system and the CO_2+crude oil+ reservoir brine system the IFT remain almost constant at different pressures, but the IFT of the latter is slightly lower at higher pressure because more CO_2 dissolves in the brine and oil phases. So CO_2 injection can be successfully used to enhance oil recovery by decreasing the IFT of reservoir fluid and water, reservoir fluid and CO_2. For the effect of temperature, different studies have provided different observations therefore the author thinks the effect of temperature of IFT is complex and must be taken into account in future studies.

Gibeau et al. (1986) conducted a series of IFT measurements versus temperature at constant pressure using the pendant drop apparatus with seven different samples of viscous crude oil using as the aqueous phases a source water for water injection, distilled water and heavy water [29]. The temperatures ranged from ambient to 160^oC. It was found that for three out of five heavy oil, there was a decrease in IFT with an increase in temperature. It was also concluded that pendant drop technique cannot be used to measure the interfacial tensions when the density difference between the two fluids is less than 0.01 g/cm^3.

Talebian et al. (2014) studied the interactions of fluids involved in foam assisted CO_2 EOR process at pressure of 7 MPa to 20 MPa, and temperature of 102°C [30]. The

equilibrium CO_2 solubility into the reservoir brine, and crude oil, and the effect of foaming agent surfactants on the CO_2 solubility into the aqueous phase were measured by using an equilibrium high pressure cell. The IFT measurements of gas-liquid and liquid-liquid systems were measured by ADSA pendant drop tensiometer. It was found that the CO_2-surfactant solution IFT values can also influence the equilibrium solubility of CO_2 in surfactant solution. The lower the IFT at the CO_2-surfactant interface would result in higher solubility of CO_2 in the solution. CO_2 dissolution in different solvents is dependent on the equilibrium pressure, and temperature. By increasing the pressure, CO_2 dissolution in both aqueous and oil systems increased. By increasing the pressure from atmospheric to 20 MPa, the IFT values decreased significantly from near 20 to 1 mN/m values.

Li et al. (2012a) in their first paper, studied the interfacial tension of different brines (salt molalities of 1 to 5 mol/kg) of (0.864 NaCl+ 0.136 KCl) with CO_2 at temperatures between 298 and 448 K (24°C and 175°C) and pressures between 2 and 50 MPa (290 psi to 7,252 psi) by using pendant drop method, generating a drop of CO_2-saturated brine surrounded by water-saturated CO_2 phase [31]. The expanded uncertainties at 95 % confidence are 0.05 K in temperature, 70 kPa in pressure, and for interfacial tension γ, the larger of 0.016γ and 0.6 mN·m−1. The results of the study indicate that the interfacial tension increases linearly with the molality of the salt solution. An empirical equation has been developed to represent the present results as a function of temperature, pressure, and molality with an expanded uncertainty of 1.6 mN·m−1

Li et al. (2012b) in another paper reported the interfacial tensions between CO_2 and different brines ($CaCl_{2(aq)}$, $MgCl_{2(aq)}$, and $Na_2SO_{4(aq)}$) each with molalities from (0.49 to 5.0) $mol \cdot kg^{-1}$ at temperatures between 343 and 423 K (70°C to 150°C), pressures

between 2 and 50 MPa (290 and 7,252 psi) [32]. The pendant-drop method was implemented in a high-pressure view cell filled with water- saturated CO_2 into which single drops of brine were injected through a suitable capillary. The expanded uncertainties at 95 % confidence are 0.05 K in temperature and 70 KPa in pressure. For the interfacial tension, the expanded relative uncertainty at 95 % confidence was 1.6 %. The results of this study show that interfacial tension increases linearly with molality. Further, it was concluded that at constant temperature and pressure, the interfacial tension is the same function of the positive charge molality for all salts investigated in this work.

Kashefi (2012) made a model on measurement of Interfacial tension between gas-water systems by generating data by performing experiments and using points generated by previous experiments done by several authors [33]. Not only data points from hydrocarbon gases were included, but also from CO_2, H_2S and N_2 were used to make IFT-solubility correlation to predict the IFT of gas-water systems. He observed that addition of salt increases the interfacial tension. Also he found that at each temperature, the effect of pressure on the IFT of each system decreases by increasing pressure. For all gases in water, IFT decreases with increase in gas solubility in water.

Cao and Gu (2013) in part of their work measured CO_2 solubility in crude oil and equilibrium IFTs of crude and CO_2 at pressures from 250 psi to 2770 psi and constant temperature 53^oC [34]. They found that up till 1200 psi, IFT tends to decrease rapidly with pressure and the cause of this decrease was the increased solubility of CO_2 in the original light crude oil. However, from 1200 up till 2770, the decrease in IFT was less, almost constant. The reason was that, lighter components of the crude oil get dissolved in the CO_2, and thereby leaving intermediate to heavy components in the crude oil and

therefore the IFT being measured was of the left-over components of the crude oil. He also observed that at low pressures, the pendant oil drop swells due to CO_2 dissolution into the oil phase. It was also observed that CO_2 solubility in the crude oil decreases as the temperature increases in a PVT cell for temperature increase from 27°C to 53°C. As the CO_2 changes into supercritical stage, the extraction ability of light hydrocarbons by CO_2 becomes stronger. However higher recovery is achieved in the second pressure range, i.e. when CO_2 is immiscible and also high temperature is desired for higher recovery in case of CO_2 flooding.

Yang et al. (2015) measured the IFT of CO_2 with two Crude oils and n-hexadecane at up till 140°C and 5500 psi [35]. According to their study, the higher is temperature, the higher is the IFT. IFT tends to decrease with pressure, however there comes a certain threshold pressure 1100 psi at which the IFT stops decreasing and becomes constant (or slightly decrease) with pressure up till 3350 psi. Crude oil A (heavier) decreases rapidly till 1750 psi, whereas crude oil B (lighter) decreases rapidly till 1450 psi. Slight decrease of crude oil A has been reported till 4000 psi whereas for crude oil B till 5500 psi at 60^oC. At lower temperature 45°C, crude oil A decreases rapidly till 1300 and slightly till 2175 psi whereas for crude oil B the two pressures are 1450 psi and 2465 psi. The reason for decrease in IFT with pressure can be explained by explaining what is happening at the molecular level. The intermolecular forces operating within the crude oil (dipole-dipole and Debye Force) are much stronger than the ones operating in CO_2 molecules (London dispersion force). Increase in pressure at constant temperature causes the molecular distances to decrease but the intermolecular forces increase. The forces in CO_2 become close (in value) to those in Oil since there is a drastic change in CO_2 molecular distance.

With these molecular forces become higher, IFT tends to decrease. Increase in temperature causes an increase in IFT is also explained by increase in molecular distances. When IFTs of all three fluids are compared, the highest IFT is shown by the lighter crude oil B and lowest is shown by n-hexadecane. According to the explanation in this work, the crude oil's IFT can be compared with each other due to same intermolecular forces. However, n-hexadecane molecules are almost linear with no-polarity therefore only London forces exist therefore the difference in intermolecular forces between CO_2 and hexadecane is smaller than those between crude oils. This is the reason for low-IFT of n-hexadecane. For n-hexadecane drop, higher the pressure smaller is the drop size and smaller is the IFT.

Awari-yusuf (2013) in his thesis measured the interfacial tension between CO_2 and crude oil at 22^oC and 60^oC and at pressures from 100 to 600 psi [36]. IFT decreases with increase in temperature and increase in pressure. He obtained a straight line for decrease in pressure that can be extended to zero IFT. This point of zero IFT is called minimum miscibility pressure (MMP). At high pressure, MMP reaches earlier at lower pressure. At the end, the author recommends that more data points need to be added to increase the accuracy and also he did not investigate the effect of gas density on IFT.

Akutsu et al. (2007) measured IFT between CO_2 and water in the presence of surfactants [37]. The surfactants used in this work are CO_2-Soluble hydrocarbon surfactants of three different ethylene oxide (EO) chains were used in this work. Both CO_2 and water-surfactant solutions were saturated with each other and interfacial tensions were measured for different surfactant concentrations. The surfactant concentration with longest EO chains showed the lowest IFT. Reason can be that EO chains are hydrophilic

and longer EO chains have strong attractive force for water surface. The EO chains penetrate into a water droplet when a surfynol molecule adsorbs on water/CO_2 interface. The IFT decreases with increasing surfactant concentration. However at a certain point all IFT values approach a same value indicating the adsorption of water droplet surface by excess amount of surfynol molecules whose hydrophobic tails are interacting with CO_2 molecules. Also the comparison at different temperatures and pressures was shown by the authors on which the fluid densities are same. It showed that IFT decreases with increase in surfactant concentration but at a point reaches a plateau.

Yang et al. (2005) in another paper measured IFT between CO_2 and brine at two temperatures (27°C and 58°C) and nine pressures from ambient pressure to 4351 psi [38]. Brine consists mainly of sodium chloride and bicarbonates and CO_2 is 99% pure. Brine and CO_2 were not in pre-equilibrium in the experiments. It was also observed that Brine drop initially swells and its volume continues to increase at the same pressure with time which is due to CO_2 dissolution in brine phase. After some time it shrinks because of the pendant brine drop mass transfer with CO_2. At high temperature, the solubility of CO_2 (drop shrinkage) increases. Thus higher the temperature the greater is the amount of brine transfer to CO_2 phase. Also they reported the solubility of CO_2 in brine. It was observed through PVT also that solubility increases with increase in temperature. Also for IFT, at higher temperature brine drop stays for shorter time because CO_2 solubility in the brine phase is lower at higher temperature. At temperature of 58^{o}C and pressure 1775 psi no interface was formed and therefore it was considered that both CO_2 and brine are miscible with each other. Generally, IFT decreases with increase in pressure however IFT increases with increase in temperature because CO_2 solubility in brine phase is higher at

high pressure and low at high temperature, also, the pressure effect on IFT is comparable with temperature effect for the brine-CO_2 system.

Rocha et al. (1999) measured interfacial tension between CO_2 and water in the presence of different surfactants [39]. According to their work, CO_2 is a poor solvent for lipophilic and hydrophilic solutes because of low dielectric constant and polarizability per volume. It is possible to disperse either lipophilic or hydrophilic phases into CO_2 with surfactants. Surfactants with low surface tensions/cohesive densities are highly soluble in CO_2. Log of IFT when plotted against temperature or pressure, decreases till a point of lowest IFT (at this point the system is balanced with respect to partitioning of the surfactant between the phases) and then increases. This increase is due to migration of the surfactant towards the other phase. Also pressure and temperature can cause change in solvent strength because of the change in density. An example is that water in propane micro emulsion was inverted to a propane in water micro emulsion by varying the pressure by 725 psi. This system undergoes a phase inversion density by analogy with the phase inversion temperature for conventional system. If the density is changed so that the surfactant prefers either phase over the other the surfactant is less interfacially active and IFT increases.

In their work, the drop is of water saturated with CO_2, whereas the bulk phase contains CO_2 and surfactant. The aqueous phase density was assumed to change less than 0.0025 g/cm3 because of the presence of surfactants. For one of the surfactants the effect of temperature was examined and it was found that both equilibrium, and minimum IFT decreases with temperature. The reason is that the interactions are strengthened due to increase in density at low temperature which favor the solvation of surfactant.

Emulsification of the water caused turbidity and the amount of water was increased to check the check the amount of emulsification by each surfactant. And high emulsification of water also corresponds with low IFT. Turbidity decreases with time. For two surfactants which produced the same amount of lowering of IFT, the one on the CO_2-philic side of the v-shaped plot emulsified more water according to Bancroft rule. A distribution coefficient is defined as the ratio of surfactant solubility in CO_2 at a particular temperature and pressure to that of water at 1 atm (14.7 psi). When this coefficient is less than 1, it means the natural curvature for those surfactants would favor CO_2-in-water droplet according to Bancroft Rule.

Ruckenstein (1996) validated and extended the Bancroft Rule which is stated as "a hydrophile colloid will tend to make water the dispersing phase while a hydrophobe colloid will tend to make water a dispersed phase" [40]. He stated that according to Binks [41], for surfactant concentrations greater than the critical micro-emulsion concentration at which a micro emulsion forms, the macro emulsion type is that of the corresponding microemulsion and that the Bancroft rule holds. However, for surfactant concentrations small compared to the critical micro emulsion concentration, the emulsions formed were of the O/W type and the Bancroft rule was violated, since the higher concentration of surfactant was in the oil phase, hence in the dispersed and not the continuous phase. Emulsions are formed by applying shear that creates oil fingers in water and water fingers in oil at the interfaces of which molecules of the surfactant are absorbed. The stability of an emulsion also depends upon adsorption-desorption process. And the type of emulsion formed depends on mixing process of the fluids. The validation/invalidation of Bancroft rule in this paper was based on two ratios, one ratio compared the interaction between

surfactant-oil to those between surfactant-water. The other ratio compared between hydrocarbon chains of the surfactant molecules of the interfacial layer and oil to those between the head groups of surfactant layers of IFT and water. When both are smaller or large than unity, Bancroft rule is obeyed.

2.2 Contact Angle Measurements

Ameri et al. (2013) determined contact angle using pendant drop shape analysis in systems with CO_2, brine, and an oil-saturated rock system [42]. Two situations were considered: Rock system I was partially water-wet, whereas rock system II is effectively oil-wet. Contact angles have been determined experimentally as a function of brine salinity and pressure. The experiments were carried out at a constant temperature of 45^{o}C and pressures varying between 0.1 up to 16.0 MPa. For rock system I, the partially water-wet substrate, brine and CO_2 system, the dependence on the pressure at constant salinity is very small. For this system, at a constant pressure, the contact angle decreases for increasing brine salinity. The results show that the carbon dioxide is the non-wetting phase in the pressure and salinity range studied. This behavior can be quantitatively understood in terms of the expected dependencies of the three interfacial tensions (IFTs) in Young's equation on pressure and brine salinity. For rock system II, the effectively oil-wet substrate, brine, and CO_2 system, the dependency of contact angle on pressure is considerable. This study proves that CO_2 becomes the wetting phase at pressures higher than 10.0 MPa. Beyond 10.0 MPa (i.e., in the supercritical region), the contact angle remains practically constant. The effect of salinity on the contact angle of the oil-wet rock system II is small. The behavior can again be quantitatively understood based on

expected trends of the three IFTs that determine the contact angle. It is also shown that use of the equation of state method makes it possible to approach the experimental data quantitatively. It was concluded that contact angle measurements form an essential ingredient to determine the efficiency of carbon dioxide flooding and storage.

Hamouda and Gomari (2006) performed a set of experiments to measure the effect of temperature on contact angle of carbonate rock samples [43]. Saturated, unsaturated fatty acids and naphthenic acids with saturated and unsaturated rings were selected for this work to alter the water-wet calcite surface over a temperature range of 25 to 130^{o}C.

Three approaches were followed by Hamouda and Gomari. In the first approach (test 1), a water pre-wetted calcite surface was modified by aging for 24 hours in a 0.01M stearic acid (SA) dissolved in n-decane at different temperatures. The second approach, the pre-wetted calcite surface was modified by aging for 24 hours in a 0.01M stearic acid dissolved in n-decane at room temperature (25^{o}C) and then immersed in water having the pre-determined temperatures. In the third approach, a water pre-wetted calcite surface was modified by aging for 24 hours in a 0.01 M stearic acid dissolved in n-decane at different temperatures as test 1, then the modified calcite at desired temperature immersed in water having the same pre- determined temperature. In these three approaches the modified calcite after treatment was dried in the air over night and contact angle was measured inside the cell at 25^{o}C.

It was observed that a steeper change in the contact angles for test 1 and 3 than that for test 2. When the temperature increased from 25 to 130^{o}C, the contact angle decreased from 160 to 68^{o} and 160 to 101^{o} for test 1 and 2, respectively. In test 3, where the contact

angles were measured on the modified calcite at the desired temperature followed by immersion in water at the same temperature, lower values than that for test 1 were observed. The lower contact angle observed in test 3 (decreased from 160 to 36^{o} with temperature increase from 25 to 130^{o}C, respectively) compared to test 1 may be explained to be caused by possible re-establishing equilibrium between the adsorbed SA / calcium stearate and water and/or desorption of SA from the calcite surface. The lower contact angles in test 1 and 3 than measured in test 2, may in general, be explained based on the available Ca^{2+} sites on the calcite surface. As the temperature increases a lesser Ca^{2+} are available for adsorption, the previously reported chemisorption of the SA, on the calcite surface5. While in test 2, the strongly adsorbed SA at low temperature, showed lesser degree of alteration of the wettability to water-wet as the temperature increases. This hypothesis was successfully quantified and verified with a simulation of solubility of calcite in an open system (presence of CO_2) was performed.

Gupta and Mohanty (2008) studied the effect of salinity, surfactant concentration, electrolyte concentration, and temperature on the wettability alteration and identified underlying mechanisms [44]. Contact angles, phase behavior, and interfacial tensions were measured with two oil (one model oil and one field oil). Most of the experiments are done with a model oil which is prepared by adding 1.5 wt. % of cyclohexanepentanoic acid to n-decane. The acid (98 % active) and n-decane were supplied by Sigma-Aldrich. It is called the model oil in this paper. The other oil used was from a West Texas fractured carbonate reservoir. It had 28.20^{o} API, 23.8 cp viscosity (at 27^{o}C), 0.2 acid number and 1.17 base number. Na_2CO_3 and NaCl were used to change salinity of the aqueous phase. Na_2SO_4, $CaCl_2.2H_2O$ and $MgCl_2.6H_2O$ used to vary

divalent ion concentration in brine were. Calcite (Iceland spar) plates used for wettability experiments. It was found that there exists an optimal surfactant concentration for varying salinity and an optimal salinity for varying surfactant concentration at which the wettability alteration is the maximum for anionic surfactants. Concentration of surfactants in the interface region can explain the occurrence of optimal salinity for wettability alteration. As the reservoir salinity increases, the surfactant concentration needed for the maximum wettability alteration decreases, but the extent of wettability alteration itself decreases. IFT and contact angle were found to have the same optimal salinity for a given concentration of anionic surfactants. Also, IFT was found to be decreasing (and in some cases reaching a plateau value) for increasing surfactant concentrations at a fixed salinity. As the ethoxylation increases in anionic surfactants, the extent of wettability alteration increases. Wettability of carbonates can be altered by divalent ions at high temperature (90°C and above).

Sulfate ions alter wettability to a greater extent in the presence of magnesium and calcium ions than in the absence. A high concentration of calcium ions can alter wettability alone. Magnesium ions alone did not change calcite plate wettability.

Alotaibi et al. (2010) conducted extensive wettability studies to determine the optimum brine salinity which results in higher oil recovery [45]. Crude oil, formation core samples (dolomite, and calcite), and synthetic brines from Middle East (formation, aquifer, and seawater) are used to evaluate wettability quantitatively, and qualitatively. All experiments were conducted at high pressure (up to 2,000 psia), and elevated temperature (up to 270°F).

Hielmeland and Larrondo (1986) [46] studied the effect of pressure, temperature, and oil composition on the wettability of calcium carbonate rocks. Temperature was found to have a large effect on the wetting characteristics. At low temperatures (22°C), the solid phase exhibited oil-wet behavior, whereas at high temperatures (≥ 60°C), it exhibited water-wet behavior. At 40°C an intermediate state of wettability seemed to prevail. No pressure effect was found on wettability. The wettability of calcium carbonate, on the other hand, was not affected by the light fraction of the oil. Advancing and receding equilibrium contact angles were obtained within 100 to 200 hours.

Saudi Arabian carbonate reservoir wettability was evaluated and compared by Lichaa et al. (1992) using USBM, Amott, and contact angle techniques [47]. Calcite, marble, and formation rocks were used in the receding contact angle measurements, as well as synthetic formation brine, seawater, and dead crude oil. A wide temperature range was examined in all experiments between 25 to 90°C. Test pressure was varied from ambient to 50 psi. Calcite surface tests became preferentially more water-wet at higher temperatures. Contact angle results for oil/brine/marble system was slightly oil-wet to an intermediate wettability, and tended to became weakly water-wet at higher temperatures. Formation rock tests, on the other hand, showed an intermediate wettability or preferentially, slightly oil-wet at room temperature and became preferentially less oil-wet at higher temperatures.

The effect of salinity on the contact angle was investigated by Almehaideb et al. (2004) [48]. Limestone rock, crude oil, NaCl solutions were all used in their study. Four runs were examined using distilled water, 1,000, 10,000, and 50,000 ppm. All experiments

were conducted at room temperature. A significant reduction of oil/water contact angle was observed at 10,000 ppm.

Yang et al. (2008) presented the wettability of the crude oil−reservoir brine−reservoir rock system at elevated temperatures, using the axisymmetric drop shape analysis (ADSA) technique [49]. Vuggy limestone rocks were used in this study with intermediate wettability. The contact angle increased as pressure increased. Slight fluctuation was reported in the contact angle measurement at pressure and temperature of 29 psi and 27°C, respectively. This contact angle fluctuation may be ascribed to be strong electrostatic interactions between the crude oil and the reservoir brine. The contact angle also decreased as increasing the fluid temperature.

Shojai et al. (2012) studied the wetting behavior of CO_2-Bentheimer sandstone-water systems was investigated by means of visual contact angle measurements at 45^{o}C and pressures between 0.1-14 MPa in a modified pendant drop cell (PDC) that allows captive-bubble contact-angle measurements at elevated temperatures and pressures [50]. Contact angle measurements were performed with water that was fully pre-saturated with CO_2. It showed that the contact angle and the size of the bubble converge to equilibrium in time. During this convergence period, the contact angle and the bubble size generally show a slight change as function of time. The experimental data shows a larger dependency of the contact angle on bubble size than on pressure. However, for bubbles with similar size, contact angle shows a slight increase as function of pressure. All data shows that Bentheimer-water- CO_2 systems remain water-wet even at high pressure.

Martavaltzi et al. (2012) studied the effect of non-ionic surfactants on contact angle with limestone outcrop core samples [51]. Indiana Limestone core samples with gas permeability ranging from 2 to 4 md were used for contact angle measurement after equilibration with different brine solutions. A 1.5 wt% naphthenic acid in decane, deionized water (pH=7.15, resistivity 305 ohm) was used for preparation of all the brines. Formation Brine is a mixture of 2.577M NaCl, 0.476M $CaCl_2$, 0.101M $MgCl_2$ and 0.003M Na_2SO_4. An inverted needle was used for sessile drop measurement to create a drop on model oil. Results show that higher salinity tended to increase the contact angle for most of the ions studied. Sulfate ions alone do not reduce the contact angle. Addition of non-ionic surfactant in 0.01M $CaCl_2$ did not induce significant improvement on the wettability of the calcite samples. The presence of the 2 first members of the 15S analogous series (secondary alcohol ethoxylates are termed 15-S in this work) led to only marginal decrease of the contact angle. Contact angle measurements on porous samples from outcrop were close to those on calcite crystals and exhibited similar trends with ionic compositions. This suggests that valid contact measurements may be made on thin end- pieces of reservoir core samples

Mirchi et al. (2014) studied the behavior of several anionic surfactants in the presence of crude oil 80^{o}C [52]. The results of these tests were used to find the best surfactants. Then dynamic interfacial tensions and contact angles of selected surfactant-in-brine/oil/shale system was measured by the rising/captive bubble technique (axisymmetric drop shape analysis). Using the same methodology, the effects of surfactant concentration (0.01 to 0.1 wt. %) and brine salinity (0.1 to 5 M NaCl) on IFT and CA at ambient and reservoir conditions (i.e. 80 °C and 3000 psig) were studied. Surfactant adsorption on shale

samples was also measured in brines at ambient conditions. It was revealed that the anionic surfactant reduced the interfacial tension of oil and brine from 23 to 0.3 mN/m at 5 M salinity. Adding surfactant into the brine increased the dynamic contact angle on the shale samples. The maximum contact angle values observed in this study were generated with surfactant concentrations close to CMC (critical micelle concentration). The anionic surfactant was more effective in increasing the contact angle and reducing the IFT at reservoir conditions than ambient conditions. Introduction of surfactant into the fluid system resulted in a significant reduction in contact angle hysteresis.

Alshaikh and Mahadevan (2014) performed sensitivity analysis of ion composition on wettability of carbonate rock samples [53]. They tried to identify the impact of six salts and three interactions. They concluded that the chlorides have the maximum impact on the contact angle change to water-wetness (22% and 31 % respectively for sodium and calcium salts). Reduction in chlorides has the obvious benefit of changing the contact angle to more water-wet. Sodium chloride and calcium chloride are the major salts that alter the calcite wettability. The percentage contributions were 22% and 31% for sodium chloride and calcium chloride, respectively. Some salts are affected due to the interactions with other salts. In this study and design of experiments these interactions were examined: the interaction between sodium chloride and sodium sulfate, the interaction between sodium chloride and magnesium chloride, and the interaction between sodium chloride and calcium chloride. The optimum brine salinity was determined after conducting 27 contact angle experiments. The optimum brine salinity consists of different salt combinations and different salt concentrations. The optimum brine was prepared by mixing 80 gm of NaCl, 0.21 gm of Na_2SO_4, 63 gm $CaCl_2$, 13.8 gm

of $MgCl_2$, 0.1 gm of $MgSO_4$ and 0.1 gm of $CaSO_4$ in one liter of DI water. A confirmation experiment using the optimum brine was performed at the reservoir pressure and temperature. The measured contact angle was 28.9° with brine salinity of 157,207 ppm.

Jaeger et al. (2010) conducted study for a thorough experimental description of a gas-crude oil-reservoir water system and its behavior under CO_2 pressure including oil density and interfacial properties [54]. They generated a drop of oil in a mixture of CO_2 and Oil. The density of CO_2 and oil mixture was measured using a gravimetric method by exposing the oil to carbon dioxide at different pressures. It was concluded that because of its strong ability to dissolve in hydrocarbon fluids, carbon dioxide has a considerable effect on phase behavior and IFT in oil and gas reservoirs. In the presence of light hydrocarbons, complete miscibility is achieved at moderate pressures. As a consequence, the IFT decreases rapidly by increasing the pressure and ultimately vanishing at the point of complete miscibility. IFT of crude oil in a CO_2 atmosphere significantly decreases but reveals the difference in miscibility at 40 and 80^oC by exhibiting higher IFT at higher temperatures. Further, carbon dioxide has a significant effect on the IFT in a crude oil-aqueous solution system, which influences the wetting via the Young's relationship. Dynamic studies reveal that the wetting liquid penetrates into porous rock structures, whereas drops of the non-wetting liquid maintain their shape after the adjacent liquid phases are saturated with carbon dioxide and an equilibrium CA is established.

Alidad (2001) in his PhD thesis has provided the dependence of contact angles and line tension on drop size by providing data of 27 solid-liquid-vapor systems [16]. He provided

that line tension ranges from 10^{-7} J/m for systems with low contact angles to 10^{-4} J/m for high energy system studied.

Kwok and Neumann (1999) discusses a review and comparison of different contact angles measured and their limitations and also generated contact angle data by using a goniometer and also by ADSA method and then used different approaches such as the three surface tension interpretation approaches (Fowkes approach, Owens-Wendt-Kaelble approach, and Lifshitz-van der Waals approach) and Equation of state approaches (Antonow's rule, Berthelot's geometric mean combining rule, modified Berthelot's rule) and then compared the results to provide positivity and limitation of each method [55].

Yuan and Lee (2013) highlighted the comparison of telescope-goniometer method, the Willhelmy balance method and DSA method [56]. Telescope-goniometer has the advantage of simplicity and that only small amounts of liquids and small surface substrates are required. However there are high risk of impurities. Captive bubble method provides better results as compared to sessile drop but it requires far more liquid which can be problematic when the solid swells after immersion into liquid or when a film on the solid is dissolved by the liquid. Willhellmy method is also a more accurate method for contact angle measurement as it measures the weight and length of the solid samble which can be measured with high accuract and also the measured force is an averaged value. But it has drawbacks that the solid sample must have uniform cross-section in the submersion direction. Sample must have same composition and topography at all sides which might be difficult to meet. Also a sufficient quantity of luquid must be used, which might cause the solid sample to swell and/or absorb vapor unintentionally. The ADSA technique is believed to be one of the most accurate techniques for high precision contact

angle measurement. With a reproducibility of ±0.2°, the ADSA method has been shown to improve the accuracy of contact angle measurement by essentially an order of magnitude, compared to the reproducibility of ±2° by direct tangent measurements.

CHAPTER 3

RESEARCH METHODOLOGY

For our research, IFT700 apparatus was used to study the change in interfacial tension at different temperatures, pressures, brine salinities, oil types and surfactant types. The apparatus consists of two manual pumps equipped with the pressure gauge, a viewing chamber (VC): whose temperature is controlled by PT100 (temperature controller) and also equipped with piezoelectric pressure transducer, Video system: 1 CCD color camera 1.4 Mega pixel, 1 macro zoom lens, 1 LED for lighting. The data acquisition is done from a DELL PC attached to the equipment with IFT software installed. In order to maintain high pressure, a pump has been used. This same equipment was used for contact angle measurements. A brief description of all the methods used in this work, the materials and the equipment as well as the detailed procedure followed in the experiments is described below.

3.1 Analysis of Interfacial measurements

3.1.1 Drop Shape Analysis:

Drop shape analysis consists of different procedures to analyze the shape of a fluid drop in order to extract its properties. The principal assumptions are

- The drop is symmetric about a central vertical axis: this means it is irrelevant from which direction the drop is viewed.

- The drop is not in motion in the sense that viscosity or inertia are playing a role in determining its shape: this means that surface (or interfacial) tension and gravity are the only forces shaping the drop.

The two principal practical advantages of the technique are

- Calibration is straightforward in that only optical magnification is needed. This can be measured with high accuracy and is easy to trace to national standards. (Density must be known by this and all methods.)
- Solid surfaces of the apparatus involved need not have any special cleanliness because their wettability, per se, does not affect the result. This is a significant advantage over such techniques as the Wilhelmy plate where cleanliness is required [57] **.**

3.1.1.1 Drop Shape Analysis (DSA) Methods:

Drop Shape Analysis is the analysis of a drop generated inside a fluid for interfacial tension or contact angle measurement with a solid surface. In historical goniometer, the drop shape analysis was done by aligning a tangent to the drop by hand on scaled rotating disk. Today the optical evaluation is a modern technique which is carried out by camera and software which provides better accuracy with high-resolution reproducibility that helps to consider maximum points on the drops. This modern method on one hand is a good step however on the other hand it required more know-how and training of the user for the equipment.

Bulk Fluid is the fluid where the drop is released. For example, a drop of oil inside water; the bulk fluid is the water. Or a drop of water inside air; the bulk fluid is air. And the

fluid of the drop is called Drop Fluid. Before carrying out the drop shape analysis, the drop configuration must be selected in the software along with the calibration of the cell. The drop configuration describes the arrangement of drop fluid in the image. There can be the following configurations:

Sessile Down:

It is an experiment to measure contact angle, where the drop fluid density is higher than the bulk fluid density. It means the needle is on the top of cell. For example: a drop of oil inside gas released on a rock plate.

Sessile up:

It is an experiment to measure contact angle, where the drop fluid density is smaller than the bulk fluid density. It means the needle is on the top of cell. For example: a drop of oil (>10° API) in water released on a rock plate.

Pendant Drop:

It is an experiment to measure IFT, where the drop fluid density is higher than the bulk fluid density. It means the needle is on the top of cell. For example: a drop of water in air.

Rising Drop:

It is an experiment to measure IFT, where the drop fluid density is smaller than the bulk fluid density. It means the needle is on the bottom of cell. For example: a bubble of air inside water.

3.1.2 Models for Analysis

Circle Method

Circle method is also called height-width method. In this method the height and width of the rectangle enclosing an arc (arc is assumed to be the drop of fluid on a solid surface as a part of complete circle) are determined. This method has a disadvantage that it uses only a few pixels at the point of inflection and at both sides instead of the whole contour. The measurement is therefore suspected to be affected by interference in this area.

Polynomial Method/Tangent Method 1

Polynomial method evaluates only the region where the phases come into contact. Therefore a drop of any geometrical shape can be measured and the polynomial adapts itself to any curve that can be thought of at the contact point of the three phases. This method can be used for inclined or very asymmetrical drops.

Conic Section Method/Tangent Method 2

Conic section method assumes an elliptical drop shape and the contact angle is determined as the angle between the baseline and the tangent at the conic section curve at the contact point of three phases.

Young-Laplace method

This method is suitable for symmetrical drop shapes that are unaffected by interferences such as sample tilting or contact with the capillary needle. It can be used to measure angles above 10^{o}. Also it cannot measure dynamic contact angles because this method is

sensitive to the contact between the drop and the needle. This method analyzes the drop shape as an effect influenced by the gravity.

Choice for Method in this work

Circle method provides good results for contact angles very low up to 20^{o}, conic section method can provide up to 100^{o} and polynomial and Young-Laplace provides throughout the whole measuring range above 10^{o}. Also for higher drop sizes, polynomial or Young-Laplace can be used. For asymmetrical drops, only the two tangent methods can be used however circle and Young-Laplace methods give good results for symmetrical (no-inclination) drops because they produce a single contact angle. Table 1 by Kruss [58] has provided the summary of all DSA methods

Table 1: DSA methods

	Circle	Conic section	Poly-nomial	Young-Laplace
Measuring range				
0-20°	✓			
10-100°		✓	✓	✓
100-180°			✓	✓
Drop weight (volume∗density)				
Low	✓	✓	✓	✓
High		✓	✓	✓
Very high			✓	✓
Deposition				
Static (contour without needle)	✓	✓	✓	✓
Dynamic (contour with needle)		✓	✓	
Contour shape				
Symmetrical	✓	✓	✓	✓
Slightly asymmetrical		✓	✓	
Very asymmetrical			✓	

3.1.3 Static or Dynamic Measurements:

3.1.3.1 Contact Angle:

When the three-phase-line of contact angle is in actual motion, the contact angle produced is called a dynamic contact angle. In actual the solid drop moves in order to wet the fresh surface with time. In order to measure this kind of dynamic contact angle, the liquid drop is expanded and contracted with time on the surface of the solid. They are called advancing or receding contact angles respectively. These angles fall within a range, with the advancing angles approaching a maximum value, and the receding angles approaching a minimum value. Dynamic contact angles can be measured at various rates of speed. At a low speed, it should be close or equal to a properly measured static contact angle. The difference between the advancing angle and the receding angle is called the hysteresis.

However, on ideal solid surfaces, there is no contact angle hysteresis. On smooth but chemically heterogeneous solid surfaces, the experimentally observed contact angle may vary in each experiment and cannot be generalized. It is recommended to have a solid surface as smooth as possible but however there are no general guidelines regarding for surface roughness so as not to affect the contact angle.

In our work, both static and dynamic contact angles have been recorded however there is no induced change in volume of the drop. The change is caused either by solubility of bulk and drop fluids, or adsorption effect onto rock disk.

3.1.1.1 Interfacial Tension:

Interfacial tension measurement is influenced by the time of contact between two fluids in order to allow the diffusion of both fluids and come to equilibrium. This diffusion measured with time provides the dynamic interfacial tension of the drop fluid with bulk fluid. Static interfacial tension is the one at which there is no change in interfacial tension with time.

In this work, both dynamic and static interfacial tensions have been recorded and provided.

3.2 Pendant Drop IFT Technique

Pendant drop technique is a static method based on the droplet shape when the drop is at mechanical equilibrium. This technique is the most adaptable method for wide range of temperatures and at high pressures [59]–[61]. Unlike other empirically derived techniques, pendant drop method uses a force balance between buoyancy and gravitational forces. This force balance defines the shape of the drop-fluid hanging out of a capillary tube (needle) immensed in the bulk fluid. Shape of the drop is analyzed at mechanical equilibrium conditions. If the two fluids are immiscible, an interface will develop between the two fluids and the curvature of this interface depends on the pressure-differential between the two fluids. A form of Laplace-Young equation describes the condition of mechanical equilibrium that governs the pendant drop.

A droplet shape is assumed spherical therefore P_{int} is the pressure inside the droplet and P_{ext} is the pressure outside. If equilibrium state is reached, the energy required to increase or decrease the droplet volume is positive. In other words, this state matches to the minimum energy level. The energy to increase the droplet volume is (-P.dV):

$$\delta W_{volume} = -(P_{int} - P_{ext})\delta V$$

Hence increasing the energy of surface area, it induces:

$$\delta W_{area} = \gamma\, \delta\, A$$

Where γ is the interfacial tension; which means that the infinitesimal energy variation to modify the radiuys of a spherical droplet is

$$\delta W = -(P_{int} - P_{ext})\delta\left(\frac{4\pi R^3}{3}\right) + \gamma\delta(4\pi R^2)$$

$$\frac{\delta W}{\delta R} = 0 = -(P_{int} - P_{ext})\times 4\pi R^2 + \gamma.8\pi R$$

Or,

$$(P_{int} - P_{ext}) = \frac{2\gamma}{R}$$

Internal pressure is higher than external pressure, more exactly; the pressure of convex side is bigger than the concave one. Therefore, the argument does not depend of the phase nature of the droplet (liquid droplet inside a gas or gas droplet inside a liquid). This relation can be extended to the shape of a real droplet. At each point of the surface area of the droplet, curve radius *i* R_i can be defined. Let S be a surface (separation fluid A/fluid B) as in Figure 1 defined by the curves dl_1 and dl_2, centered in O_1 and O_2, with radius R_1 and R_2. In O, at equilibrium, a force *f* counterbalances the vertical resultant force from interfacial tension:

$$\Delta P.S = \Delta P.dl_1.dl_2$$

$$f_i = \sigma.dl_i$$

$$\Delta P = 2\sigma\left(\frac{\cos\alpha_1}{dl_1} + \frac{\cos\alpha_2}{dl_2}\right)$$

$$(P_{int} - P_{ext}) = \gamma\left(\frac{1}{R_1} + \frac{1}{R_2}\right)$$

Moreover, taking into account the fundamental equation of the equilibrium of the forces at a point of the drop, ($\Delta P.S = m\vec{g}$). Taking into account, any kind of drop, the Laplace equation is:

$$\frac{dx}{ds} = cos\theta, \qquad \frac{dz}{ds} = \sin\theta,$$

$$\frac{d\,\theta}{ds} = 2b + cz - \frac{\sin\theta}{x} \quad \text{..... (1)}$$

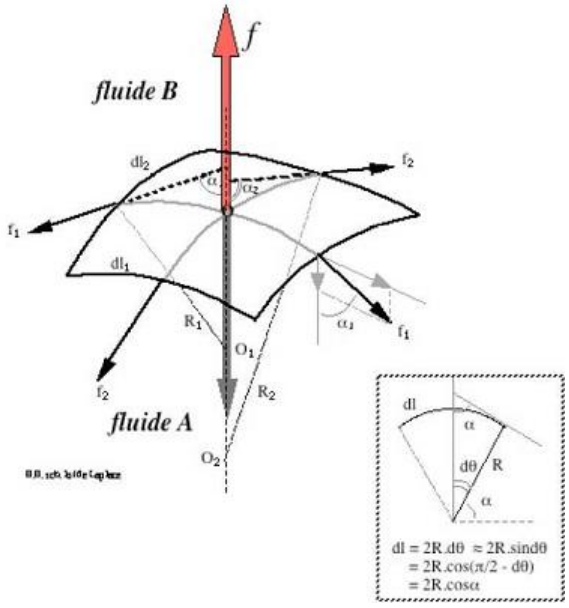

Figure 1: Force Balance of Interfacial Tension

This equation (1) does not have analytical solution and a numerical solution is required. Vinci Technilogies has developed house software dedicated for oil & gas laboratory toi proviude accurate and fast results. An old generation of IFT softwares used only two or three main parameters (Equatorial diameter, Apex diameter, refer to Adamson table) to compute the IFT. Subsequently the accuracy of the results was based on only few parameters. To enable maximum accuracy, all the points from shape of the drop are taken

into account to solve the Laplace equation. Fast computation is performed thanks to an advanced numerical scheme of resolution. To sum up, the IFT700 enables to determine the interfacial tension from the Laplace-Young equation based on the complete shape of the droplet [62].

3.3 Sessile Drop and Contact Angle (Young's Angle)

A way to study liquid-solid interaction resides in leaving a fluid-droplet on a cleaned and polished area of a solid. It is called sessile droplet (in opposition with pendant/rising droplet). The droplet would spread over the face even more solid-liquid interactions are more "attractive" than the liquid-liquid ones. Making sure that equilibrium state is reached (many minutes can be required); contact angle (also called Young's angle) can be measured.

For tension between liquid and gas, tension between solid and gas and tension between liquid and solid. At each interface, tension is not equivalent, and equilibrium state means:

$$\gamma_{liq-gas}.cos\theta + \gamma_{liq-solid} = \gamma_{solid-gas}$$

$$\gamma_{liq-gas} \leftrightarrow \sigma_l \ and \ \gamma_{solid-gas} \leftrightarrow \sigma_s$$

As the measurement of interfacial tension, the IFT700 enables to determine the contact angle thanks to computer processing of video frames. Liquid can be classified according to this angle. For "wetting liquid", the contact angle reaches very low values.

3.4 Materials

3.4.1 Core Sample

Guelph Dolomite core of 12” length and 1.5” diameter were used in the experiments. The core samples were procured from Kocurek Industries (USA). The porosity of the cores lies in the range of 10% – 19%. The supplier specified brine permeability was in the range of 45-100 md and gas permeability was in the range of 100-170 md. In addition, the core samples contain 98% dolomite with minute traces of silica.

3.4.2 Brine

Brine was prepared as synthetic sea water by using the salts mentioned in Table 2:

Table 2: Components of Brine 1

Salt Name	**Mg/L (ppm)**
$NaHCO_3$	165.246
Na_2SO_4	6339.02
NaCl	41172.4
$CaCl_2.2H_2O$	2387.13
$MgCl_2.6H_2O$	17644.1
Total	**67707.9**

Other three brines were prepared by diluting this brine by 50%, 25% and 12.5% with deionized water.

3.4.3 Surfactants

Surfactants used in this work are :

1- Alfoterra L167-4S 90
2- Armovis EHS
3- FS-50

3.4.3.1 Alfoterra

Anionic surfactants are surface-active agents having a net negative charge. Alfoterra L167-4S 90 (a branched alkyl alcohol propoxy sulfate) is an anionic surfactant containing 4 moles of Propylene oxide (PO) distributed by “Sasol North America Corporation”. It has the following chemical structure:

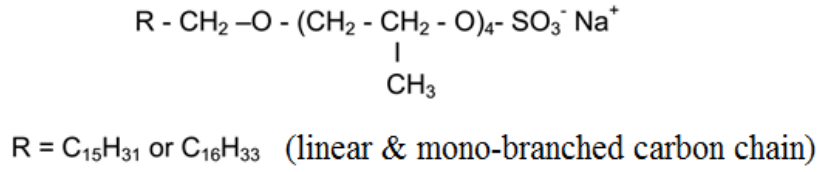

$$R - CH_2 - O - (CH_2 - \underset{\displaystyle CH_3}{\underset{|}{CH}} - O)_4 - SO_3^- Na^+$$

$R = C_{15}H_{31}$ or $C_{16}H_{33}$ (linear & mono-branched carbon chain)

These anionic surfactants are good candidates for EOR because they create very low IFT at very low concentrations and without any co-surfactant or alkaline agent [63]. Alfoterra L167-4S 90 is best suited for use at low temperature (less than 60^{o}C) and salinities below 40,000 ppm.

It exhibits unique extended surfactant structures allowing improved solubilization of oily materials in an aqueous medium by extending the interface. The monobranched alkyl hydrophobe allows for greater interaction with the oil phase while maintaining good solubility.

3.4.3.2 Armovis EHS

“Armovis ® EHS” by “AkzoNobel” is a patented viscoelastic surfactant (VES) that offers a range of unique benefits when used in acidizing of hydrocarbon-bearing

carbonate reservoirs. It is zwitterionic and contains 50% total solids with 1 specific gravity and PH of 8.

In case of VES surfactants when certain salts are present in the aqueous fluid within a particular concentration range, the micelles assume a rod-like structure similar to polymer strands. These spherical (rod-like) micelles becomes entangled, viscoelastic behavior develops, and fluid movement is hindered. However this packing is affected by conditions such as temperature and surfactant concentration. Also it may be influenced by changes in miceller chain length and dissymmetry that cause an increase in surfactant's spontaneous curvature, ultimately determining whether surfactant's molecules will form spherical or cylindrical micelles [64].

Viscoelastic surfactants have been for mobility control and lowering the IFT [65]. They are found to form foam with CO_2 and have been used in some studies as a fracturing fluid where VES fluids were found to be compatible with CO_2 [66], [67].

3.4.3.3 FS-50

FS-50 is an amphoteric fluorosurfactant that significantly reduces the surface tension of aqueous solutions and is also useful in providing sustained foam. Fluorosurfactants are synthetic organofluorine chemical compounds made up of multiple fluorine atoms. As surfactants, they are more effective at lowering the surface tension of water than comparable hydrocarbon surfactants. They have a hydrophilic head and a fluorinated tail. Some fluorosurfactants, such as PFOS, are detected in humans and wildlife. It is based on six flourinated carbon molecules that cannot break down to PFOA in the environment.

The electronegativity of flourine reduces the polarizability of the flourinated molecular surface due to which they are not suspectible to London dispersion force due to which they are lipophobic. The carbon-fluorine bond is quite strong which makes it suitable for the fluorosurfactants to be used in harsh conditions.

3.4.4 Deionized Water

First grade deionized water was used for preparation of Brines and surfactant solutions. In addition, it was also used to clean the entire IFT Equipment before and after each experiment in order to avoid presence of any impurity inside the cell.

3.4.5 Oil

Following Oils were used in this experiment:

1- Crude oil 1: Arabian Oil of API 30°

2- Crude Oil 2: Arabian Oil of API 40°

3- Model Oil 1: 98% Squalane ($C_{30}H_{62}$) a colorless odorless hydrocarbon with API 43°

4- Model Oil 2: 99% Pure Toluene

5- Model Oil 3: 99% Pure Penta-decane ($C_{15}H_{32}$)

Properties of Crude Oil 1:

Percentage of Aromatics	Percentage of Saturates	Percentage of resins	Percentage of Asphaltenes
49.51	35.36	11.64	3.49

Properties of crude oil 2:

Percentage of Aromatics	Percentage of Saturates	Percentage of resins	Percentage of Asphaltenes
57.90	32.84	8.66	0.63

3.4.6 Gas

The following two gases were used in the experiments:

1- Industrial grade N_2 gas was obtained in sufficient quantity in the form of gas cylinders. Nitrogen gas was used to provide pneumatic control to the ISCO pump for pressurizing the CO_2 accumulator.

2- 99% pure CO_2 in the form of gas cylinders was obtained.

3.4.7 Toluene

Pure Toluene was used during this experiment as a solvent for cleaning the IFT equipment, accumulator and densitometer.

3.5 Equipment

3.5.1 HPHT IFT Equipment

Vinci Technologies IFT700 (Figure 2) was used to measure interfacial tensions and contact angles. It consists of:

- Two manual pumps equipped with the pressure gauge, one is called drop pump and other is called bulk pump, both equipped with a temperature sensor and an electric heater. These pumps act as a storage for bulk and drop fluids and also contain valves that can be screwed to increase or decrease pressure. The drop fluid can be filled by an injector filled with fluid. However, in order to fill the

bulk pump, the fluid from the other injector has to pass through the cell in order to reach the bulk fluid. In the configuration used in this experiment, the injector of bulk pump has been replaced with the accumulator containing CO_2 and the bulk pump is not being used to pressurize the cell. The accumulator is being pressurized which causes an increase in pressure of the cell. The drop can only be generated when the pressure of drop pump is higher than bulk fluid

- A cell called viewing chamber in which the experiment takes place having the capacity of 20 cc fluid volume. It has maximum capacity of 10,000 psi with glass on both sides, one side allows the light source while the other side allows camera to capture the pictures.
- Capillary Needle which generates drop. This Needle is connected via a valve to drop pump. This equipment comes with different sized needles. Needle size depends on the viscosity of the fluid. Since no fluid of very high viscosity is to be used, therefore the smallest needle has been used.
- A control panel containing temperature regulator and pressure indicator. It does remain only on the time when equipment has to perform experiment. And it takes almost 5 to 6 hours for stabilization of a low temperature such as 30^{o}C and take almost 1 hour for high temperatures such as 90^{o}C. For 60^{o}C it takes almost 1.5 to 2 hours.
- 1 CCD color camera 1.4 Mega Pixel and 1 LED light. The camera captures live video of the drop from which stills can be captured at particular moment. The

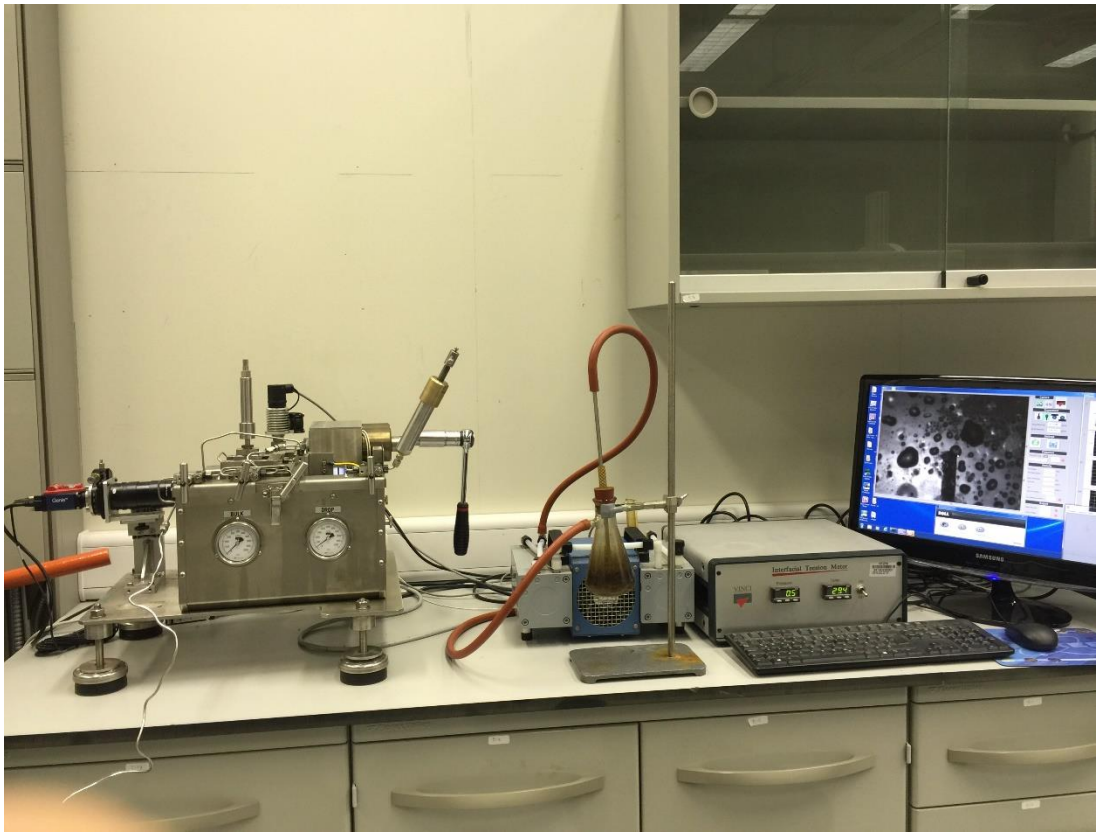

Figure 2: IFT Apparatus

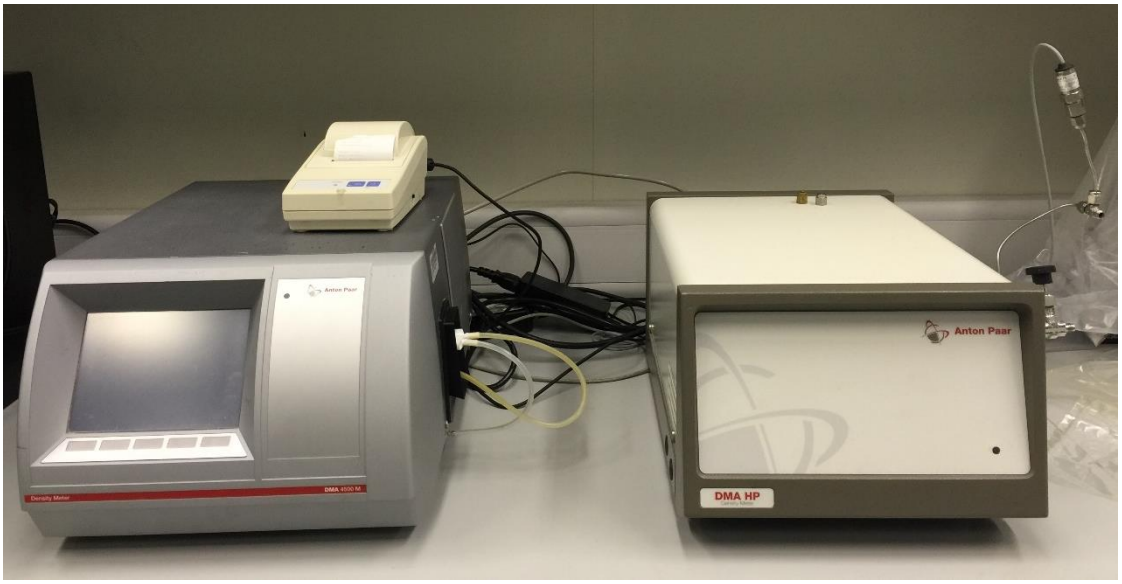

Figure 3: DMA 4500 and DHA HP by Anton Par

computer software can be set to take a picture after every 5 second in order the study the change in properties of the drop.

- Computer with IFT software installed. This software uses Drop shape Analysis technique and use Young-Laplace method. This software is calibrated for each experiment for being completely vertical and with stabilized pressure and clean glass and also proper focus.

Equipment Configurations:

1- For IFT:
    a. Pendant Drop: When Bulk Fluid is lighter than the Drop Fluid.
    b. Rising Drop: When Bulk Fluid is heavier than the Drop Fluid.
2- For Contact Angle:
    a. Sessile Down: When Bulk is lighter than drop fluid
    b. Sessile Up: When Bulk Fluid is heavier than drop fluid

3.5.2 ISCO Pump

A pneumatic controlled ISCO syringe pump with automatic refilling capacity and two cylinders. Each cylinder had 265ml capacity, maximum 7500 psi pressure, and a flow rate of maximum 45ml/minute. This pump is connected to an accumulator of 5 litre capacity which contains high purity CO_2. Figure 4

3.5.3 HPHT Densitometer

Densitometer by Anton Par (DMA-4500) was used along with an HPHT accessory (DMA-HP) as shown in the Figure 3.

Figure 4: ISCO Pump with N_2 Cylinder for pneumatic control

Figure 5: Analytical Weight Balance

Figure 6: Specially Fabricated Disk Holder for Grinding disks

3.5.4 Analytical Weight Balance

A high accuracy analytical weight balance (Sartorius Cubis® Precision Balance MSE5203S-000-DE) was used to measure the weight of the salts for brine preparation. The weight balance is shown in Figure 5.

3.5.5 Disc Holder

A grinder was used to make the dolomite disks smooth and horizontal. The disc was inserted in a fabricated holder (Figure 6) that could fit in the grinder.

3.6 Methodology

3.6.1 Experimental Plan

In order to study the IFT of various parameters on IFT and Contact Angle and to find a low IFT system, it was decided to conduct a number of experiments. The experimental layout was divided in four main parts:

i. The first part deals measurement of IFT of CO_2 with four types of Brines with different salinities on 3 temperatures and 9 pressures each.
ii. CO_2 with Brine-Surfactant Solutions containing three different types of surfactants on 3 temperatures and 9 pressures each.
iii. CO_2 saturated with Brine-Surfactant Solutions inside the cell, with five different oils and that saturated CO_2 on 2 temperatures, and 9 pressures each.
iv. The last part consists of making contact angle measurements in the last system that was selected for IFT, on a Guelph dolomite at one temperature and 9 pressures with different oils as drop fluids.

The parameters that were kept constant are:

i. Surfactant Concentration:
    - For FS-50: 0.15%
    - Alfoterra 0.1%
    - Armovis: 0.1%
ii. Brine-Surfactant concentration in Cell: 0.1 ml
iii. Core: Guelph Dolomite
iv. Brine for Brine-Surfactant Solutions: Brine 4

The parameters that were varied to study the IFT are mentioned below:

i. Temperature
    - Experiments without Oil: 30, 60 and 90 C
    - Experiments with Oil: 30 and 60 C
ii. Pressure: from 1500 to 5500 psi

iii. Brine Salinities from: 67708 ppm to 8464 ppm

iv. Oil types: Two crude oils and three model oils

An experimental layout for performing IFT has been given in Table 3:

Table 3 Experimental Layout for IFT Experiments

	Interfacial Tension (mN/m)			
Temperatures	30°C	60°C	90°C	**Compositions**
	Experiment Number			
Pressures: 1500 to 5500psi each experiment number	1	2	3	Brine1 with CO_2
	4	5	6	Brine2 with CO_2
	7	8	9	Brine3 With CO_2
	10	11	12	Brine4 With CO_2
	13	14	15	BSS1 with CO_2
	16	17	18	BSS2 with CO_2
	19	20	21	BSS3 with CO_2
	22	23	24	CO_2 + BSS3 with Crude oil 1
	25	26	27	CO_2 + BSS3 with Crude oil 2
	28	29	30	CO_2 + BSS3 with Model oil 1
	31	32	33	CO_2 + BSS3 with Model oil 2
	34	35	36	CO_2 + BSS3 with Model oil 3

The parameters for Contact Angle Measurements are:

i. Temperature: 60°C

ii. Pressure: 1500 psi to 5500 psi

iii. Rock Sample: Dolomite

iv. Oil Types: Two crude oils and one model oil

An experimental layout for performing CA has been given in Table 4

Table 4: Experimental Layout for Wettability Experiments

Composition	Pressures (psi)	Contact Angle Readings at Temp: 60 C
Bulk: CO_2 + BSS3 Drop: Crude oil 1 Rock: Dolomite	**1500**	Exp 37
	2000	Exp 38
	3000	Exp 39
	3500	Exp 40
	4000	Exp 41
	4500	Exp 42
	5000	Exp 43
	5500	Exp 44
Bulk: CO_2 + BSS3 Drop: Crude oil 2 Rock: Dolomite	**1500**	Exp 45
	2000	Exp 46
	3000	Exp 47
	3500	Exp 48
	4000	Exp 49
	4500	Exp 50
	5000	Exp 51
	5500	Exp 52
Bulk: CO_2 + BSS3 Drop: Model oil 1 Rock: Dolomite	**1500**	Exp 53
	2000	Exp 54
	3000	Exp 55
	3500	Exp 56
	4000	Exp 57
	4500	Exp 58
	5000	Exp 59
	5500	Exp 60

3.6.2 Density Measurements

The first step in conducting the IFT experiments was to determine the densities of the fluids. IFT software requires the densities of both the bulk fluid and the drop fluid. For bulk fluid, we use CO_2 in almost all of the experiments whose densities at required temperatures and pressures can be easily found in the literature. Therefore, only the densities of drop fluids were measured.

The densitometer was calibrated using N_2 and deionized water with known densities. Then at values were recorded at desired pressure and temperature conditions and a formula (polynomial) was devised and added into the equipment software. Now the equipment became ready to measure densities of other fluids.

The 1st step consists of density measurements of 4 Brines, each at 30, 60 and 90^{o}C and temperatures from 1500 psi to 5500 psi. An accumulator was filled was 35ml of Brine 1 and tightened closed. Then it was connected to the inlet of DMA HP. But the outlet was kept slightly open so as to allow the air in the pipelines to escape. Then the accumulator was pressurized to 100 psi. When the fluid filled DMA HP and started coming out of the outlet, the outlet was tightly closed and the apparatus was set to stabilize at a particular temperature, say, 30°C.

At that particular stabilized temperature and required pressure, say we started from 1500 psi, reading was taken. Then the pressure was increased to 2000 psi and temperature was again allowed to stabilize and then the reading was taken. This continued till 5500 psi.

Now to take readings at 60°C, the fluid inside the DMA HP was allowed to flow out and new fluid from the accumulator was allowed to displace it. Then similar procedure of

closing the outlet and temperature stabilization was carried out. Procedure was repeated for 90°C.

3.6.3 IFT Measurements

After measuring the densities of brines, the IFT experiment needs to be performed on each of the brine sample. Then the brine that shows lowest IFT will be selected for further experiments.

3.6.3.1 Interfacial tension between CO_2 and Brines

The Table 5 shows labelling of brines for easy explanation. Brine 2, 3 and 4 are simple dilutions of Brine 1 as mentioned already. The experimental parameters for performing IFT measurements between Brine and CO_2 are shown in Table 6.

Table 5: Brine Labels

Brines Labels	**Salinity ppm**
Brine 1	67708
Brine 2	33854
Brine 3	16927
Brine 4	8463

Table 6 : Experimental Parameters for Brine- CO_2 IFT Experiments

Experiment Parameters	
Drop Fluid	Brine
Bulk Fluid	CO_2
Temperatures (ºC)	30,60,90
Pressures (psi)	1500 to 5500
Brine Salinities (ppm)	67708 to 8464
Type of CO_2	99% Pure

The view cell was thoroughly cleaned with toluene and deionized water and then dried with tissue and nitrogen was also circulated. The pipelines, valves, pressure gauges, bulk and drop pumps, injectors were also cleaned with toluene and deionized water and dried by vacuum pump to make sure no traces of water or impurity is left. Then the pipelines and cell was reconnected. Brine1 was injected through injector 1 keeping the valve for drop generation closed so that it may fill Drop pump 1. Then CO_2 was charged into the cell from the connected accumulator that was pressurized using an ISCO Syringe Pump. Then cell was then covered and the equipment was allowed to stabilize on $30^{O}C$. It takes almost 5 to 6 hours to stabilize on $30^{O}C$. After stabilization, the valve from the drop pump is slowly opened to allow the flow of fluid through the capillary needle. Due to this, the drop is formed at the tip of the needle by using a specially designed high pressure syringe delivery system. Some of the CO_2 enters the needle and pipelines therefore initially that CO_2 comes out of the needle followed by drop fluid. After the drop is formed in the CO_2, its digital image is well focused and stored automatically in the computer memory. The IFT keeps decreasing with time till a point where it comes to an equilibrium with the bulk fluid. At this point the IFT is called “equilibrium IFT”. Both the IFTs changing with time and the ones when they came in equilibrium have been reported in this work. The output data of this DSA program also includes the radius of the curvature at the apex point, the volume and surface area of the brine drop. Each experiment gave readings at one temperature and nine pressures. After each experiment, the equipment was thoroughly cleaned with toluene and deionized water and then vacuum dried.

In order to take readings at 60°C the whole process from cleaning to drop generation and analysis was repeated. Similar case for readings at 90°C.

3.6.3.2 IFT measurements between Brine-Surfactant Solutions and CO_2

Brine 4 was selected from the experiments of the 1st step because it showed the lowest IFT. This Brine was then used to prepare three solutions for three different types of surfactants. Their name and composition has been mentioned in Table 7

Table 7: Brine-Surfactant Solution (BSS) Labels

Brine-Surfactant Solution Labels	**Composition**
BSS 1	Brine 4 containing 0.1 % Alfoterra
BSS 2	Brine 4 containing 0.1% Armovis
BSS 3	Brine 4 containing 0.15% FS-50

The experimental parameters for this Experiment have been given in the Table 8:

Table 8: Experimental Parameters for IFT measurement of BSS & CO_2

Experiment Parameters	
Drop Fluid	Brine4 containing Surfactant
Bulk Fluid	CO_2
Temperatures (°C)	30,60,90
Pressures (psi)	1500 to 5500
Brine Salinity	8464 ppm
Surfactants	FS-50, Alfotera, Armovis
Type of CO_2	99% Pure

The concentration of surfactants typically found in literature is 0.1% however, it was found that fluorosurfactants are effective till 0.15% and then a constant plateau is reached in terms of their ability to decrease IFT. Therefore, BSS3 contains 0.15% FS-50.

These brine-surfactant solutions were then used as drop fluids with CO_2. The same procedure was repeated as in 1st step for both cleaning, filling and temperature stabilization. The readings in this case were also taken at 9 different pressures from 1500 to 5500 psi for each temperature 30^{O}C, 60^{o}C and 90^{o}C.

IFTs were quite small and drops were unstable therefore the drops did not sustain for much longer time. However, their equilibrium IFT was recorded at a point where IFT stopped changing with time.

3.6.3.3 IFT Measurements between CO_2 (saturated with brine-surfactant solution) and Oils

This part of experiment is different from the previous experiments because previous experiments were between two single phases. This one is between a two phase CO_2 i.e. CO_2 saturated with BSS 3. The reason for selecting BSS 3 is that it gave the lowest IFT as compared to the other two surfactants.

The experimental parameters of this experiment have been given in Table 9.Some drops of BSS3 were dropped inside the cell before closing it. Then the cell was filled with CO_2 and allowed to stabilize with temperature and come at equilibrium with BSS3. On the required temperature and pressures, reading were obtained one by one. Both Equilibrium and changing IFTs were recorded with time.

Although the CO_2 was saturated with BSS3, the density used for this experiment is the density of pure CO_2 since the two phases of Brine and CO_2 have very limited solubility, this difference in densities is expected to be close to the difference between pure brine and pure CO_2 at desired temperature and pressures. However, at low temperatures and high pressures, where change in density is small, errors in the phase densities can have large influence on the derived values of IFT. [31], According to Hebach et al. at pressures up to 30MPa and temperatures between 10°C and 50°C they found out that density of CO_2 rich phase did not differ from density of pure CO_2 within the experimental uncertainty of 0.15%.

Table 9: Experimental Parameters for IFT measurements of Oils & CO_2-BSS3

Experiment Parameters	
Drop Fluid	Oil
Bulk Fluid	CO_2 and approx. 0.1ml BSS3
Temperatures (°C)	30,60
Pressures (psi)	1500 to 5500
Brine Salinity	8464 ppm
Surfactant	FS-50
Type of CO_2	CO_2 Saturated with Solution
Oils	Crude oil 1, 2, Model Oil 1,2,3

3.6.4 Contact Angle Experiments

After the completion of all IFT experiments, the next challenge was to perform contact angle experiments in the same manner and with the same components as used in the last IFT experiment i.e. all 4 fluids (CO_2, Brine, Surfactant, and Oil) with dolomite rock.

3.6.4.1 Preparation of Dolomite Disks

A core of Guelph Dolomite with properties mentioned in the previous chapter was cut into disks of 1 inch x 2.5 mm. Then these disks were polished by a grinding machine using a specially fabricated holder. These disks were then put in the respective oils for aging for 24hrs at 60^{o}C because the experiments would be performed at 60^{o}C. (Figure 7)

Figure 7: Dolomite disk aged in squalane, pasted on disk holder of the cell

Another method of polishing the disks by using silicon epoxy could also be used but it could alter the composition of the rock and also the contact angle. Three test experiments were performed with different disks to see what could be the effect of polishing method.

3.6.4.2 Procedure

The disks after aging were pasted on the holder of the cell with a glue, making sure fingers don't touch the top side of the disc. Then the cell was closed after putting some drops of BSS3 inside the cell and allowed to stabilize at 60^{o}C meanwhile CO_2 was also injected inside the cell. When the temperature stabilizes, the disc is analyzed for its surface. Sometimes a lot of foam accumulates on the surface of the rock. This foam would make it difficult for the camera to differentiate between foam and the oil drop. In

this case, leave the equipment for 6 hours for the foam to disappear. The foam is more when there is crude oil as compared to any single component model oil.

Since horizon of the disk is an important factor for solution of Young-Laplace equation on the drop, the disk is matched with a horizontal reference line to make sure it is horizontal.

At the desired pressure and temperature, a drop is generated from the capillary needle. Some CO_2 comes out of the needle followed by drop fluid. Since we have a disk below, therefore the valve is opened with much care so as not to allow more than one drop to come out of the needle and fall on the disk.

The size of the drop doesn't matter as long as the weight of the drop doesn't act. Therefore, the smallest needle was used for all experiments.

Then the drop was recorded and reading were taken for the whole time until the drop comes to an equilibrium with bulk fluid. For some cases such as Squalane at higher pressures the drop would disappear because it was partially miscible into CO_2. Therefore, an equilibrium value was recorded because, although the squalane would be miscible the CO_2, the drop would become smaller and smaller the contact angle remained constant even with the decrease of drop volume.

After taking the readings at a single temperature and pressure, it was desired to take readings at other pressure. However, the same place on the rock cannot be used because it has already wetted the specific surface of the rock. Therefore, there can be two ways, either to turn off the equipment, deplete the gas, clean the cell and the equipment, change the disk and perform the experiment on a new disk. Or any way one could change the

place of drop on the disk. The holder on the cell could be rotated which could change the place of the drop. Hence this second method was used for ease. After the reading was taken for one drop at one pressure, the disk was rotated a little bit to change the location, pressure was increased till the desired pressure and then a new drop was generated and made to fall on a new place on the disk. This however depends on the volume of drop generated on the rock surface. If the drop is of high volume and there is no space left on the rock surface to measure at next pressure, the experiment was to run all over again with a new rock sample at required pressure and temperature conditions.

At the all of the results from contact angle experiments and IFT experiments were compiled and conclusion was derived from the results. For some of the values of contact angle, the experiments were repeated to confirm the trend.

CHAPTER 4

RESULTS AND DISCUSSION OF IFT EXPERIMENTS

The main purpose of an EOR process is to reduce the oil saturation which therefore increases the oil recovery. An EOR process like Surfactant-Alternating-Gas is used when simple CO_2 or simple Water injection does not give significant results.

The interfacial tension between SAG fluids co-existing in the reservoir have been measured in this series of experiments whose experimental plan and procedure have been mentioned in the previous chapter. The results of each step are described in the sections below:

4.1 Density Measurements:

Densities of the following fluids which were needed for IFT experiments:

1- CO_2
2- Brine 1
3- Brine 2
4- Brine 3
5- Brine 4
6- Brine4 containing 0.1% Alfoterra
7- Brine4 containing 0.1% Armovis
8- Brine4 containing 0.15% FS-50

9- Crude oil1

10- Squalane (Model oil 1)

11- Crude Oil2

12- Toluene (Model Oil 2)

13- Pentadecane C15 (Model Oil 3)

Density of Fluids increase slightly with pressure and decrease with temperature. Trends of different fluid densities have been below. Details of density values have been provided in Appendix A.

4.1.1 Carbon Dioxide (CO_2)

Carbon dioxide follows the following phases at different temperature and pressure conditions.

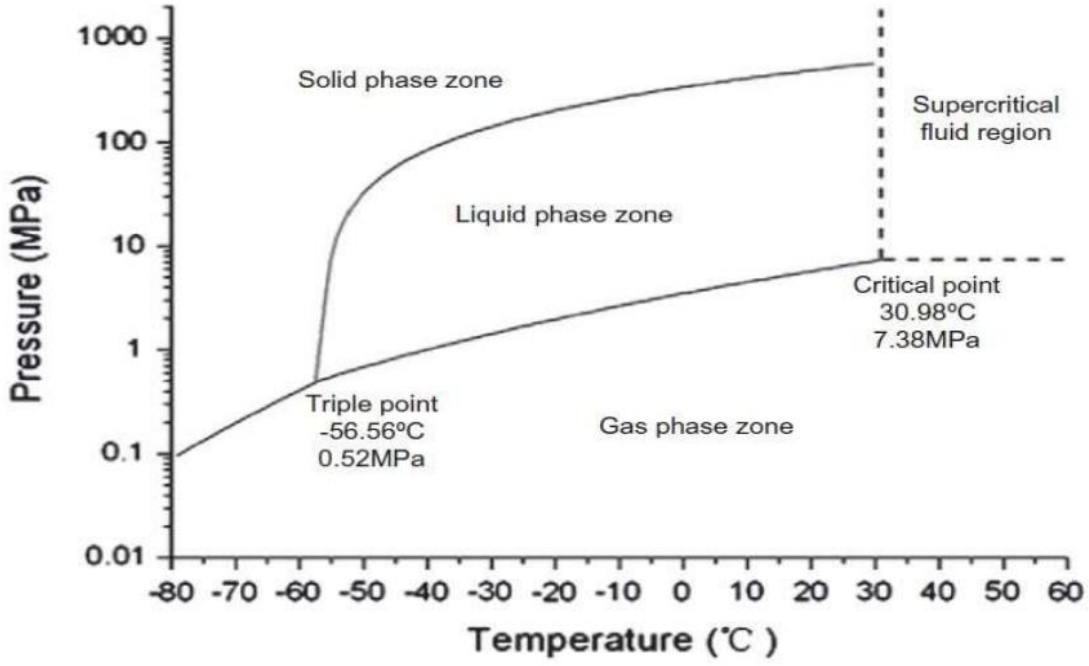

Figure 8: Phase Diagram of CO_2 [36]

Density of CO_2 has been calculated by Ouyang (2011) correlation and given in Appendix A [68]. However the variation with pressure and temperature has been shown in Figure 9.

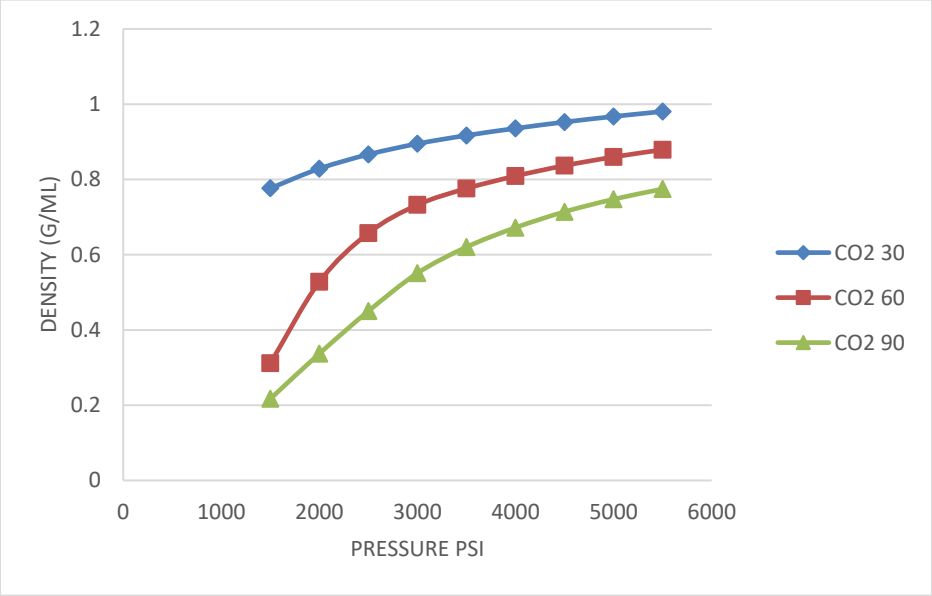

Figure 9: CO_2 Densities as a function of Pressure at Different Temperatures

4.1.2 Densities of Brines:

The higher is the salinity, the denser is the brine as shown from the above figures. Also density increases with pressure and decrease with temperature.

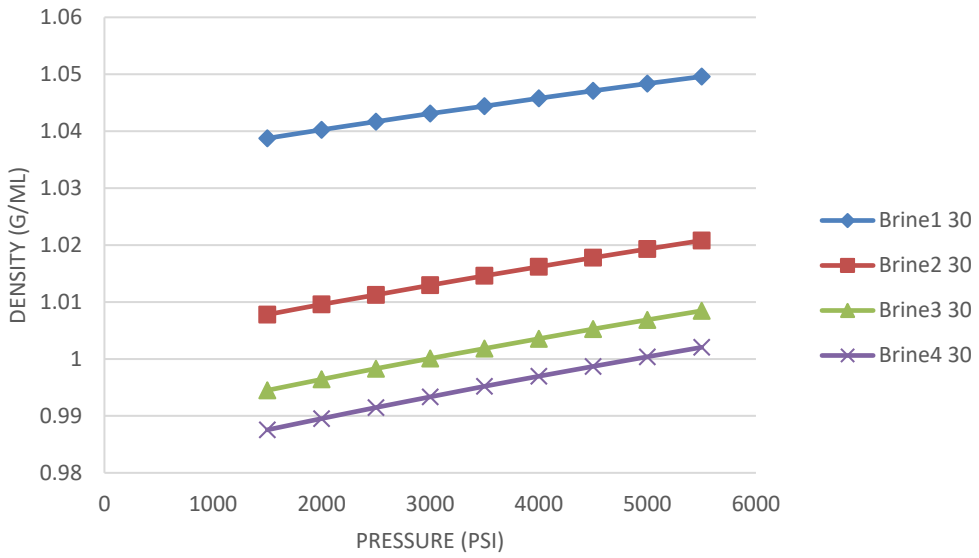

Figure 10: Densities of Brines at 30°C

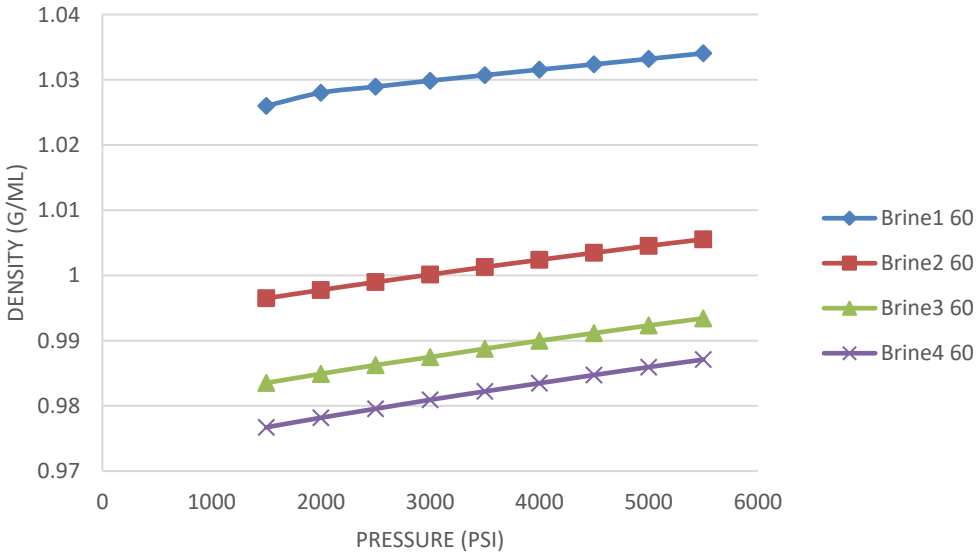

Figure 11: Densities of Brines at 60°C

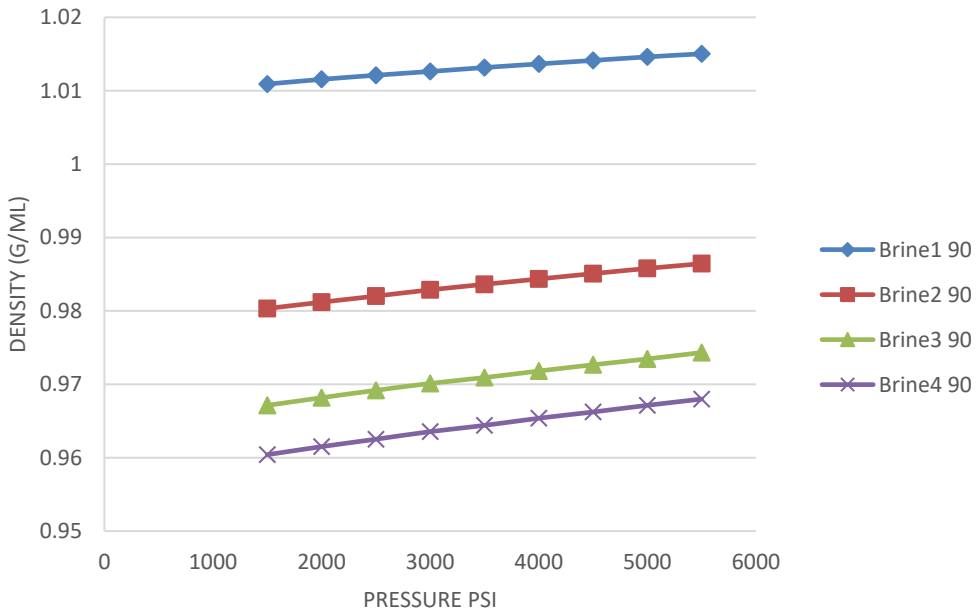

Figure 12: Densities of Brines at 90^{o}C

4.1.3 Density of BSS

In Figure 13 to Figure 15, for brine-surfactant solutions, density change is minute with pressure. The graphs have been drawn for small range to show the effect.

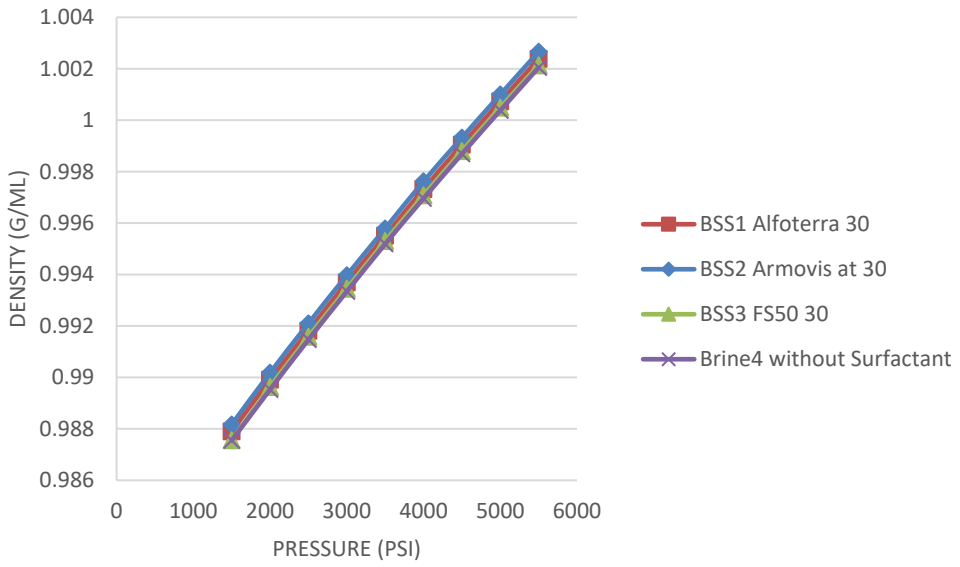

Figure 13: Densities of BSS at 30°C

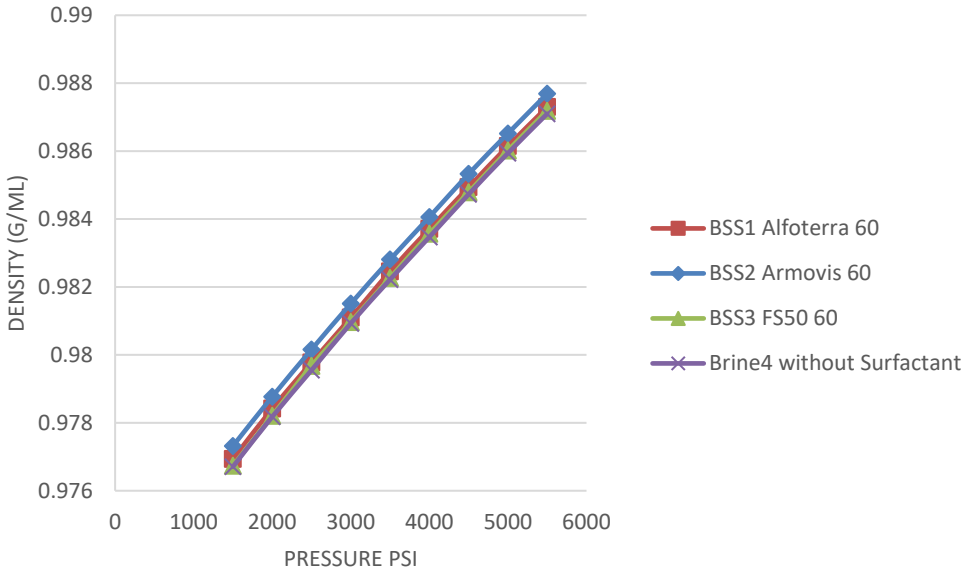

Figure 14: Densities of BSS at 60°C

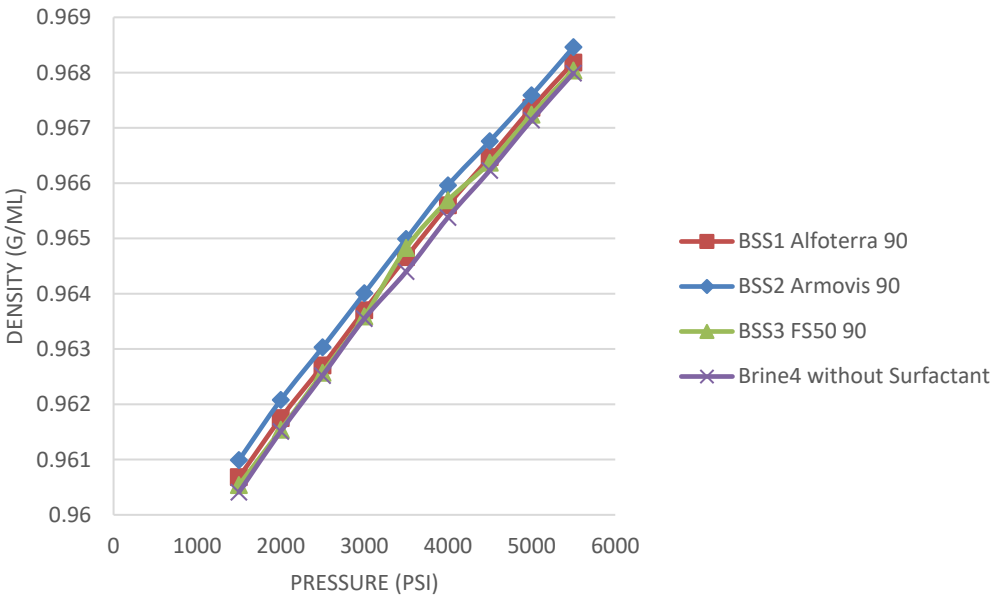

Figure 15: Densities of BSS at 90°C

4.1.4 Density of Oils

Densities increase almost linearly with the increase in pressure and decrease in temperature. This trend is continuous for all fluids.

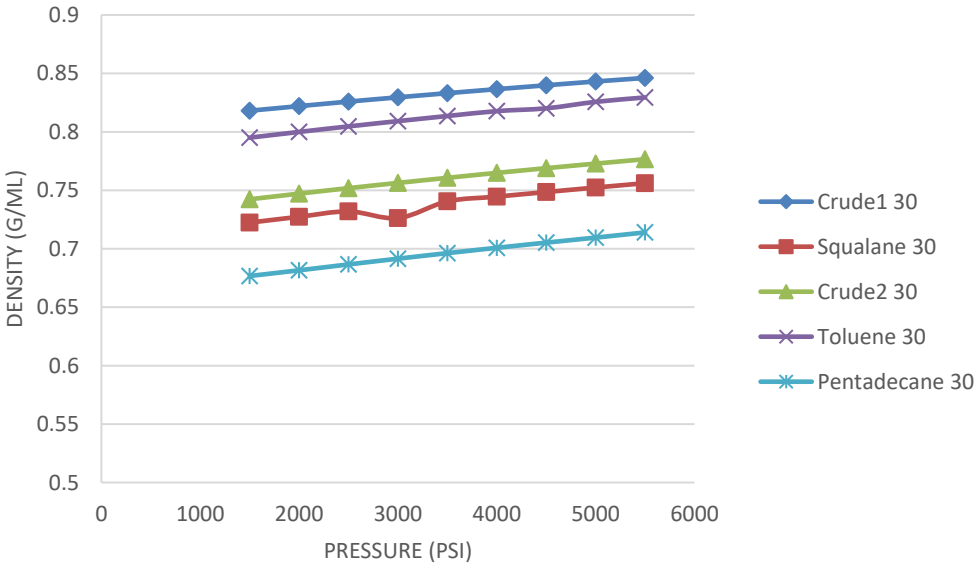

Figure 16: Densities of Oils at 30°C

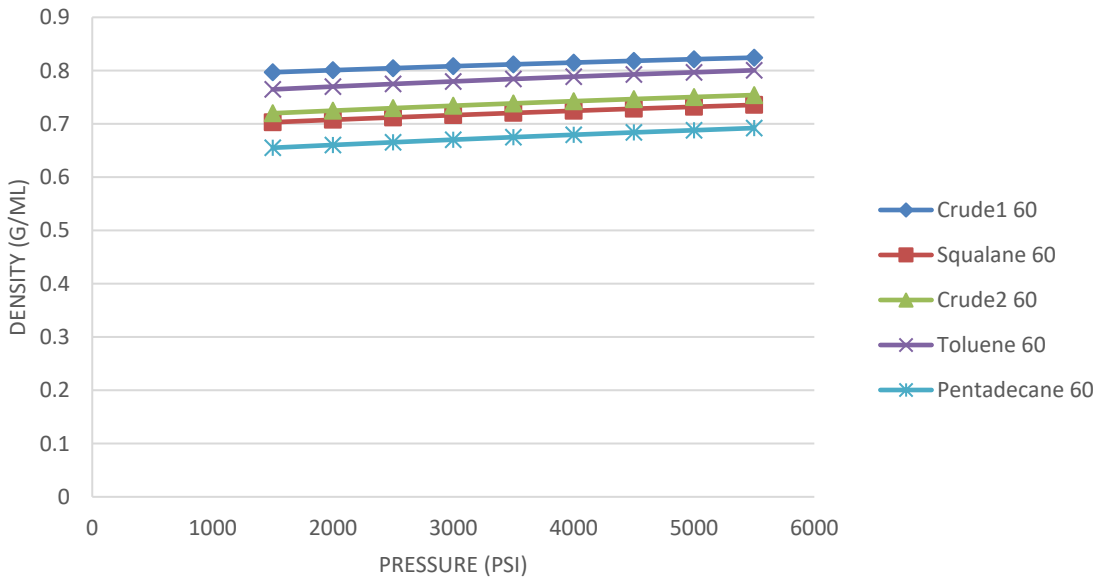

Figure 17: Densities of Oils at 60°C

4.2 IFT

According to the experimental plan mentioned in Table 3 interfacial tensions have been measured between the following fluids:

1- Brines as drop fluids and CO_2 as Bulk fluid
2- Brine-Surfactant Solutions as drop fluids and CO_2 as Bulk fluid
3- Oils as drop fluids with CO_2 as bulk fluid in the presence of brine-surfactant solution

4.2.1 Brines as drop fluids and CO_2 as Bulk Fluids:

4.2.1.1 Effect of Temperatures and Pressures:

General trend found in literature is that higher is the temperature, higher is the IFT [18], [31]. However according to Chiquet et al. (2007) [69] IFT decreases with increase in temperature for water/CO_2 systems. According to Bikkina et al. (2011) [70] in the

supercritical region of CO_2, the IFT with pure water is constant with both temperature and pressure. Yang et al. (2005) [38] found that IFT decreases with increase in pressure at 27°C but increase with increase in temperature, however they found that their brine was miscible at 58°C and 1100 psi since the interface disappeared.

In this work it was observed that brines with lesser salinity follow the trend observed by Li et al. (2012) that higher temperature causes increase in IFT and high pressure causes decrease in IFT [31]. For brine1, the brine with highest salinity, the IFT is independent of pressure and temperature matching with results by Li et al.

Initial decrease is high till 2000 psi at 30°C because at this point the system is in the supercritical phase at a point closer to gaseous phase (Figure 8). This rapid decline is due to solubility of CO_2 in brine according to Xing et al., (2013) [28].

At 60°C the IFT increases till 2500 psi. This behavior has been seen in the literature [70] but not highlighted and some authors have not measured values between these points. For Yang et al. (2005), at 58°C which is close to our temperature, the brine became miscible and no interface was formed [38]. Chun (1995) and Chalbaud et al. (2010) observed it at 71°C, Bikkina et al. (2011) at 40°C, Rocha et al. (1999) at 45°C, and Hebach et al. (2002) at 45°C, all in the same range of pressure that lie closer to points where CO_2 is behaving partly supercritical and partly gas [22], [39], [70]–[72] . Interestingly Hebach et al. (2002) observed the reason why IFT increases instead of decreasing in this region [72]. Any error in the zone where density is varying strongly with pressure would cause a large deviation in the results. Hebach et al. (2002) did two experiments to conclude that a temperature sensor/thermometer near the pendant drop inside the bulk phase would

produce less error as compared to the one placed in the equipment enclosure. In this work, it was observed that density varies significantly in this region (1500 to 2500 psi at 60°C) as shown in Figure 9.

From 1500 psi (10MPa) to 2500 psi there is a drastic density change in CO_2 at 60°C as shown in Figure 9 and from the phase diagram Figure 8 it can be observed that this point is sensitive to pressure changes.

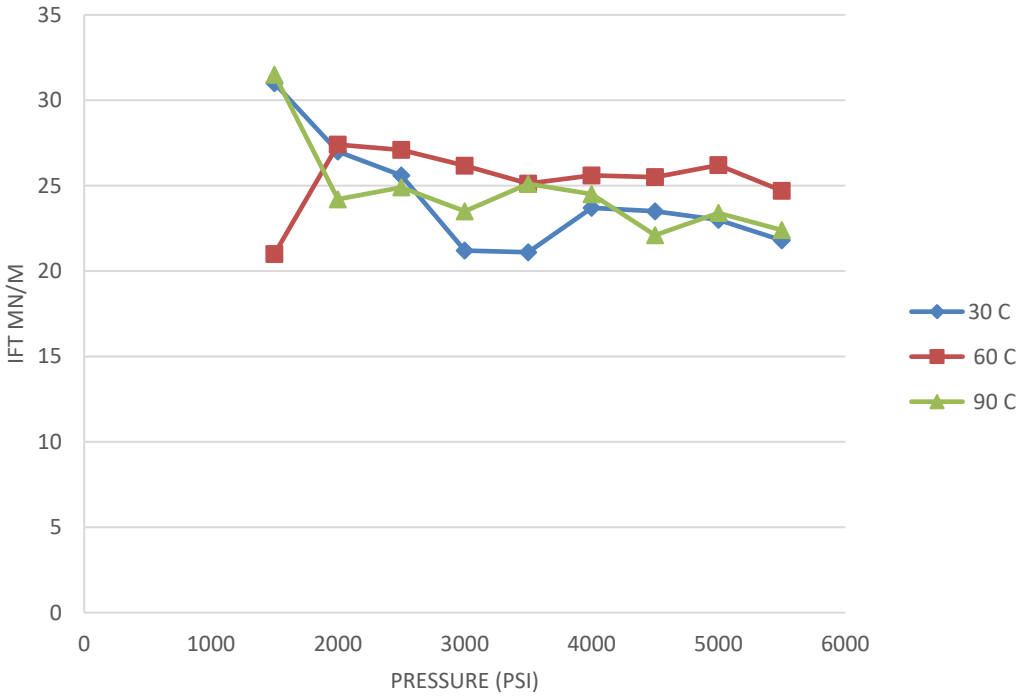

Figure 18: Interfacial Tensions of Brine 1 at different temperatures

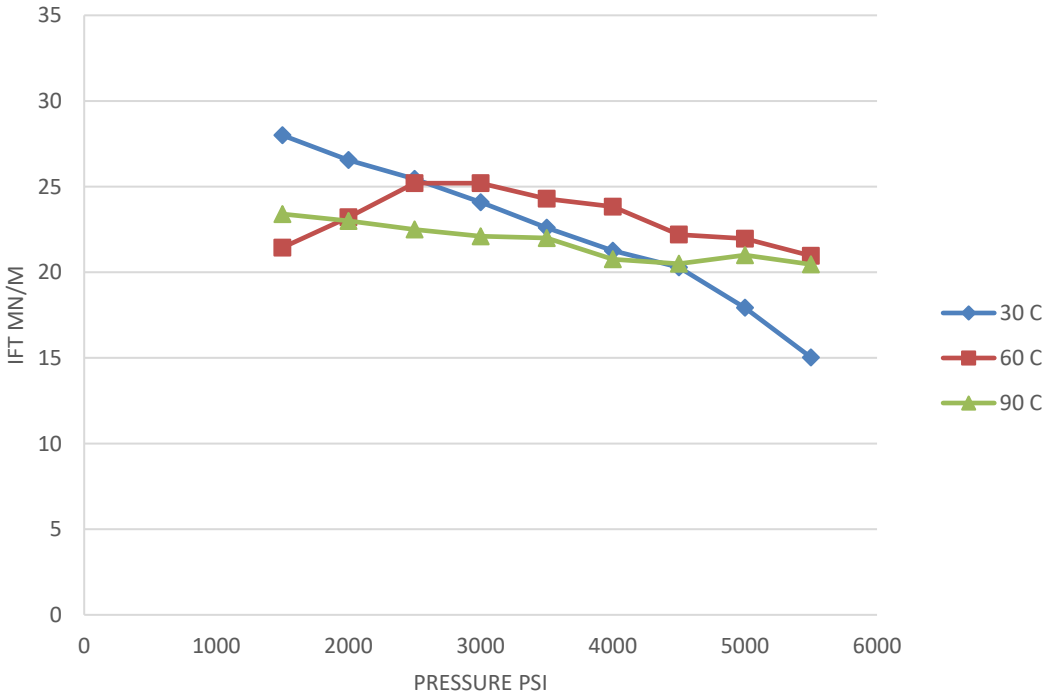

Figure 19: Interfacial Tensions of Brine 2 at different temperatures

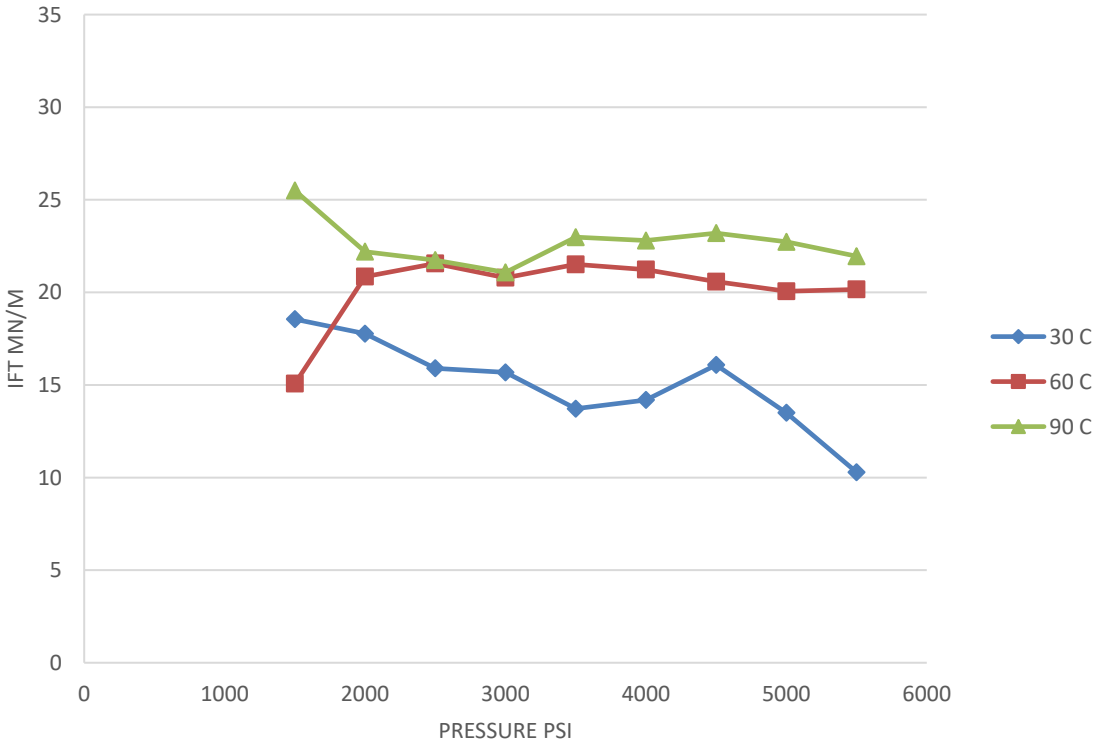

Figure 20: Interfacial Tensions of Brine 3 at different temperatures

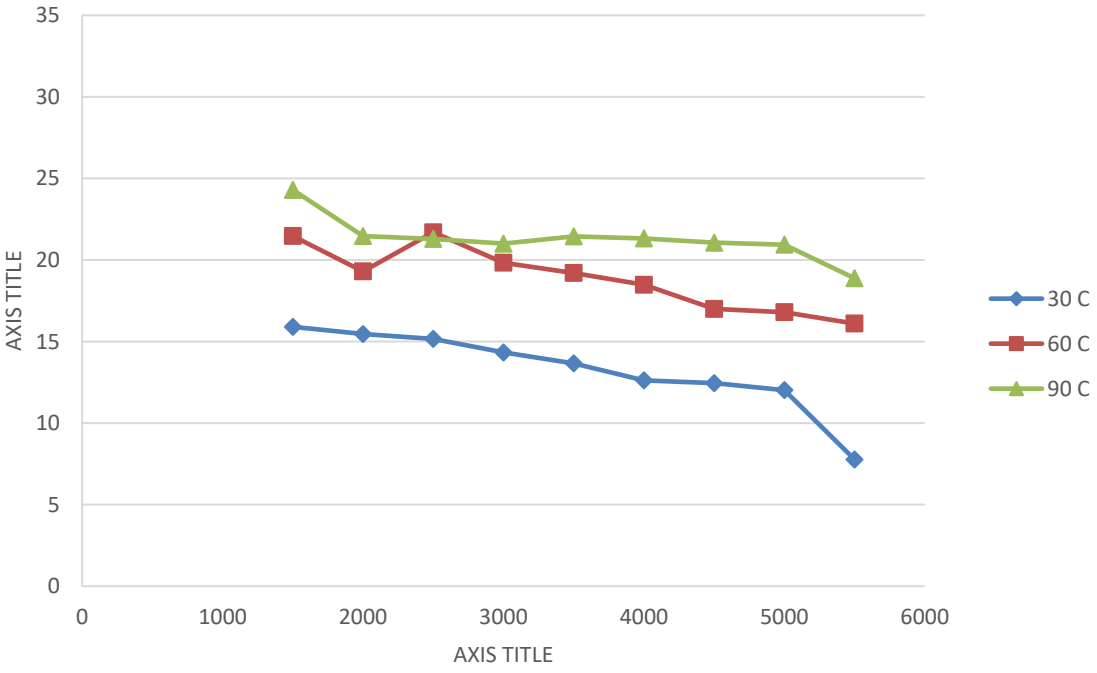

Figure 21: Interfacial Tensions of Brine 4 at different temperatures

Another interesting trend has been observed by Chalbaud et a. (2009) that higher the salinity, lesser is the deviation as shown in Figure 22.

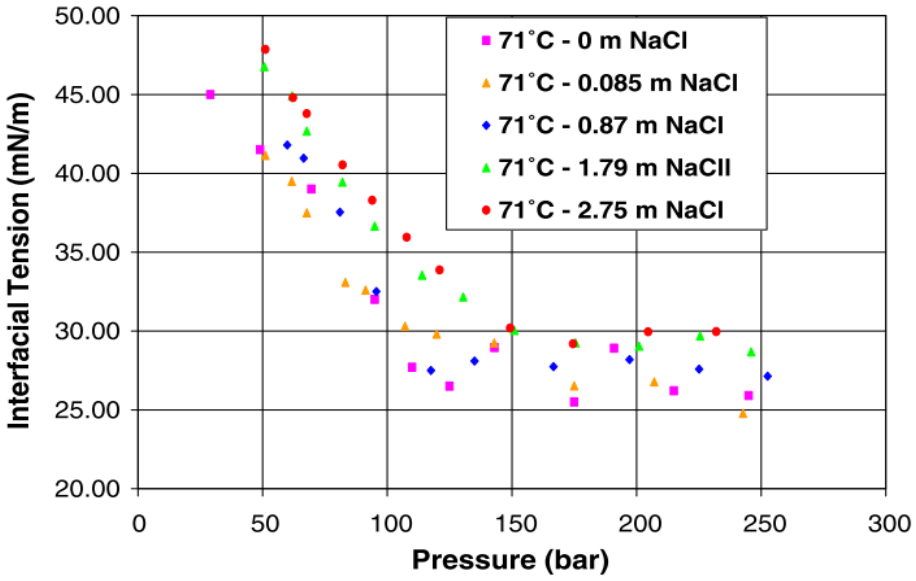

Figure 22: IFT versus Pressure for different conc. of NaCl [73]

This same trend has been observed in this work. For Brine1, the increase is only till 2000 psi whereas for other brines that are in lower salinity the increase is till 2500 psi.

4.2.1.2 Effect of Salinities

For Figure 23 to Figure 25, at same temperatures and pressures, it is observed that higher the salinity, higher is the interfacial tension. The same trend was observed by (Li et al., 2012) .

From Figure 26 to Figure 28 increase in IFT with salinity does not follow a specific trend of increase. Previously Chalbaud et al. [73] observed that the relation between average IFT increase and salt concentration (Figure 29) is linear in case of simple NaCl brine and similar kind of linear relation is true for many other chlorides. However, they mention that the relation is not linear with higher concentrations of salts and for multi-component brines. Since the brine used in this work is a multi-component brine, therefore no relation can be made between them however trends show that the average IFT increase will increase with increase in brine salinity.

4.2.1.3 Effect of Solubility of Brine and CO_2

Spycher et al. (2003) and Spycher (2005) made a literature review and correlation for measurement of CO_2 and water/brine solubility at different temperatures and pressures [74],[75]. They observed that CO_2 solubility in H_2O decreases with increase in temperature, but increase with increase in pressure for all pressure and temperature ranges. However the solubility of H_2O in CO_2 increases with both pressure and temperature (Figure 30).

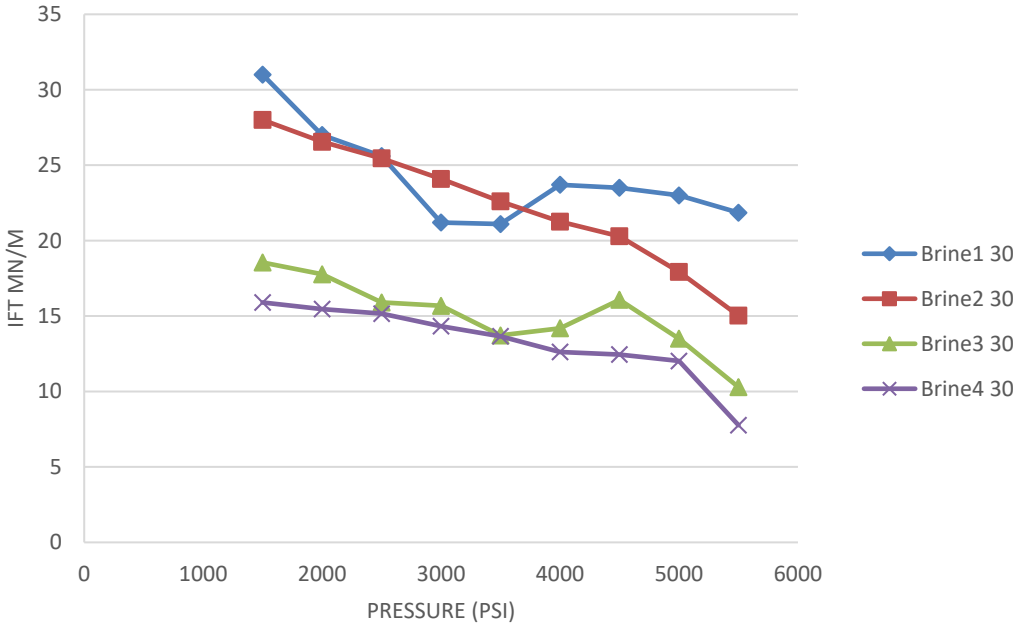

Figure 23: Interfacial Tension of Brines at 30°C

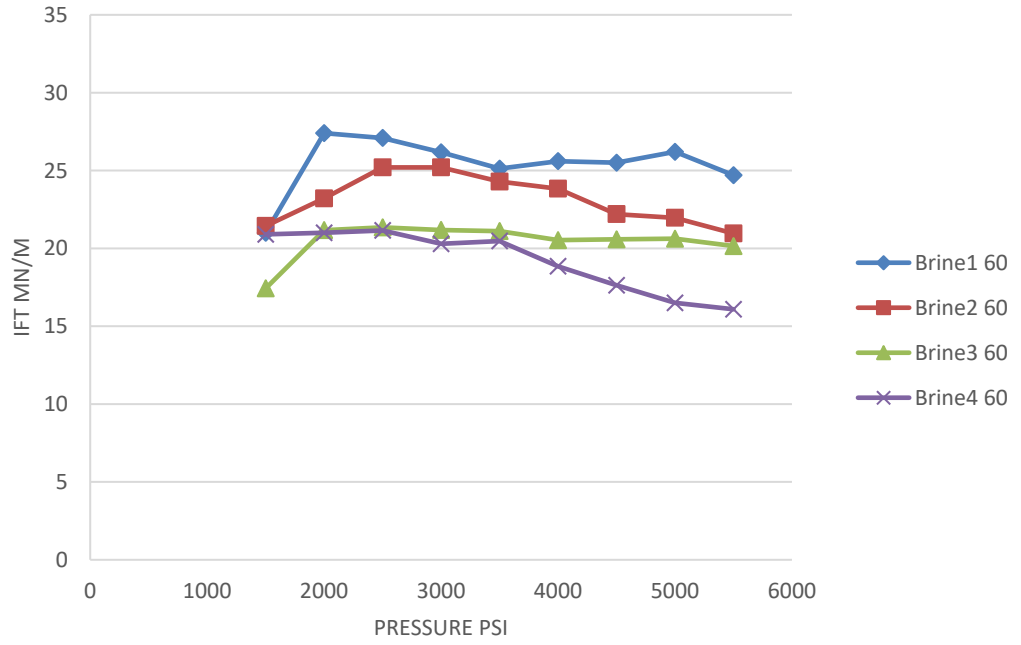

Figure 24: Interfacial Tension of Brines at 60°C

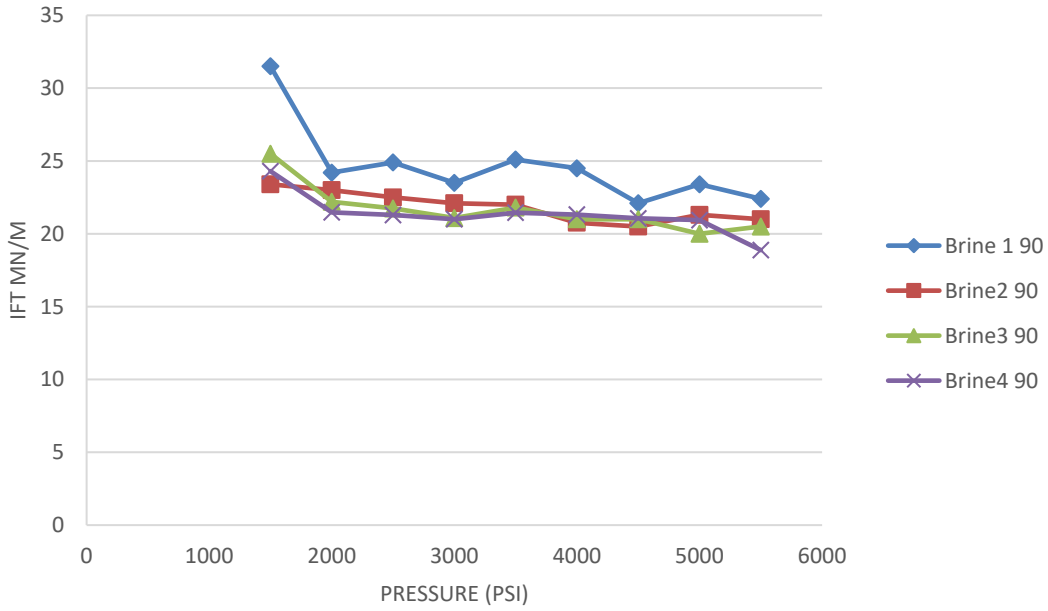

Figure 25: Interfacial Tension of Brines at 90°C

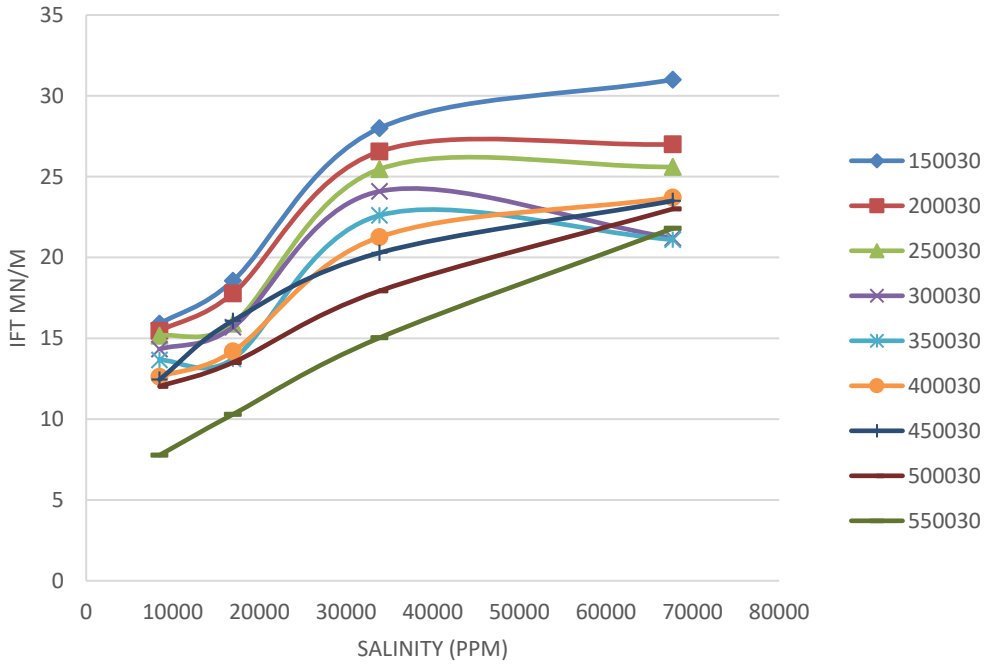

Figure 26: IFT vs Salinities at 30°C and all pressures

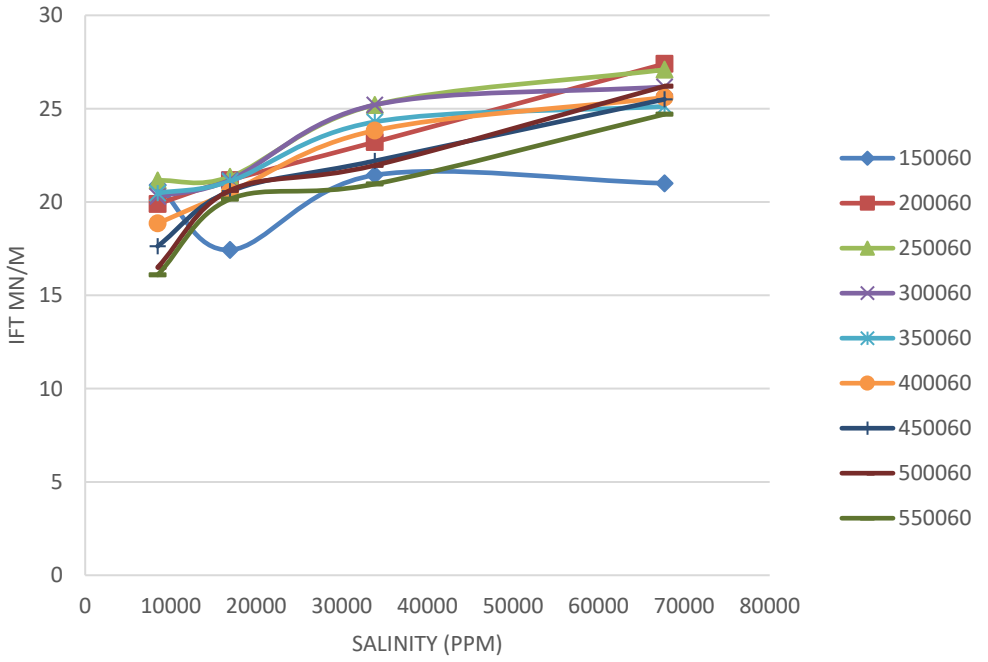

Figure 27: IFT vs Salinities at 60°C and all pressures

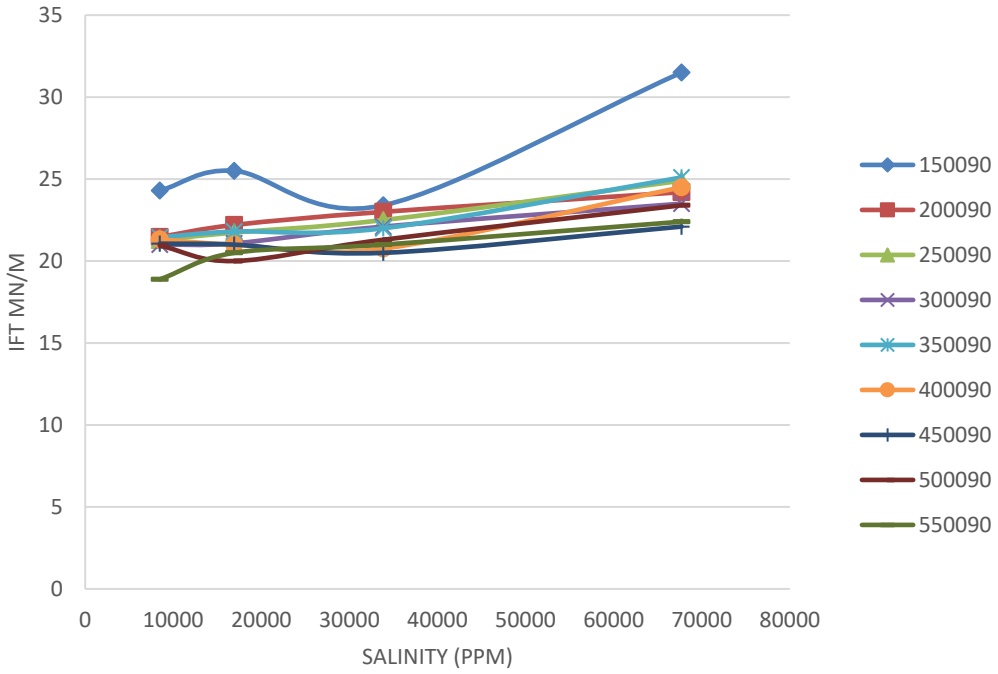

Figure 28: IFT vs Salinities at 90°C and all pressures

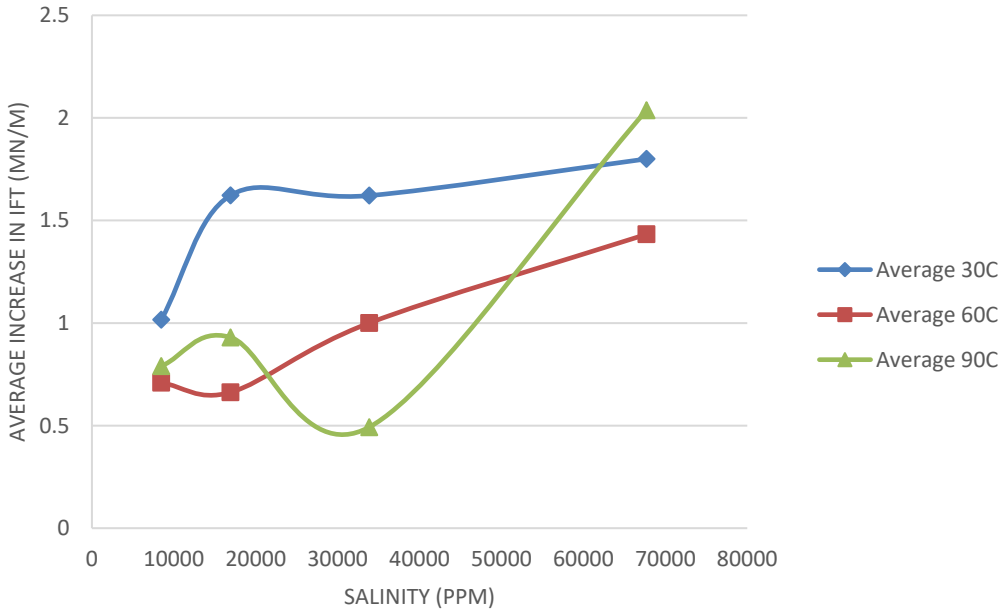

Figure 29: Average IFT increase as function of brine salinity for different T

Yang et al. (2005) explored the relationship between IFT and Solubility of brine and CO_2 [38]. He observed that solubility of CO_2 (using equation of state for real gas) in brine increases as the pressure increases whereas it decreases with increase in temperature and this increase and decrease had a direct influence on IFT. As temperature increases, the brine molecules achieve high kinetic energy to escape the brine interface. Also CO_2 molecules are in high random motion making it easier to diffuse into and out of brine and capture and dissolve brine molecules. The higher is the dissolution of fluids into each other, lesser is the density difference and therefore lesser is the IFT. Yang et al. (2005) explained this dissolution from the work of Teng (1998) that at low temperatures, mass transfer is mostly one-way i.e. CO_2 dissolves into water [38], [76]. However, at high temperatures, there is a two-way mass transfer because CO_2 solubility increase with temperatures. Work of Spycher et al. (2003) also proves the same point [74] . This mass transfer can be observed by swelling and shrinkage of the pendant drop [38].

From Figure 96 to Figure 107, it can be observed that on increasing pressures, for same temperature, the size of the drop increases for all brines. This is due to increase in solubility of CO_2 in brine drop causing the expansion of brine particles in the drop. However, at very high pressure, the drop size either remains constant or decreases a little bit. This is due to the vapor pressure at such high pressure trying to act on the drop surface and therefore decreasing the drop size and also making it difficult to stabilize it for longer times.

Increased salinity of the reservoir brine results in significantly reduced CO_2 solubility [38]. At 30°C, from Figure 96 to Figure 99, Figure 96 is for the Brine with highest salinity and Figure 99 is for brine with lowest salinity. Brine 4 has larger drops and the drop size decreases when salinity is increased for Brine 3, Brine 2 and Brine 1.

However as previously mentioned, not only solubility but vapor pressure and time stabilization is affecting the drop profile, that's why sometimes at high pressure the drop tends to be small.

4.2.1.4 Effect of Brine-CO_2 density difference on IFT

From Figure 31 it has been observed from our experimental values that IFT depends on density difference. Although here the density difference takes into account the effect of pressure, temperature and salinity. Nevertheless, density difference is not the only parameter to predict the IFT here and in Figure 32 it has been shown that at same density difference IFTs can be obtained and that this is mainly the consequence of salinity.

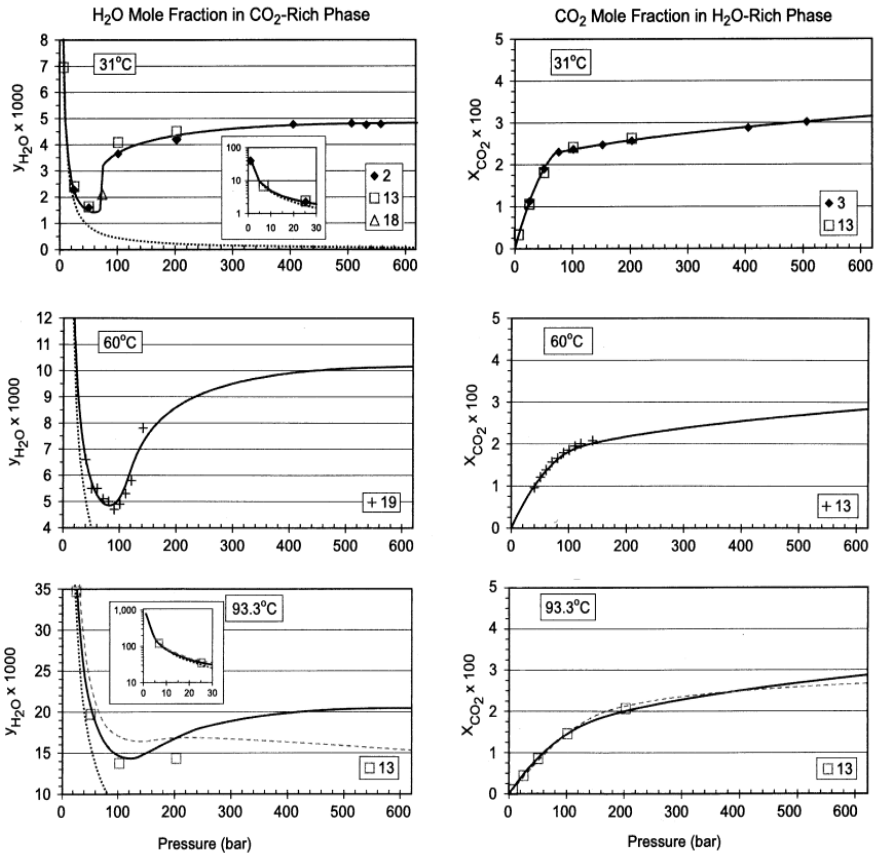

Figure 30: (Spycher et al., 2003) Solubility of CO_2 and water

However, the density difference variation follows the same trend making it easier to predict the behavior of IFT with density difference.

Similar results were plotted by [73] however they did not plot at points where density difference is less than 0.2 g/ml. IFT increases linearly till density difference of 0.2 g/ml and forms a plateau (or a region of less increase) at certain region of density difference and as the density difference increases further, the IFT slope changes again making it almost linear increase.

4.2.1.5 Change of Brine IFT with time

Many authors have reported the an experimental trend of change in IFT in their work [22], [37], [38], [70], [72], [73], [77] similar to the one shown in Figure 33.

Once the drop was generated from the capillary needle, it was maintained for at least 10 minutes in this work for brine and CO_2 system. Initially the drop comes into contact with the bulk fluid (CO_2) and, since both fluids are unsaturated, the drop is initially enlarged due to intake of CO_2. Later the mass transfer of water into CO_2 takes place. Due to this dissolution IFT decreases till a point of equilibrium for some time.

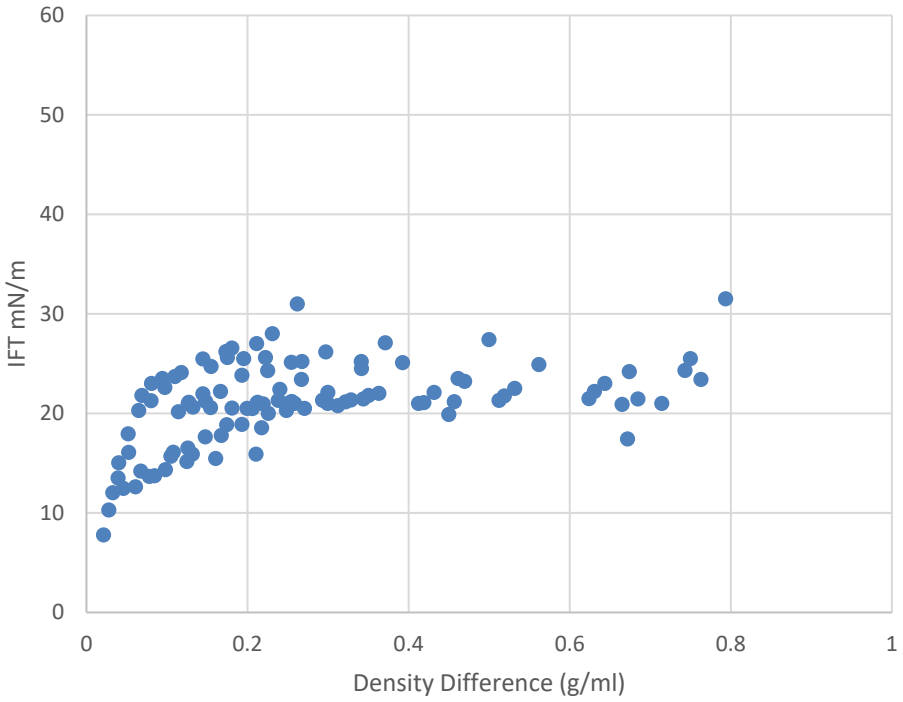

Figure 31: Variation of IFT with Brine-CO_2 density difference

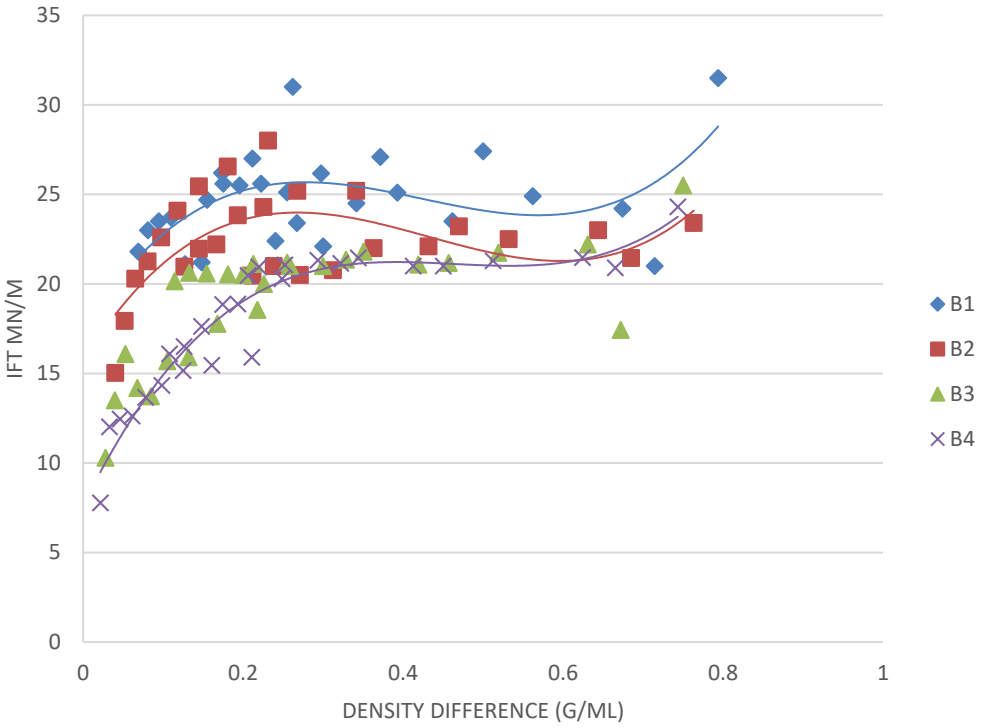

Figure 32: Trends of IFT with density difference

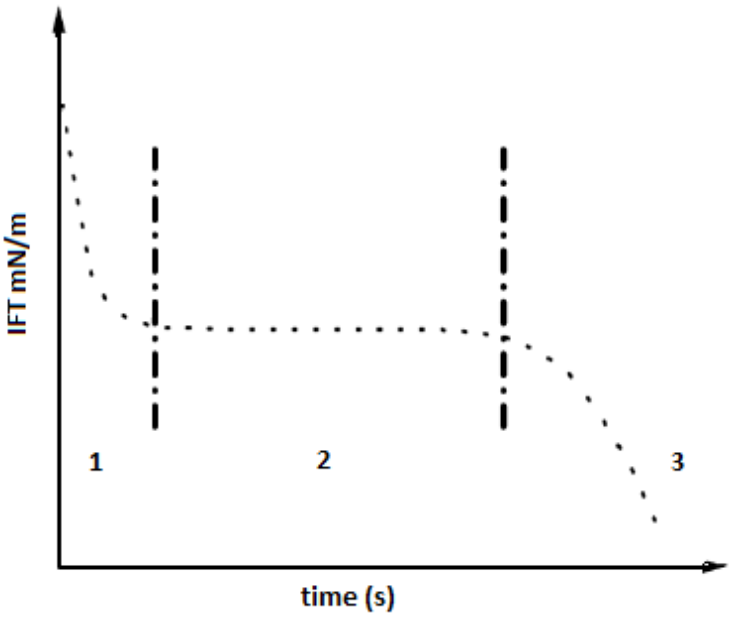

Figure 33: Time dependence of IFT

This 2nd region is the best time to measure the IFT values. IFT continues to decrease with time afterwards because the vapor pressure above a positively curved surface is higher

than that above a flat surface. Therefore, it is difficult for the drop to maintain equilibrium for longer time and as a consequence it becomes smaller with time and therefore the volume of the drop changes. While the dia of the needle remains constant, the drop shape changes and thereby causing error in IFT calculation below a certain drop volume.

For this work, IFT variation with time has been shown in Appendix D.

4.2.1.6 Determination of Minimum Miscibility Pressure

If the difference between the intermolecular forces is small, the interfacial tension between the two phases is small and vice versa the interfacial tension between the two phases is large. Only if the intermolecular forces operating with two phases are equal, the molecules on the interface between the two phases are under balance of forces. As a result the interface between the two phases disappears, the value of interfacial tension between the two phases is zero and the two phases are miscible [78].

Minimum miscibility pressure is defined as the pressure at which no drop for IFT can be formed and IFT is therefore zero. This can be estimated by extrapolating the decreasing lines, on plot of pressure vs IFT, till x-intercept i.e. where y-axis value (IFT) becomes zero.

Table 10: Minimum Miscibility pressures in psi of brines

Temperatures	**30**	**60**	**90**
	MMP (psi)		
Brine 1	17707	46990	21204
Brine 2	10986	19640	30552
Brine 3	12848	55722	27702
Brine 4	11231	12685	30040

The minimum miscibility pressures for all four brines at each temperature have been given in Table 10. Since at high temperatures, the solubility of CO_2 in H_2O decreases it becomes difficult to make them miscible and very high pressure is required. There is a need for more points at high pressures to predict the effect of salinity on MMP using the plot of IFT vs Pressure.

4.2.2 Brine-Surfactant Solutions (BSS) as drop fluids and CO_2 as Bulk Fluid

Since the lowest IFT was given by Brine4 (i.e. the brine with lowest salinity), therefore this brine was selected for next step of system for comparison of three different surfactants.

4.2.2.1 Effect of Temperature and Pressure

From Figure 34 to Figure 36 it can be seen that IFT increases with increase in temperature and decreases with increase in pressure. This trend is continuous for all surfactants except for Alfoterra at 90^{o}C. Alfoterra can give ultra-low IFT at low temperatures (less than 60^{o}C) and low salinity of NaCl [63]. 40,000 ppm is the minimum salinity defined by the manufacturer. Alcohol ether sulfate surfactants have poor hydrolytic stability at high temperatures (above 65^{o}C) and therefore decompose [79]. However addition of co-surfactants or alkali (sodium carbonate) in low concentration can increase the stability of this surfactant till 120^{o}C [79], [80].

In this work, brine consists of several components and therefore the effect of sodium carbonate cannot be separated. Also salinity is 8464 ppm but sodium carbonate concentration is quite high. Therefore, the surfactant inside the brine drop is decomposing at such a high temperature and pressures. BSS1 couldn't show any ultra-low IFT however

IFT is still lesser than the brine without surfactant. IFT initially decreases with increase in pressure but after a certain point it continues to increase with pressure. Similar kind of increasing IFT has been reported when the surfactant is used in highly saline system by [63]. Another cause of this behavior could be the presence of divalent cations in the brine which are a great threat to aqueous solubility and cause precipitation with the ether sulfate surfactant [81]. All of the above factors could also be the reason for no-ultra low IFT, however IFT is still quite low.

IFT of Armovis EHS also increases with increase in temperature. [65] has also used a viscoelastic surfactant for lowering the IFT and observed a similar kind of increase in IFT with increase in temperature. Effect of pressure on IFT has not been observed before in the

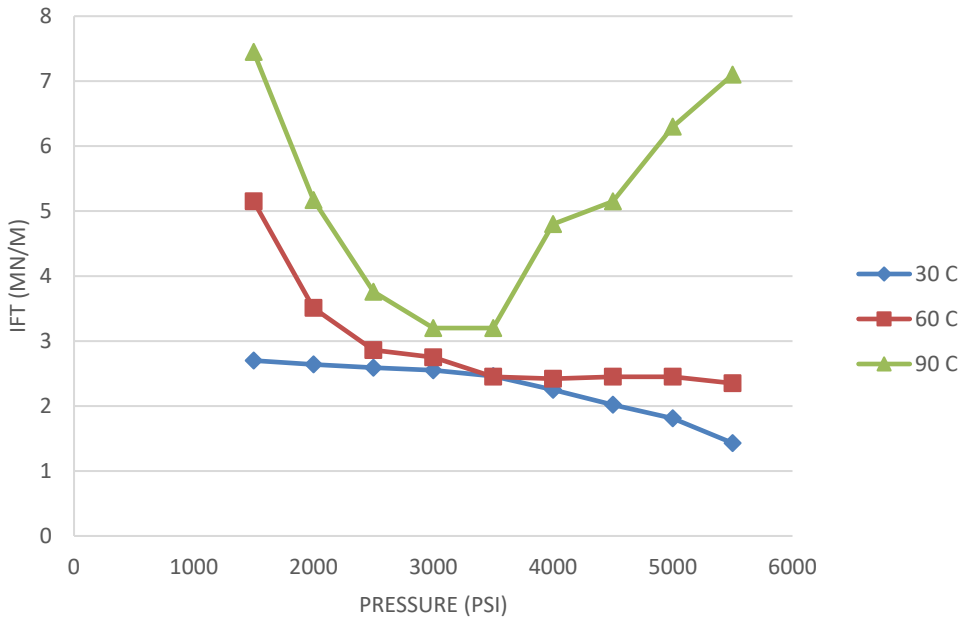

Figure 34: Interfacial tensions of BSS1 at different temperatures

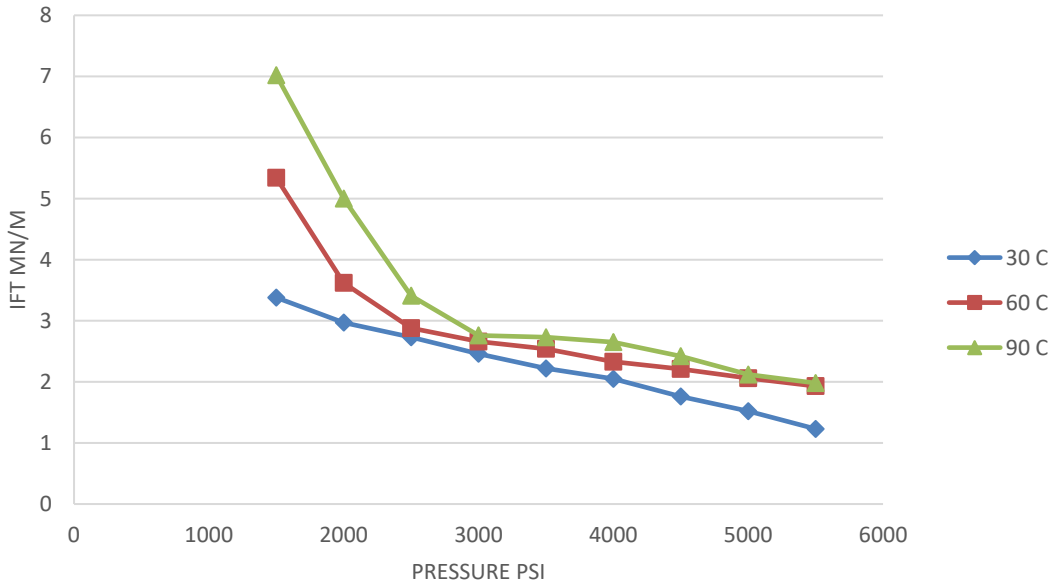

Figure 35: Interfacial tensions of BSS2 at different temperatures

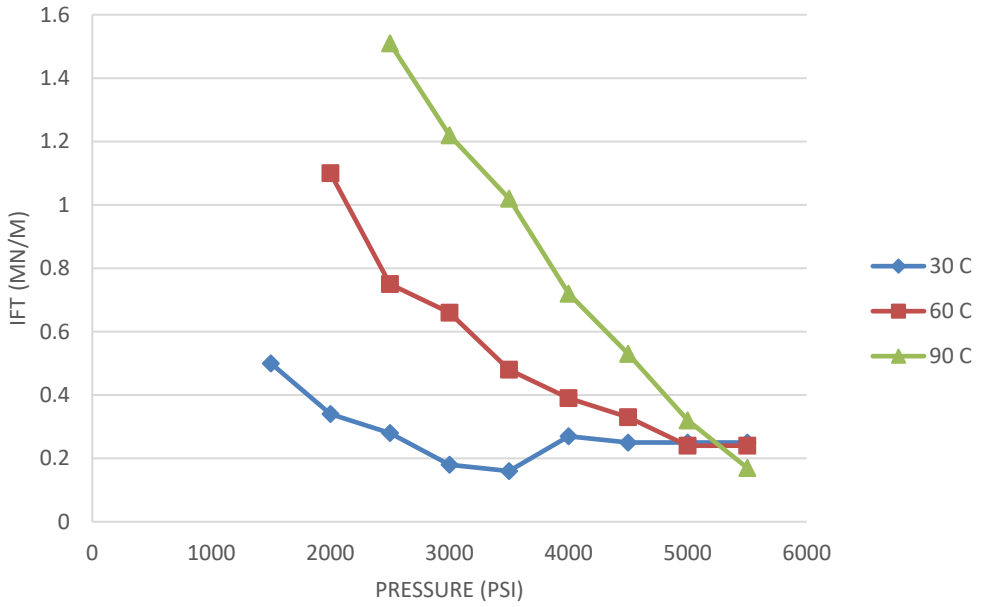

Figure 36: Interfacial tensions of BSS3 at different temperatures

literature. IFT decreases with increase in pressure at each temperature and this behavior is attributed to solubility.

For FS-50 (fluorosurfactant) ultra-low IFTs have been achieved. This makes it the best surfactant for this system and conditions. Also due to its lipophobicity, it is oil repellent and can be used to decrease IFT and wettability with oil systems.

IFT decreases with increase in pressure but increase with increase in temperature. However, at pressures 5000 and above, IFT becomes almost independent of pressures and temperatures. This point is the limit of solubility of CO_2 and Brine. From Figure 108 to Figure 116 it can be observed that drop becomes hazy with increase in pressure at all temperatures. This is due to increased solubility of CO_2 in brine and making emulsions with surfactant and at high pressure, no further emulsification is possible therefore IFT becomes constant and independent of pressure and temperature.

4.2.2.2 Effect of Surfactant type

From Figure 37 to Figure 39 it can be observed that IFT has been reduced to a very less value because of the use of surfactants as compared to simple brine without surfactants. This is because generally CO_2 is a poor solvent for both lipophilic and hydrophilic solutes [82] and surfactants can disperse these lipophilic or hydrophilic phases (which may both be considered CO2-phobic) into supercritical CO_2 in the form of micro-emulsion, emulsions and micelles [83] [39].

Because of very less polarizability and dielectric constants of CO_2, any CO_2-philic type of functional group in a surfactant will provide low energy-density. The ones with low cohesive densities and surface tensions are the most soluble [83]. Fluorosurfactants have given the ultra-low IFT because of their best suitability to the system. Although its boiling point is 82^{o}C for a pure surfactant, but when mixed as 0.15% in Brine it

performed very well at 90ºC. It has low surface tension of pure surfactant. Also its function is not affected by salinity.

4.2.2.3 Solubility of BSS and CO_2

Although what exactly governs solubility in CO_2 is not entirely clear but researchers have investigated the design of so-called "CO_2-phillic" surfactants that are soluble in CO_2 at moderate temperatures. K. Consan and R. Smith are notable authors who investigated almost 130 surfactants with CO_2 at 50ºC and pressures from 1500psi to 7250 psi [84]. They observed that commercially available surfactants exhibit low solubility in CO_2 however some fluorinated surfactants appreciably dissolve in CO_2.

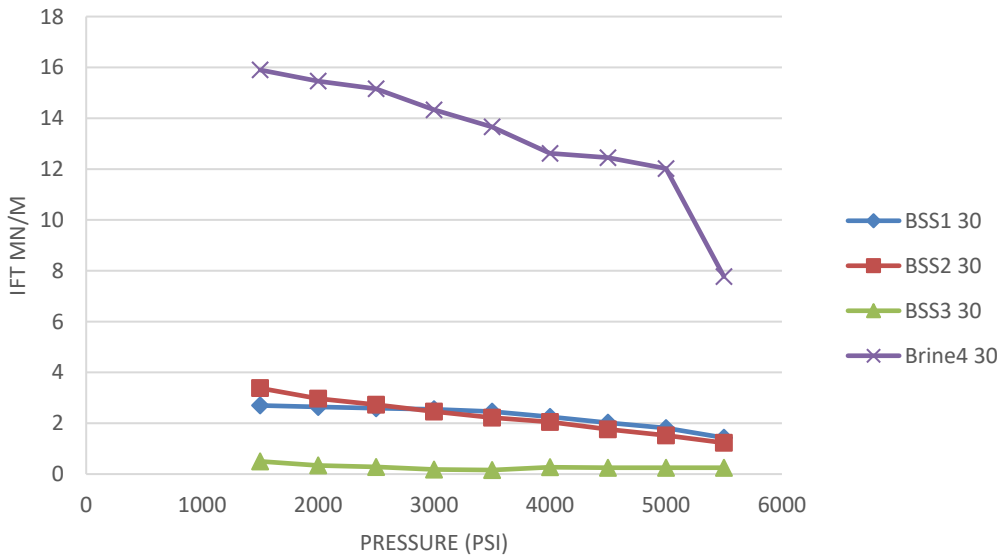

Figure 37: Interfacial tensions of Brine-Surfactant Solutions at 30ºC

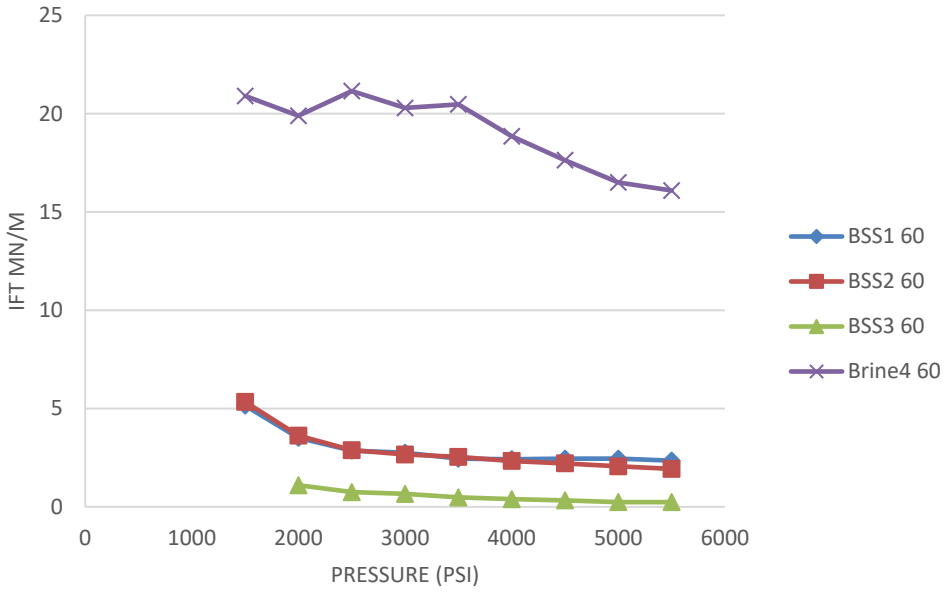

Figure 38: Interfacial tensions of Brine-Surfactant Solutions at 90°C

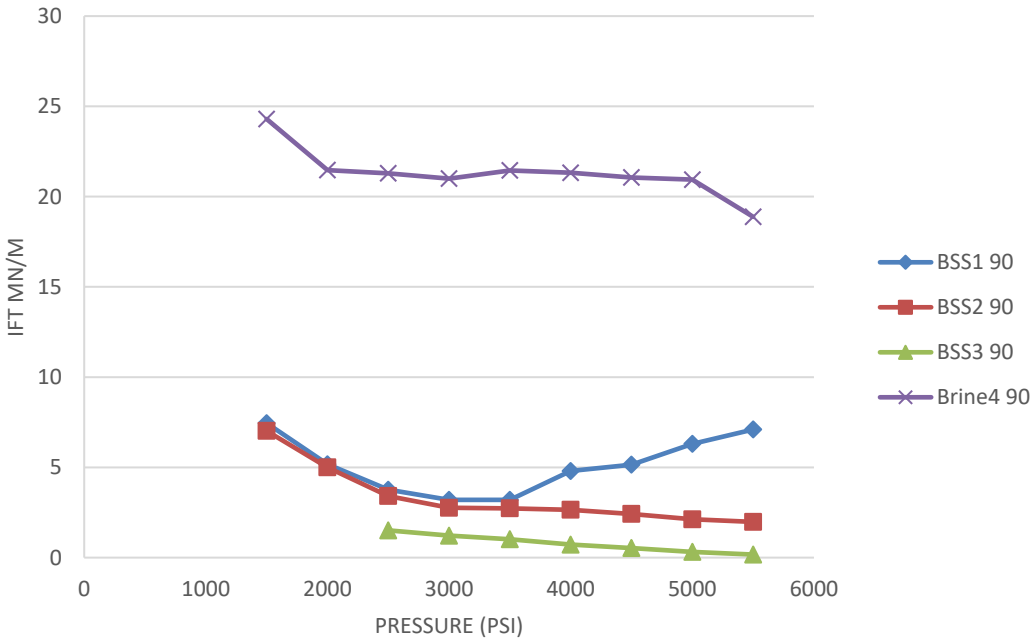

Figure 39: Interfacial tensions of Brine-Surfactant Solutions at 90°C

This work proves the same point that ultra-low IFT values have been obtained with fluorosurfactant FS-50 Solution.

If a substance is partially soluble, the formation of fog upon slight decompression is taken as evidence for some degree of solubility [84]. From Figure 108 to Figure 116, increase in pressure causes an increase in fog inside the bubble which explains the increase in solubility with pressure. Increase in solubility with increase in pressure is similar to the system of Brine-CO_2 mentioned earlier.

4.2.2.4 Effect of BSS-CO_2 density difference on IFT

From Figure 40 we can deduce that incase of BSS, IFT is depending on density difference making a trend similar to Figure 32 except for a few outliers.

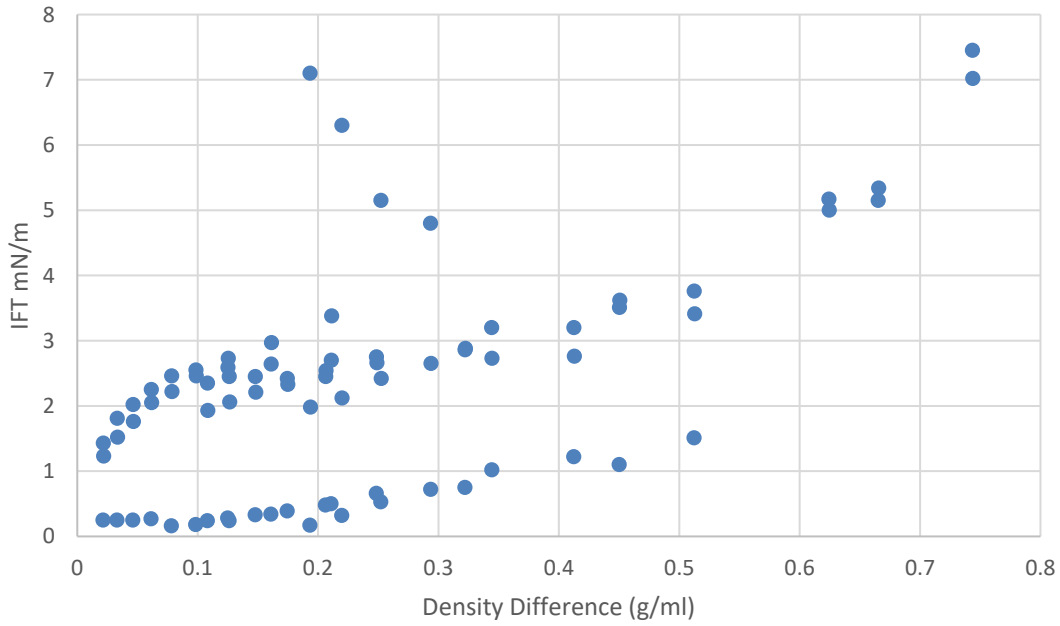

Figure 40: Trends of IFT with density difference for BSS

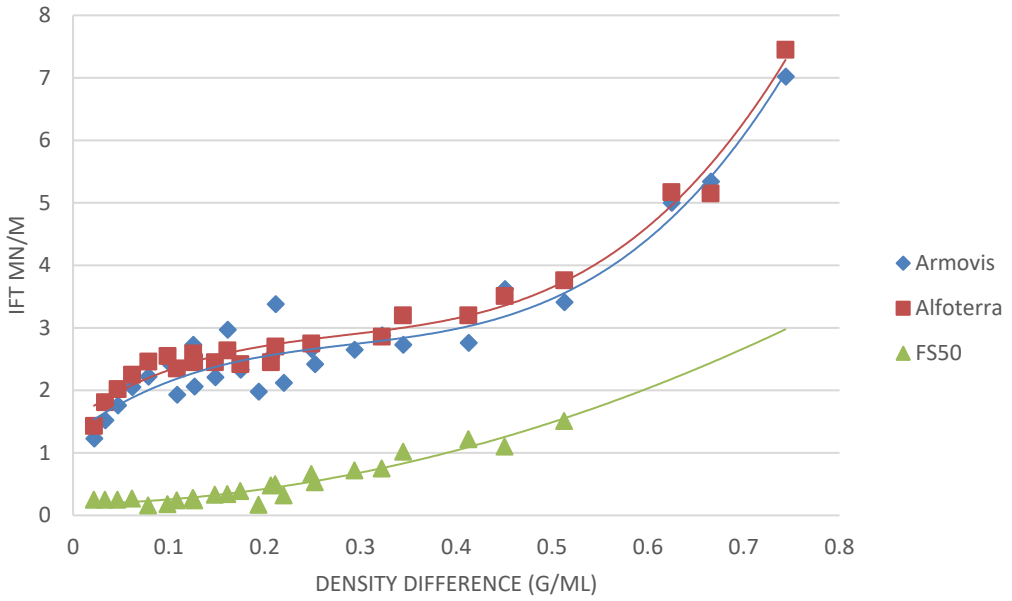

Figure 41: Effect of Density Difference on IFT for BSS

Since the outliers were due to decomposition of surfactant, we have excluded them in Figure 41. Since Armovis and Alfoterra are of similar chemical nature, they make a similar trend w.r.t to density difference. For density difference less than 0.2, there is a rapid linear increase in IFT with respect to density difference. Up till 0.6 the increase is gradual and afterwards the increase is linear again. This is the same trend that was observed for case of simple Brine-CO_2 systems (Figure 32). However, FS50 is a fluorosurfactant and the trend was found to be linear.

4.2.2.5 Determination of Minimum Miscibility Pressure

Minimum miscibility pressure is defined as the pressure at which no drop for IFT can be formed and IFT is therefore zero. This can be estimated by extrapolating the decreasing lines, on plot of pressure vs IFT, till x-intercept i.e. where y-axis value (IFT) becomes zero

However, in case of surfactant solutions, MMP cannot be properly determined because the surfactant is present in the system and a small change in pressure and temperature can have large influence on density and thus the solvent strength of CO_2 and BSS. Emulsion formation occurs inside the system which will be explained in detail in the next part of experiments with oil and the system undergoes a phase inversion and surfactant preference for either phase changes due to which IFT starts increasing instead of decreasing [39] which makes it impossible to predict the miscibility pressure.

4.2.2.6 Change of BSS-CO_2 IFT with time

The trend similar to Figure 33 for Brine holds for BSS-CO_2 system. Alfoterra takes more time to stabilize as compared to other two Brine-Surfactant solutions as shown in Appendix D. This is because Alfoterra is a fluid with density and viscosity higher than other two surfactants depicting strong intermolecular forces thereby taking more time to come to equilibrium.

4.2.3 Oils as drop fluids and CO_2 as a bulk fluid in the presence of BSS3

Since the lowest IFT has been shown by BSS3, our next experiments were carried out on this Brine-surfactant solution.

As mentioned in the previous chapter that some BSS3 drops (approx. 0.1 ml) were dropped inside the cell and CO_2 was filled and allowed to stabilize for some time at the desired temperature and pressure. Five oils were used one by one as drop fluids at one

temperature (60^{o}C) and nine different pressures. Their results have been shown in Figure 42 to **Error! Reference source not found.**.

4.2.3.1 Effect of Temperature and Pressure

In these experiments, at some pressures, the density of the bulk fluid (CO_2) became heavier than the density of drop fluid (oil) therefore the configuration of IFT equipment had to be inversed i.e. inverse pendant drop.

According to the literature and work done by Li et al. in 2012, for simple systems without surfactant, Interfacial tension decreases with increase in pressure [31].

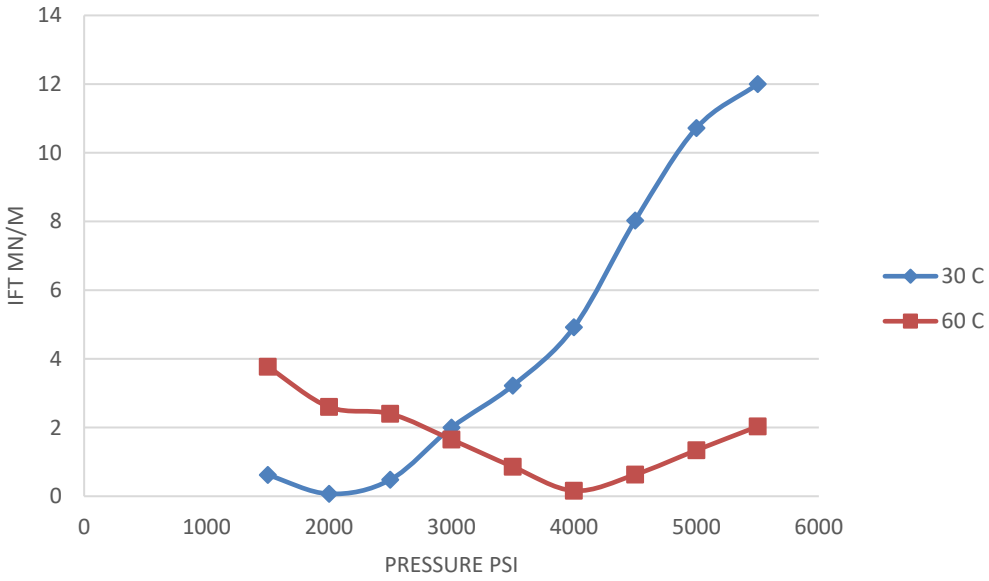

Figure 42: Crude oil 1 as a drop fluid at two temperatures

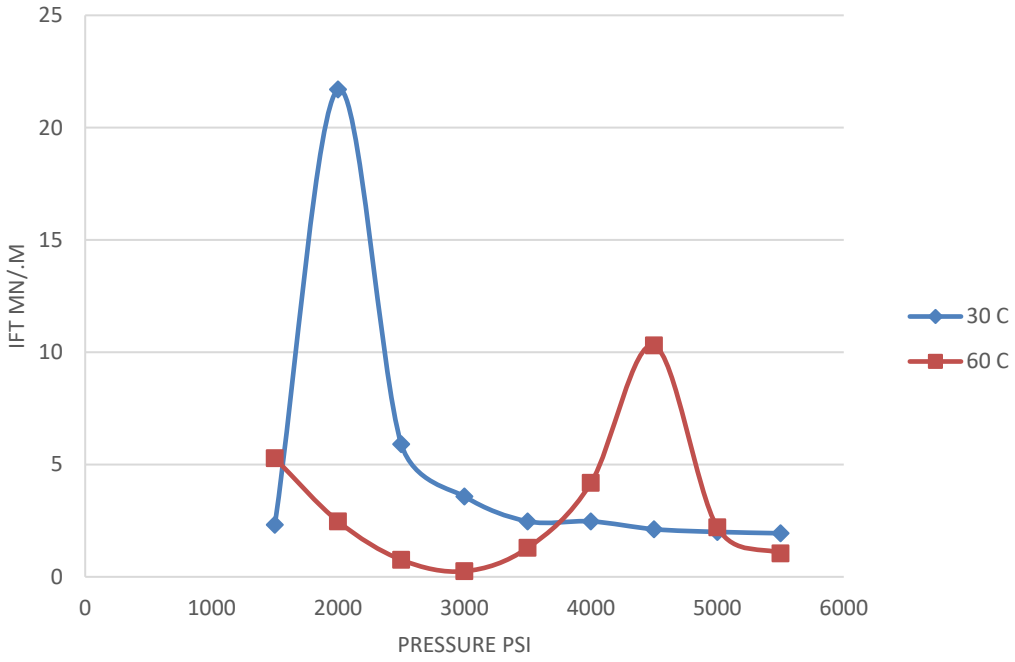

Figure 43: Interfacial tensions of Squalane at two temperatures

However the results in this work (Figure 42 and Figure 43) show that for Crude oil 1 Crude Oil IFT decreases till 2000 but then continues to increase with pressure. However, at 60^{o}C it decreases till 3500 psi and then increases. For Squalane which is a single component model oil, the IFT continues to decrease with pressure till 3000 psi at 60^{o}C. After 3000 till 4500, an increase is IFT is observed. After 3000 psi, CO_2 becomes denser than squalane however still the falls downwards until 4000 psi. At 4500 psi, the configuration of the equipment was changed and the drop was generated which resulted in very high IFT.

At 30^{o}C, only one experiment at 1500 psi could be performed in pendent drop configuration. Later all the values were taken with inverse pendant drop configuration

because of the density inversion, a high value of IFT was measured, just like the one at 4500psi at 60°C. Afterwards, IFT keeps decreasing with pressure.

The above results can be explained as the effect of formation of emulsion/micro-emulsion inside the cell due to surfactant. Shear causes oil fingers in water and water fingers in oil at the interface of which molecules of a surfactant are adsorbed. These fingers break up forming Oil/water and water/oil emulsions [40]. This same phenomenon is valid for supercritical CO_2 and Oil in presence of surfactants. [85] investigated the formation of emulsions, micro-emulsion, phase behavior and curvature for an oil/water micro-emulsion by plotting it on log of IFT. Da Rocha in 1999 summarized this kind of behavior for CO_2, water and surfactant systems in Figure 44 [39].

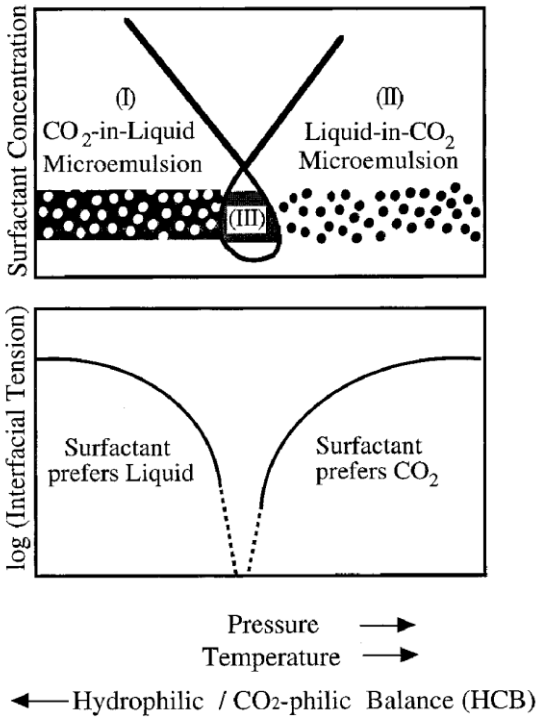

Figure 44: [39] Phase behavior in system of CO_2, H_2O and surfactant

Log (IFT) plots for Oil-CO_2 IFTs, in the presence of Brine-surfactant solution, have been shown from Figure 45 to Figure 48

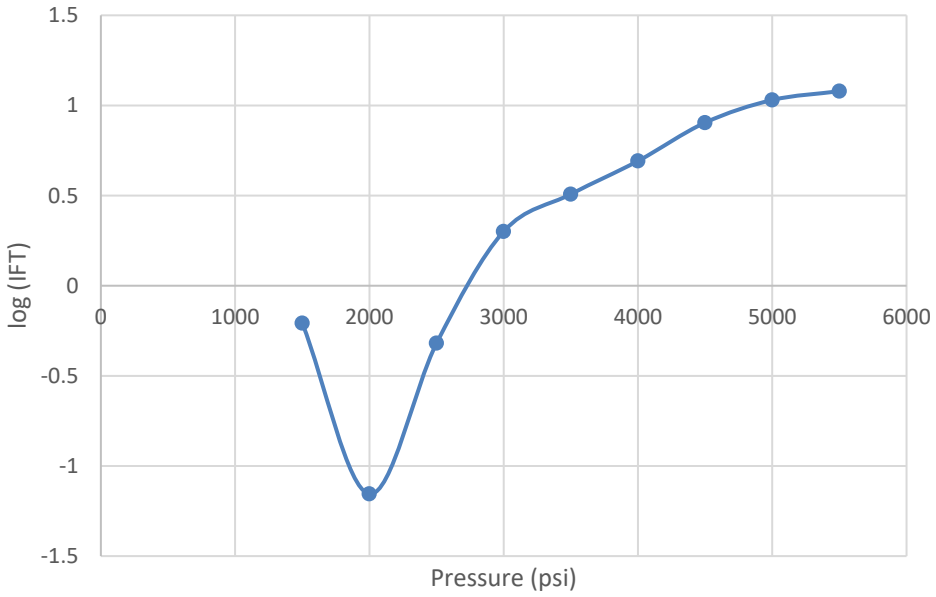

Figure 45: Log (IFT) vs Pressure for Crude oil 1 at 30ºC

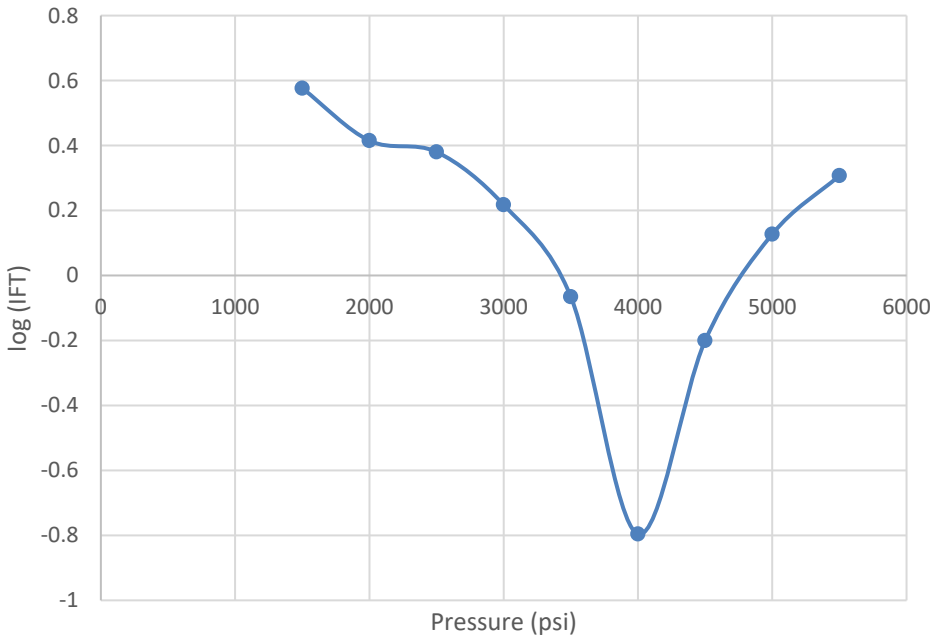

Figure 46: Log (IFT) vs Pressure for Crude oil 1 at 60ºC

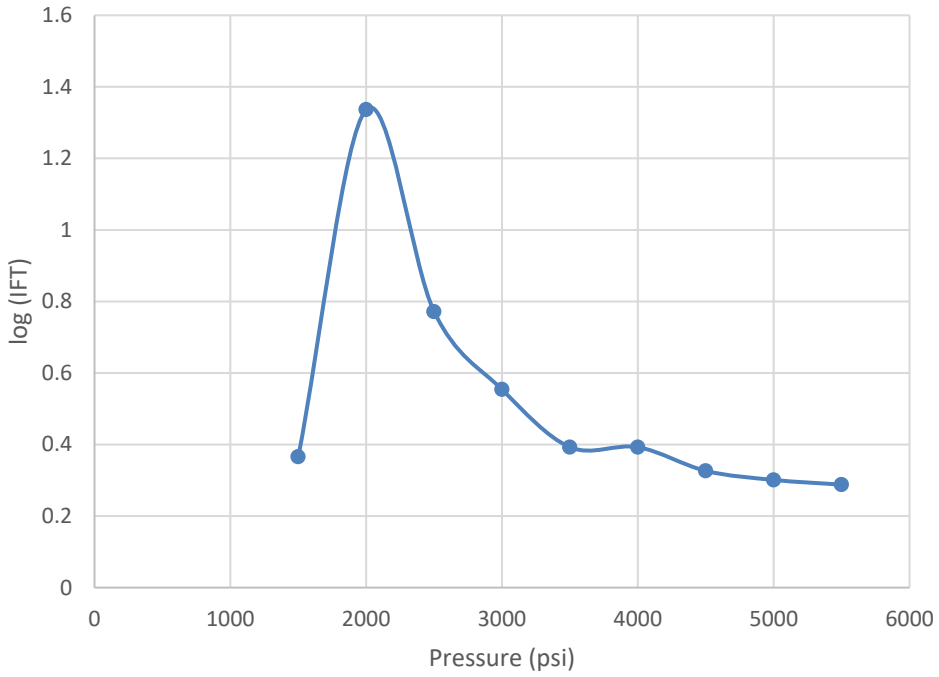

Figure 47: Log (IFT) vs Pressure for Squalane at 30ºC

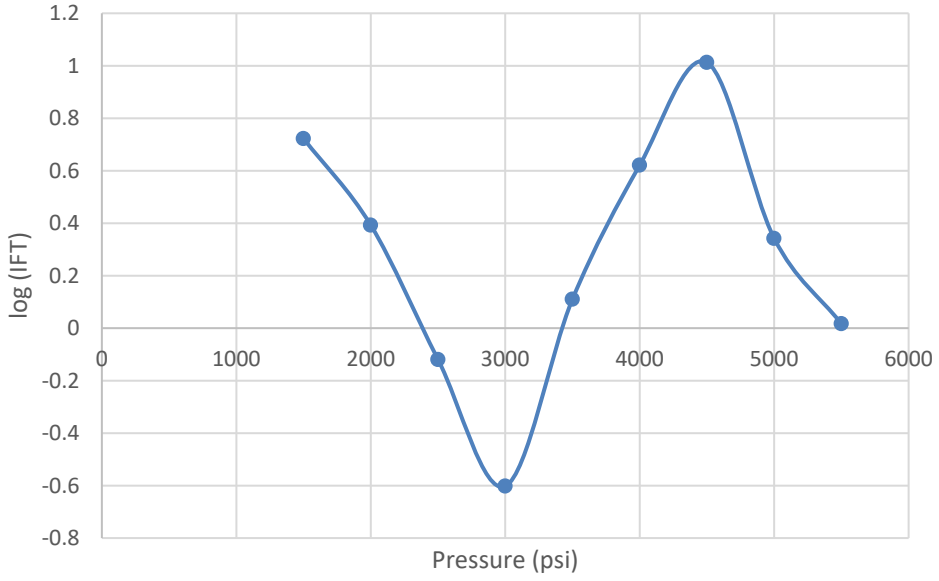

Figure 48: Log (IFT) vs Pressure for Squalane at 60ºC

The phase which contains most of the surfactant become the continuous phase while the other becomes dispersed phase for both micro emulsions and macro emulsions [40]. When the system is balanced w.r.t partitioning of the surfactant between both the phases, a minimum in IFT value is observed. This point is called phase inversion point and a change in any temperature, pressure (for compressible fluids) or hydrophilicity/hydrophobicity ratio (or in this case hydrophilic/CO_2-philic ratio) will cause the surfactant to migrate towards one of the phases [86].

This phase then becomes the external (continuous) phase [40][39]. During emulsification the droplets are deformed and/or broken. Then the surfactant approaches and adsorbs into deformed/broken newly formed droplets. The surfactant lowers the IFT and thus the Laplace pressure, thereby facilitating droplet breakup by reducing the energy required to break/deform the interface of the droplet [87].

Consider for Crude oil 1, increase in pressure is causing a shift from surfactant's preference for Oil (CO_2-in-liquid micro-emulsion) to surfactants preference for CO_2 (liquid-in- CO_2 micro-emulsion). However, the brine is also being emulsified inside CO_2 which is indicated by the fog inside the cell making it difficult to view. However, this Brine emulsion in not completely stable and disappears in 5 to 8 hours and the system was kept in this state prior to the first reading at 1500 psi for each of the two temperatures.

From Figure 49 at high temperature, the point of phase inversion/HCB (Hydrophilic-CO_2 philic Balance) point is delayed. This is in accordance with literature and previous

discussion that a small change in temperature can have a large influence on solvent strength of supercritical CO_2

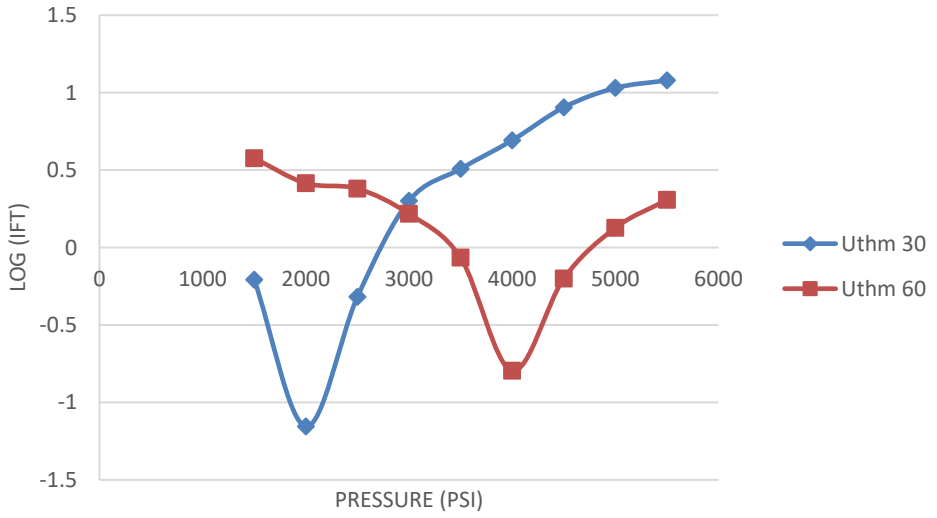

Figure 49: Effect of Temperature on Crude oil 1 for Log (IFT) vs pressure

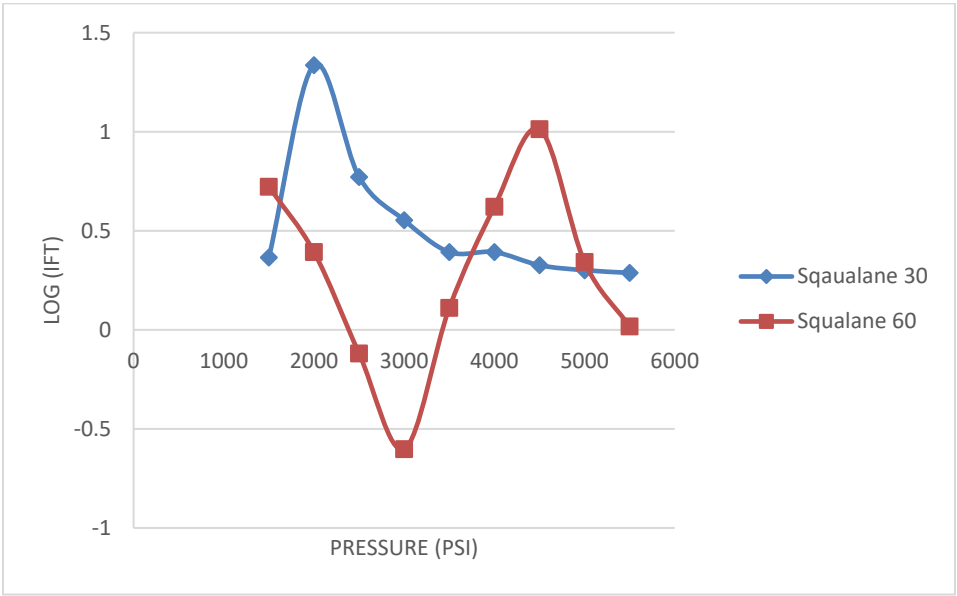

Figure 50: Effect of Temperature on Squalane for Log (IFT) vs pressure

. Since phase density has a big role in surfactant preference [39][86], increase in temperature is causing a change in density of the phase due to which surfactant changes its preference. At high temperature, the CO_2-in-liquid micro-emulsion is stronger for

quite higher pressures and phase inversion pressure (PIP) changes from 2000 psi to 4000 psi.

For Squalane, considering both Figure 47 and Figure 48, at 2000 psi, 30^{o}C and 4500 psi, 60^{o}C, the density configuration of the system has to be changed because at these pressure and temperature conditions, CO_2 became denser than and the Squalane drop rose upwards (Figure 117 and Figure 119). On these conditions, the IFT again starts to decrease but this time, no oil-in-CO_2 emulsion was formed in the system judging from the semi-log plot since the curvature in not following the decreasing downward slope. Rather the decrease is due to increase in pressure that causes an increase in the solubility of CO_2 and also due to the role of intermolecular forces. However the system still remained foggy (Figure 117 and Figure 119) which means that brine was being emulsified in CO_2 at 30^{o}C. But at 60^{o}C system remained clear.

The experiments could not be performed at 90^{o}C because, at this temperature, emulsification of Brine in CO_2 was quite high making the glass of the cell foggy therefore making it difficult to see the drop through the camera. Also some foam along with mist would accumulate on the glass. Only results of 30^{o}C and 60^{o}C could be shown in this work.

4.2.3.2 Effect of types of Oils

From the trends it is clear that we cannot generalize the outcome of IFT and neither can we consider one oil to be better candidate than the other. One is a crude oil, the other is a model oil. It all depends on the density of the oil, pressure, temperature and compositions of the oil

Squalane is soluble in CO_2 in the presence of surfactant at experimental conditions and values mentioned in this work are the ones at which Squalane drop was most stable.

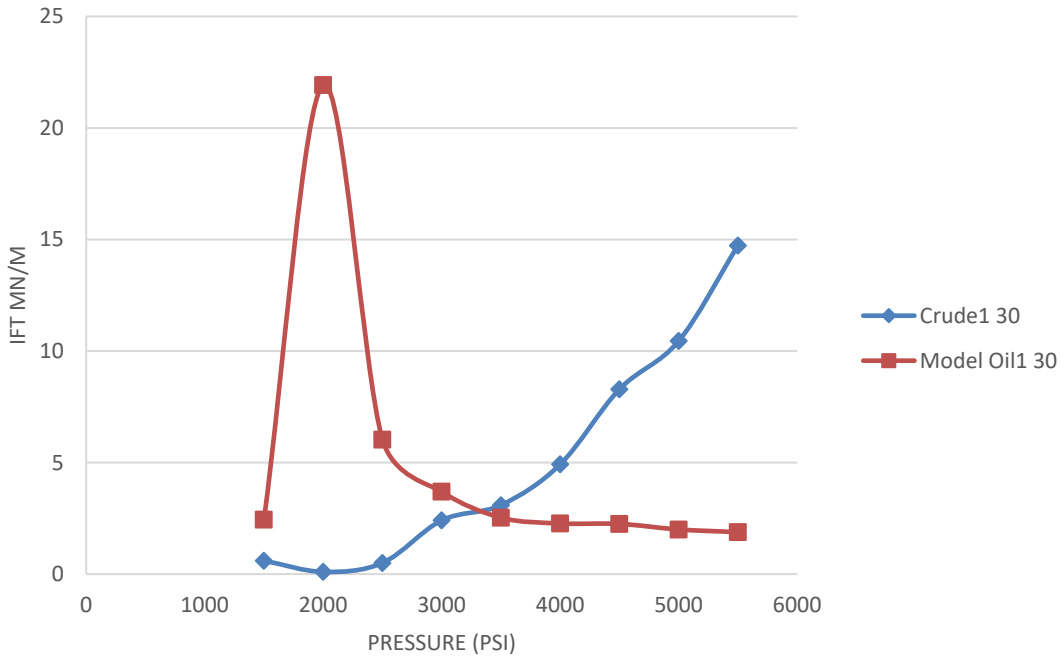

Figure 51: Interfacial tensions of Oils at 30°C

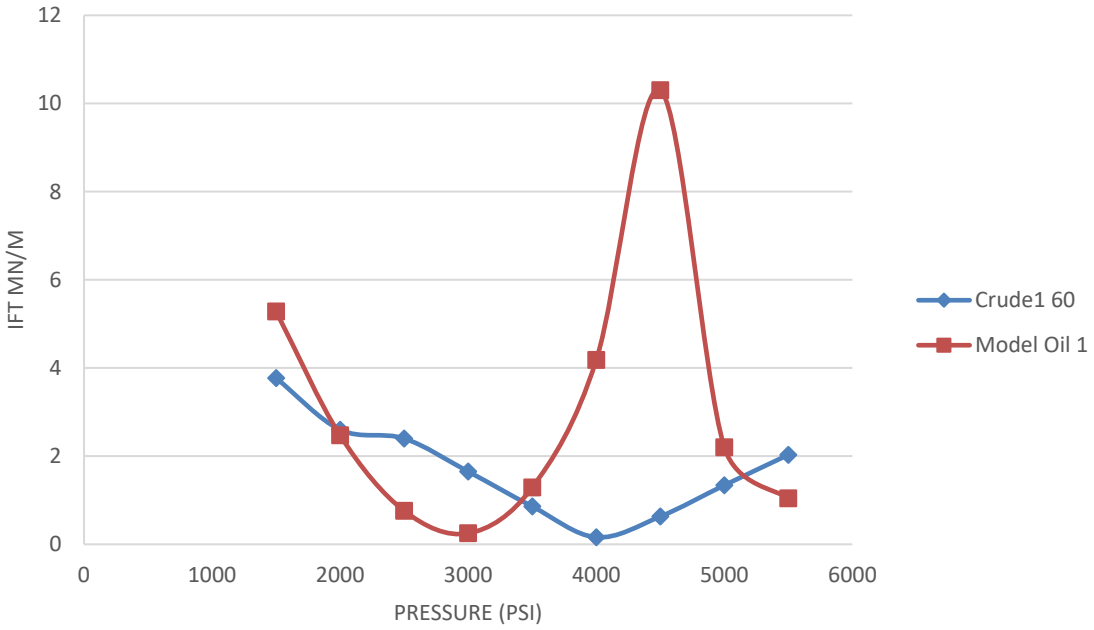

Figure 52: Interfacial Tensions of Oils at 60ºC

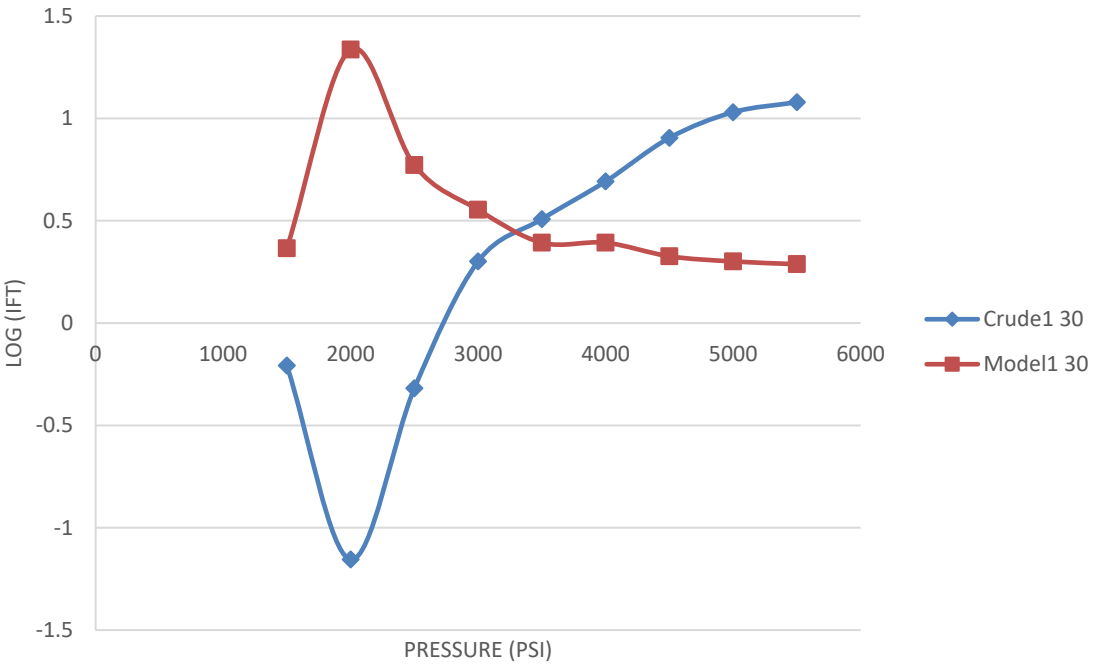

Figure 53: Log (IFT) vs Pressure for Oils at 30ºC

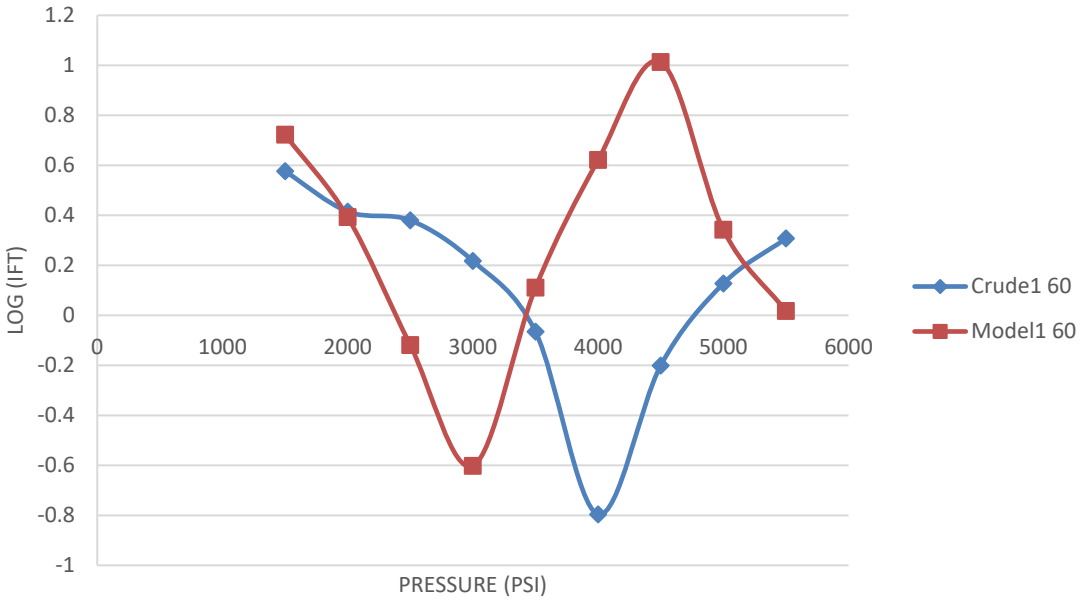

Figure 54: Log (IFT) vs Pressure for Oils at 60°C

Solubility of Squalane in CO_2 increases with increase in pressure therefore at high pressures, drop remains stable for very short period. Different readings were taken for the same point to get an average.

4.2.4 Experiments which were unsuccessful

Other oils that were used for IFT experiments but the results could not be generated have been mentioned below:

4.2.4.1 Toluene

This single model was very light and did not form a drop in CO_2 at either 30 or 60°C. It would become a gas and mix with CO_2.

4.2.4.2 Pentadecane

Pentadecane would produce a drop only at low pressures however higher values could not be taken. Since this same oil had to be used for contact angle and IFT experiment was not successful, therefore it wasn't used for contact angle experiments as well.

4.2.4.3 Crude Oil 2

This an API 40 crude oil of a Saudi Arabian field. During IFT experiments, the lighter components of the oil are highly soluble in CO_2 making it difficult to measure correct values of IFT (Figure 121). Since for Young-Laplace equation to be solved for IFT, the drop has to be perfectly in balance with the gravity, hanging itself. Therefore, IFT values could not be generated. However, contact angle values were measured with this oil.

Also there were other types of experiments that could not be performed were:

4.2.4.4 Use of (50% BSS3 and 50% CO_2) as Bulk Fluid

For this experiment, instead of few drops of BSS3, 10cc of cell was filled with BSS3 (since the whole cell has a capacity of 20cc). The remaining would be filled by CO_2. CO_2 does not have very high solubility for Brine even at very high temperatures and pressures. Therefore, the cell would remain half filled with liquid at all pressures, also a layer of foam would accumulate on the interface between CO_2 and BSS3. Therefore, if a drop was generated, it would be generated in the CO_2 portion of the cell but when the drop grown larger, it would touch the interface and therefore mix with it which would make it impossible for the DSA software and camera to distinguish between oil drop and the foam on the interface. Also BSS3 is heavier than Oil, therefore it would not allow the drop to enter the liquid region and therefore it distorted the drop shape of the oil.

4.2.4.5 Use of (CO_2+ Oil) as bulk fluids and BSS3 as drop fluids

Oil could not be used in the bulk phase as it would make whole of the cell and its glass "black" making it impossible to see through the camera. No experiment in the literature has been performed with crude oil as a bulk fluid for the same reason.

CHAPTER 5

RESULTS AND DISCUSSION OF CONTACT ANGLE EXPERIMENTS

Contact Angle is the measure of Wettability of a fluid with a rock surface. Higher the contact angle means lesser is the wettability and vice versa.

Wettability is an important parameter for Enhanced Oil recovery processes since the sole purpose of EOR is to decrease the residual oil saturation inside the reservoir. In case of Surfactant-Alternating-Gas (SAG) process, use of surfactant can not only decrease the interfacial tension of the fluids, but also decrease the wettability of the fluids. Experiments were performed where CO_2, Brine, Surfactant and Oil would coexist on a dolomite rock in order to study the wettability and the effect of pressure at a particular temperature (60^oC in our case).

The purpose of performing these experiments was to change the wettability of dolomite rock from oil wet to gas-wet. [88] first used the word gas-wetting in their work where they used two chemical to alter the wettability of rock from liquid wetting to gas-wetting. Fluorosurfactant has the ability to adsorb on the mineral surface for long-term wettability alteration.[89]

Before the start of actual experiments, three experiments with Squalane were performed on different rock surfaces to test the effect of surface polishing.

5.1 Test Experiments

Three experiments were performed to study the effect of polishing and saturating the rock surface.

5.1.1 Polishing with silicon epoxy, not saturated with oil

This experiment was performed where the rock disk was polished with silicon epoxy. Use of silicon epoxy completely sealed the porosity of the rock. Use of silicon epoxy has a disadvantage that it changes the composition of the rock by entering inside the pores and therefore the value for contact angle measurement will not be actual representative of dolomite.

5.1.2 Unpolished, unsaturated rock disk

Rock disk was not polished neither was it saturated with oil prior to performing the experiments in order to study the effect of adsorption of oil on contact angle.

5.1.3 Polished by grinding the surface, saturated with oil

Rock disk was polished by grinding machine using a specially fabricated holder. Later the prepared disk was kept dipped in a closed container containing oil (squalane). This container was kept in the oven at experimental conditions ($60^{o}C$) for 24 hours.

The results of above three experiments has been shown in **Error! Reference source not found.**. Because of least absorption, epoxy-polished gave higher contact angle values. The unsaturated and unpolished rock gave lowest because of high effects of absorption. The non-epoxy, polished and saturated rock disk's results were considered logical to be used for all experiments since saturated rock is representative of real rock situation and

polishing rock by merely grinding (not epoxy) makes the rock horizontal and smooth allowing for accurate measurement of contact angle.

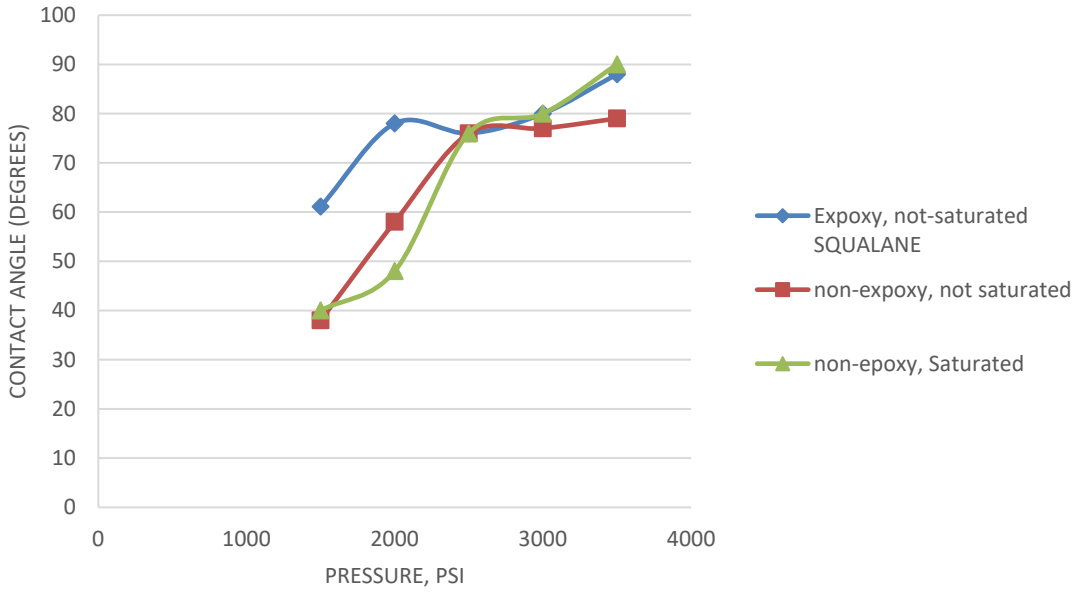

Figure 55: Results of Test CA Experiments with Squalane

According to the experimental plan in chapter 3, contact angle experiments of three different oils were performed with oils as drop fluids and CO_2 saturated with BSS3 as bulk fluid. The core disk used was Guelph Dolomite for all experiments.

5.2 Oil drop on Guelph Dolomite in the presence of CO_2 and BSS3

The decrease in oil wettability from Figure 56 to Figure 60 can be explained by the water and oil repellency of Fluorosurfactants because of its small Van der Waal's forces between fluorine and carbon atoms.

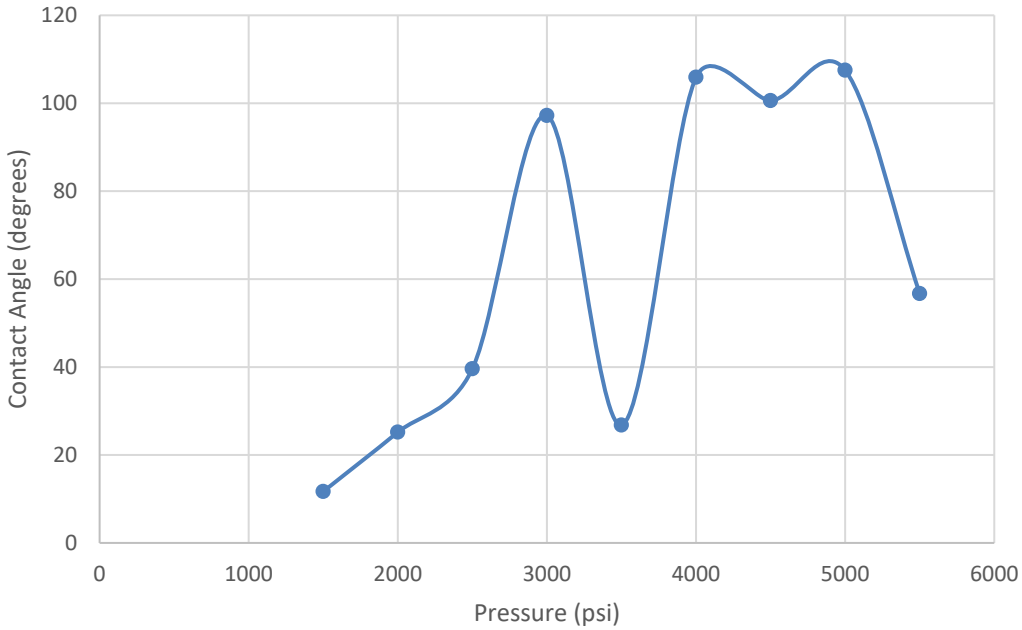

Figure 56: Contact Angle of Crude oil 1 at 60°C and different pressures

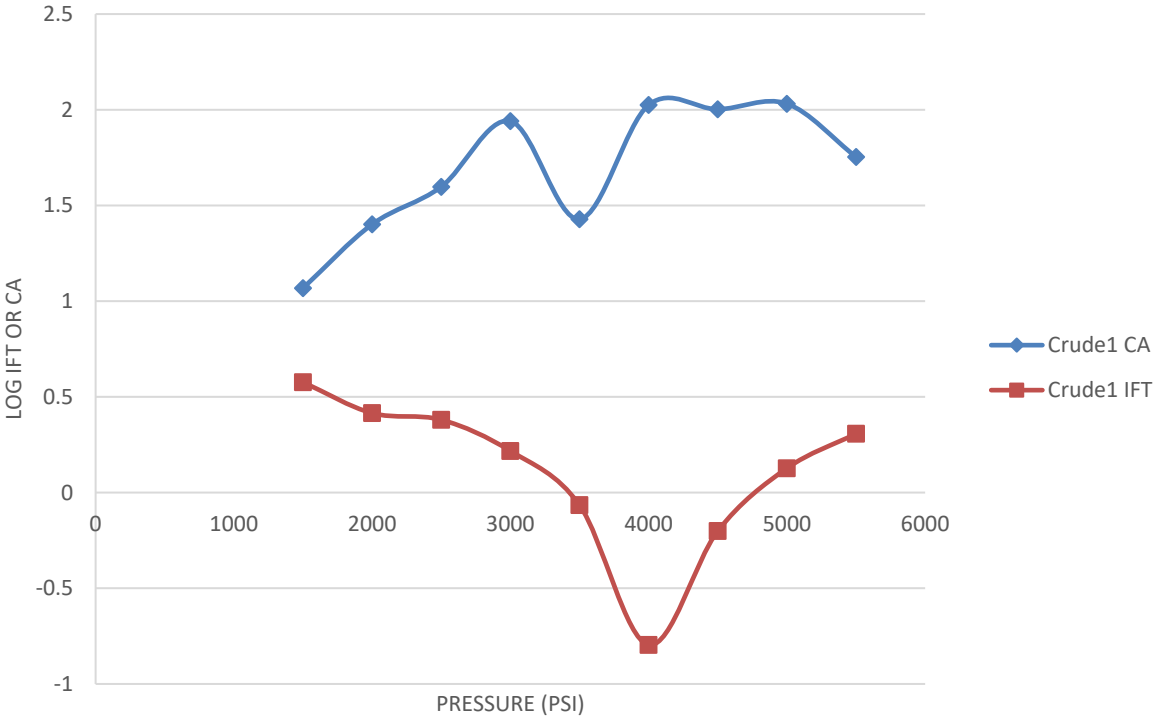

Figure 57: Semi-Log plot of both IFT and CA for Crude oil 1

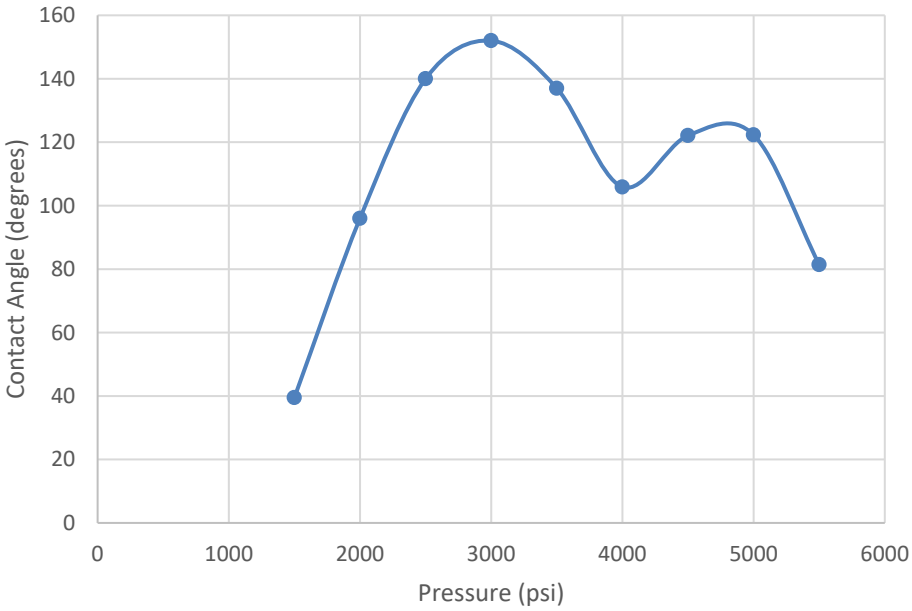

Figure 58: Contact Angle of Squalane Drop at 60°C at different pressures

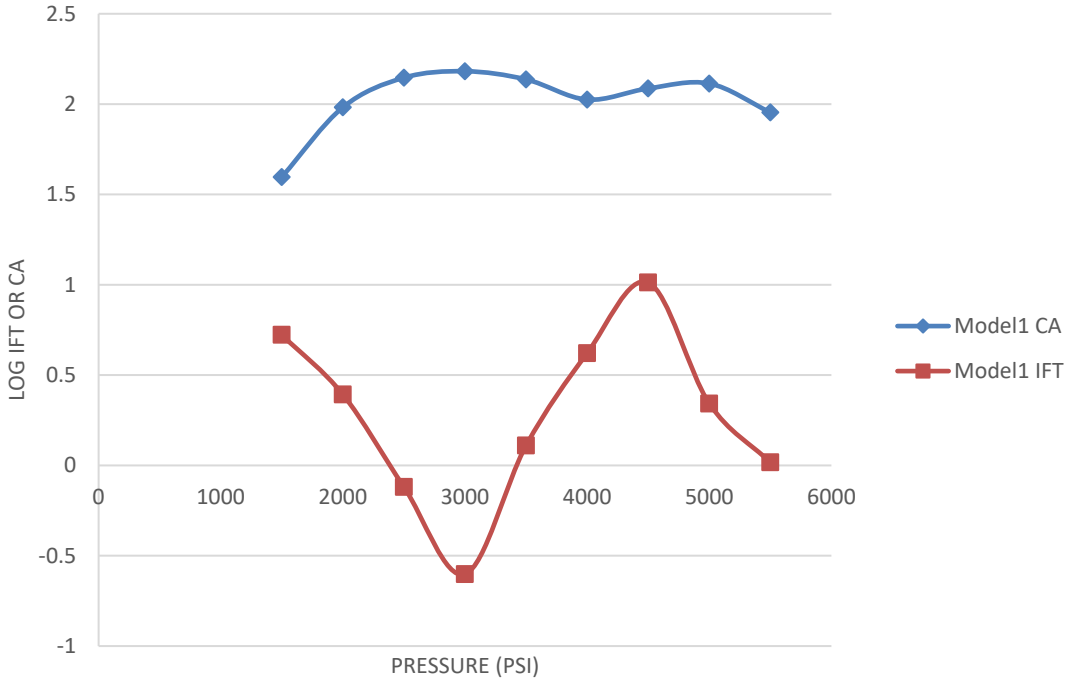

Figure 59: Semi-log Plot of both IFT and CA for Model Oil 1

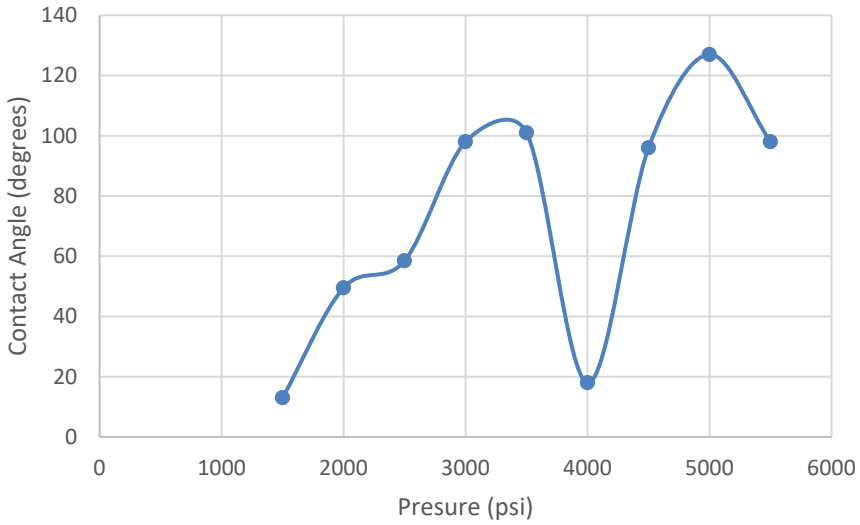

Figure 60: Contact Angle of Crude oil 2 at 60°C and different pressures

5.3 Comparison of All three oils (Crude oil 1, Arabian Light, Squalane)

Figure 61 and Figure 62 show the comparison of all the previously mentioned contact angle experiments on a single graph.

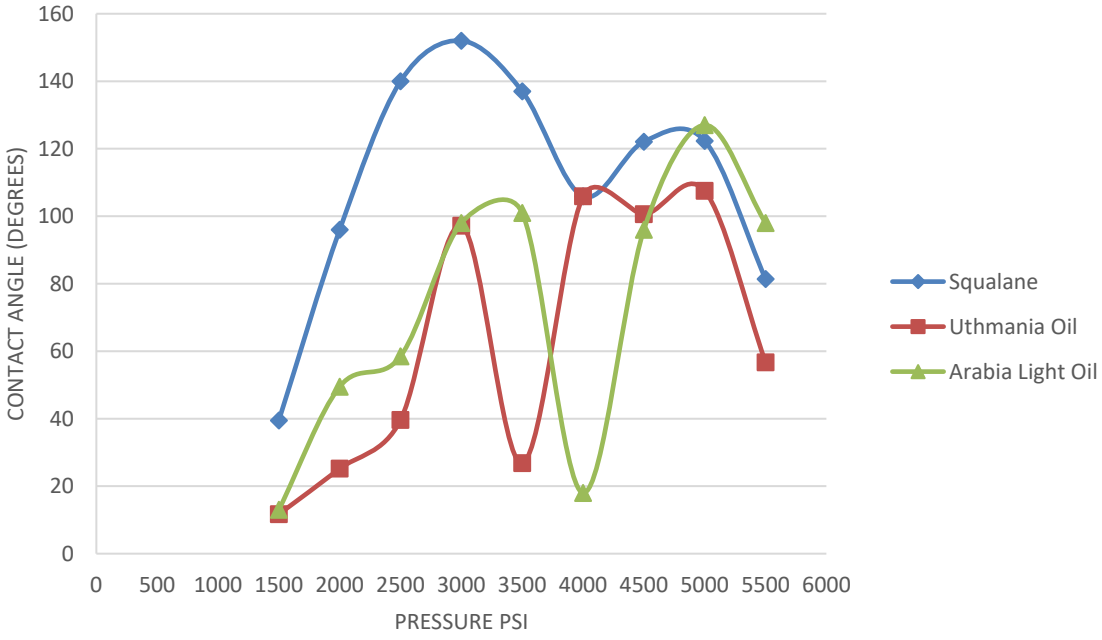

Figure 61: Contact Angles of Oils at 60°C at different pressures

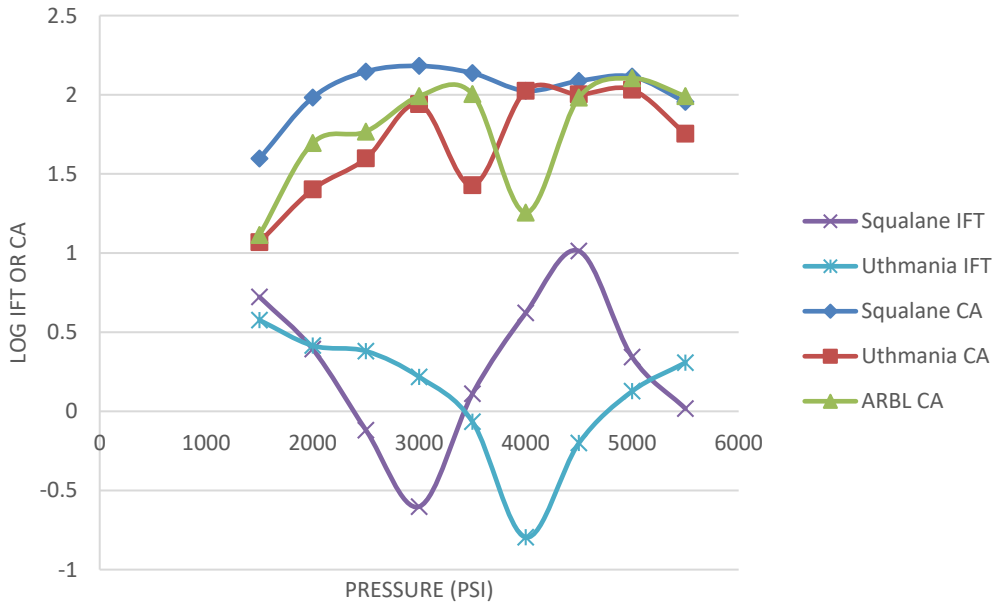

Figure 62: All Log plots of oils

Fluorine atoms had a very strong electronegativity of 4.0. On the contrary, fluorocarbon molecules were extremely resistant to oxidation because fluorine atoms, with an electronegativity of 4.0, were attached to their carbon atoms, thereby bringing the carbon atoms into a more oxidized state than that of those bound to the oxygen atoms of an electronegativity of 3.6. Halogens were generally strongly electronegative with high bond energy between carbon and fluorine (in particular) which had the strongest bond energy at 484 kJ/mol. Moreover, fluorine atoms were small in size (next to the smallest hydrogen atoms) and their van der Waals and covalent bond radii were larger than those of the hydrogen atoms by only 10%, or so. This rather small difference in size caused the hydrocarbon chains to have a zigzag structure and the fluorocarbon chains to have a rigid rod-like shape with a period of twist with 13 carbon atoms. In addition, the carbon

skeleton (within this rigid structure) was covered by densely packed fluorine atoms that were attached to the carbon atoms, much like a rod with a fluorine sheath on it. The protective action of the fluorine atoms is shown in Figure 63.

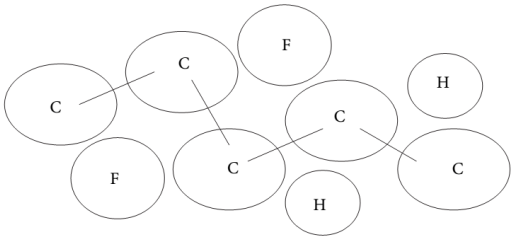

FIGURE 5: Protective action of fluorine atoms.

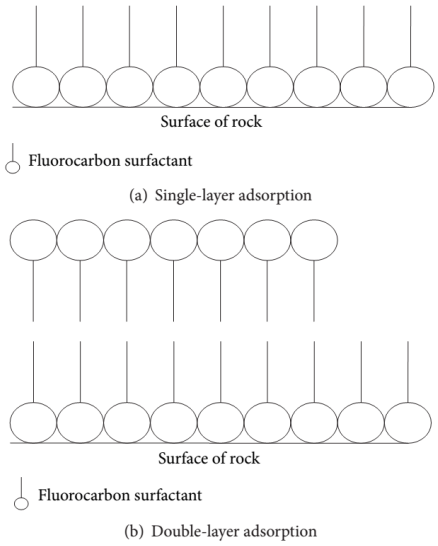

Figure 63: Adsorption of Fluorosurfactant on rock surface [90]

The nature of fluorine atom leads to the water and oil repellency characteristic of the Fluorosurfactants. Fluorine atom has the strongest electronegativity and the smallest atomic polarizability among the elements. Its atom radius is also smaller than other elements except for hydrogen. This enables the formation of a strong carbon-fluorine bond thereby forming the perfluoroalkyl group having weak intermolecular Van der Waals force and small interaction with other substances such as water and hydrocarbons.

Then, the surfaces of the disks get altered to gas-wetting because of the water and oil repellency characteristic of the fluorosurfactant.

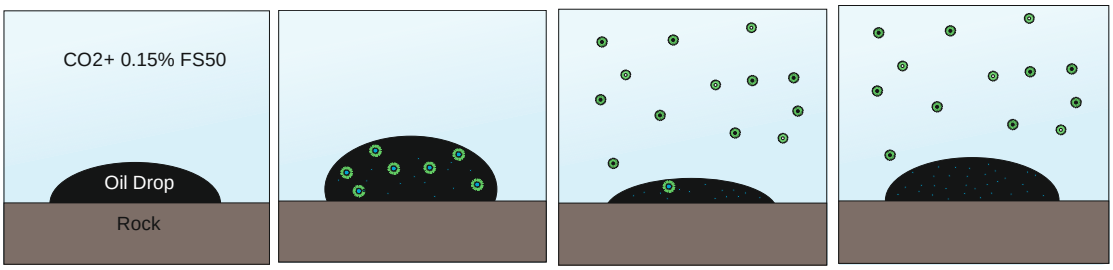

Figure 64: Formation of micro-emulsions explained graphically

However, between 3000 psi to 4000 psi, the CA would show a decrease i.e. the rock becomes oil wet. But a further increase in pressure causes the wettability to come back to its original trend of decreasing value i.e. increasing contact angle. This trend of sudden decrease is continuous in all kinds of oils; therefore, it is due either due to any property of CO_2 or the fluorosurfactant used. The explanation for similar behavior has been given by Wang et al. in 2013 that the cause of reduction in gas-wetting is due to double-layer adsorption of the fluorosurfactant (Figure 63) but this is valid if high surfactant/unoptimistic concentrations are used [90]. Since in our case the pressure of the system is causing a change, our surfactant is forming micro-emulsions inside the system and it is always close to the PIP (phase inversion pressure) which can observed from Figure 62 therefore the whole process can be explain graphically using Figure 64. For every pressure, a new drop was formed on a fresh surface and then allowed to stabilize for some time. Increase in pressure causes an increase in CA i.e. decrease in oil wettability. This is due to CO_2-in-oil micro-emulsions and also due to CO_2 being dissolved in the oil. However, as the system reaches the transition zone, the micro-

emulsions become unstable and start breaking until a certain point where oil-in-CO_2 and Brine-in-CO_2 micro-emulsions form. Contact angle then continues to increases with increase in pressure due to dissolved CO_2.

5.4 Correlation Based on Experimental Data Using Artificial Neural Network (ANN)

The above trends can be made into a correlation that depend on pressure, density and IFT.

$$CA_n = \left[\sum_{i=1}^{N} w_{2_i}\left(\frac{2}{1+e^{-2\left(w_{1_{i,1}} P_n + w_{1_{i,2}} IFT_n + w_{1_{i,3}}|\rho_{CO_2}-\rho_{Oil}|_n + b_{1_i}\right)}}\right)\right] + b_2$$

Where the w_1, w_2, b_1 and b_2 are the weight matrix of input layer, weight vector of hidden layer, bias vector of input layer and bias of hidden layer respectively.

i = Number of hidden layer neurons

N = Total number of neurons in hidden layer

b_1 = Bias vector for input layer

b_2 = Bias of hidden layer

n = Subscript ‘n’ shows normalized parameter

w_1 = Weight matrix of input layer

w_2 = Weight matrix of hidden layer

IFT = Interfacial tension (mN/m)

CA_n = Normalized output of the output layer

P = Pressure

$\rho_{CO_2} - \rho_{Oil}$ = Density diff of CO_2 and oil

This correlation was made using two of the five oils used (Crude Oil 1 and Model Oil) for CA and IFT measurements because IFT values of crude oil 2, model oil 2 and model oil 3 could not be obtained.

70% of data was used for training the ANN model and finding weights. It was then tested using 30% of the data. Figure 65 shows a plot between ANN Model data and Experimental results. Except for two points, the model shows good agreement with experimental data. Figure 66 is a similar plot for testing data of ANN model with experimental results which shows good agreement.

Both experimental values and values predicted from the model have been plotted in Figure 67 and Figure 68. The model can predict the rise and fall of contact angle but not all points could be accurately predicted. A lot more experimental data for oils is required at more ranges of pressure and temperature in order to decrease the error.

This correlation can be used for densities, pressures and IFTs lying in the range used in this work and at 60^{o}C.

Correlation buildup parameters have been mentioned in Appendix F. This correlation requires IFT, Density difference of the Bulk and drop fluids, and Pressure as input parameters to find Contact Angle on a surface of Dolomite. The results of correlation match with experimental data with 8.4% average error.

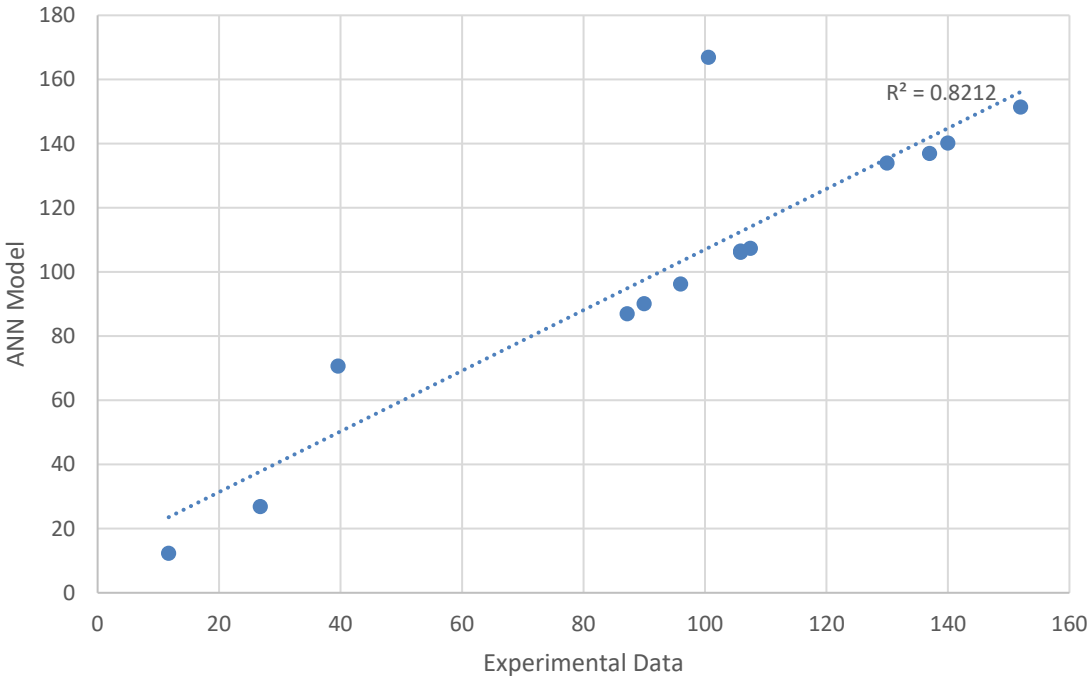

Figure 65: Comparison of training data for experimental and ANN Model results

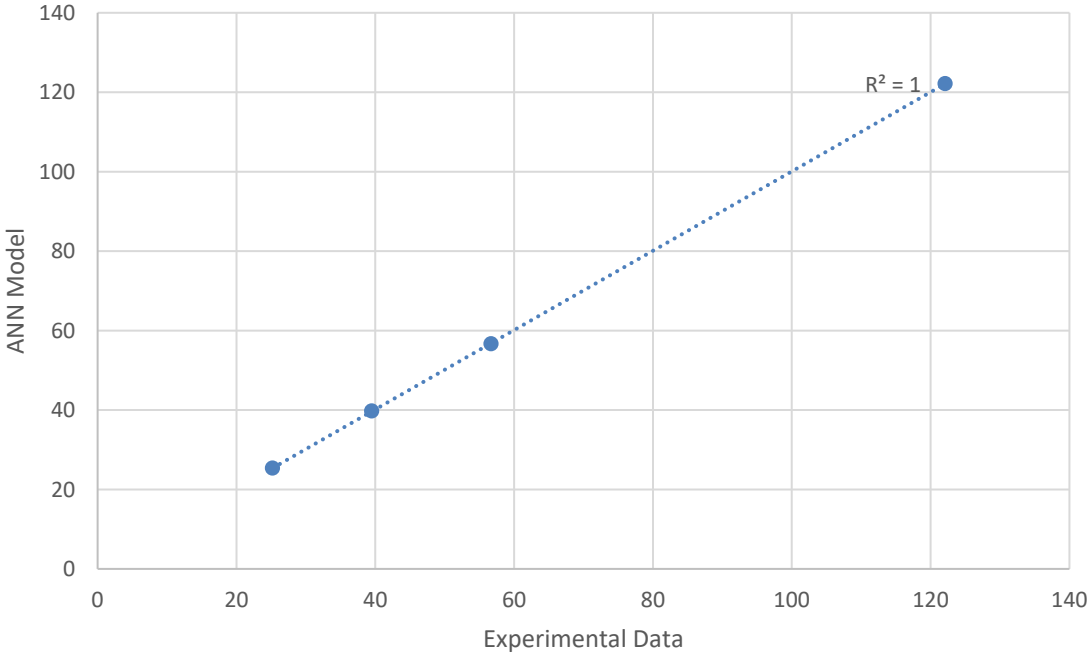

Figure 66: Comparison of Testing Data for experimental and ANN Model results

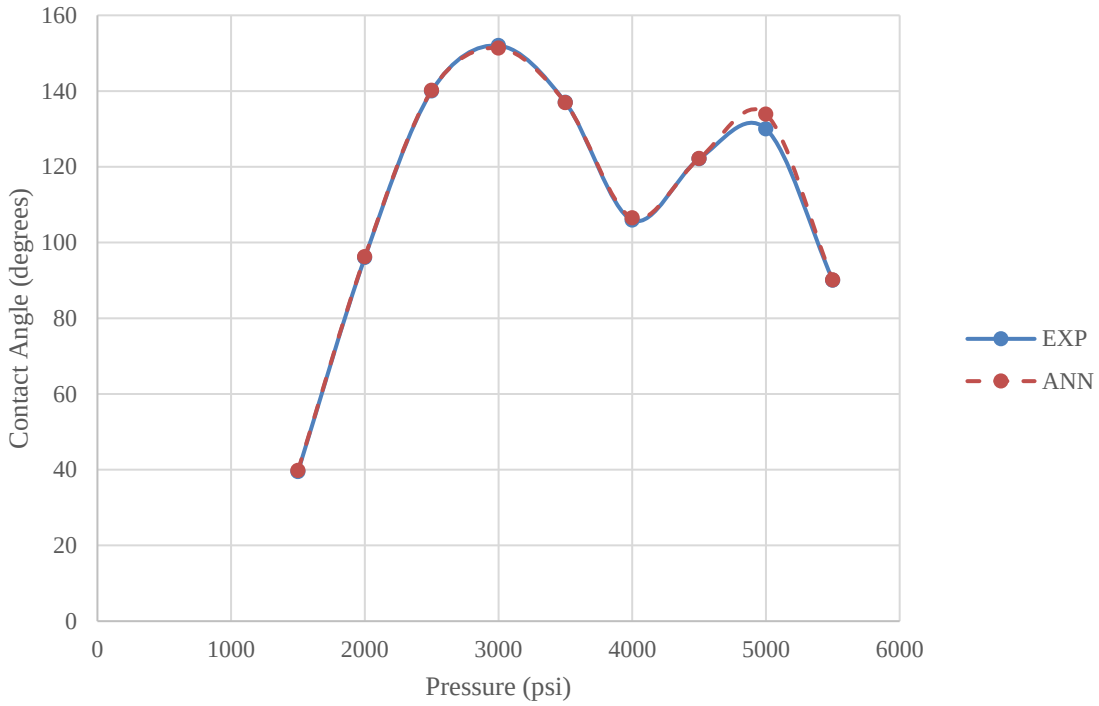

Figure 67: Plot of Model Oil1, Dotted: ANN Model, Line: Experimental

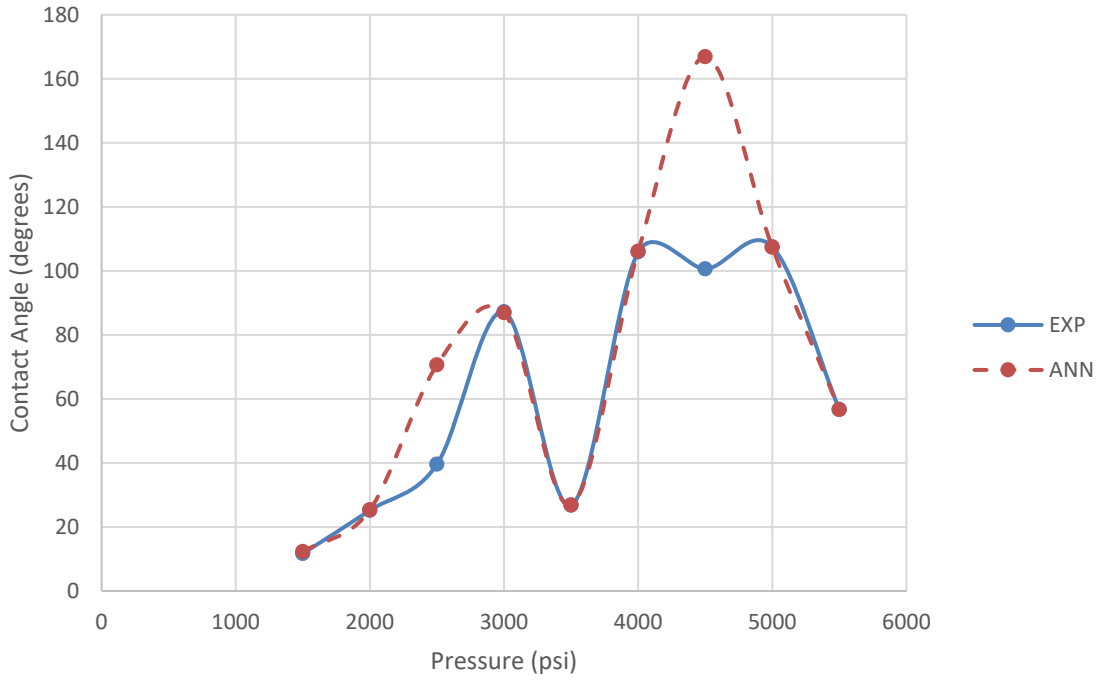

Figure 68: Plot of Crude Oil1, Dotted: ANN Model, Line: Experimental

5.5 Discussions

The ultimate objective of this thesis research was to understand the interfacial phenomenon of fluids which co-exist during (Surfactant-Alternating-Gas) processes. If the interfacial tension and contact angle could be reduced, high oil recovery by an EOR process can be achieved. The data set obtained from this experiment can also help understand the use of different surfactants during SAG processes.

Usually in Middle East, sea water can be easily utilized for injection during EOR process. This work explains how good it can be if sea water could be diluted to reduce the salinity to enhance the oil recovery. Also, Crude oil 1 and Crude oil 2 are two crude oils used in this work from Saudi Arabian oil field, both having different APIs to see the effect of Oil densities at interfacial level. Squalane is a model oil that has been used as a test case but however the trends lie matching the trends of crude oil therefore giving a good idea how multi or single component oils can behave in similar conditions.

Brine1 used was a recipe of sea water prepared in laboratory. It is a multi-component brine that behaved almost similar to other single component brines in the literature, however the values may be different. Effect of Brine salinity was observed by diluting this same brine with deionized water and then running experiments on them again. Effect of Pressures was measured every time on a new drop. Alfoterra and FS-50 behave almost similarly but FS-50 gives a much lower interfacial tension that is why FS-50 was considered for further experimental sets.

Interfacial tension experiments were performed on the following systems:

1. CO_2 and 4 types of Brines

2. CO_2 and Brine4 (lowest salinity) with 3 types of Surfactants

3. CO_2 (saturated with Brine4 Containing FS50) with 5 types of Oils but three were unsuccessful.

At 9 different pressures from 1500 to 5500 psi and 3 temperatures 30^oC, 60^oC and 90^oC.

Contact Angel experiments were performed on the following system:

1. CO_2 with 5 types of Oils in the presence of Brine Surfactant Solution (FS-50) (two were unsuccessful).

At 9 different pressures from 1500 to 5500 psi and at 60°C.

CHAPTER 6

CONCLUSIONS & RECOMMENDATIONS

6.1 Conclusions

The results from IFT experiments that were described in chapter 4 lead us to the following conclusions:

1- Density of Fluids increase with increase in temperature

2- At high salinity, IFT is independent of temperature.

3- Lesser the salinity, lesser will be the interfacial tension of the fluids

4- For brines and brine-surfactant solutions IFT decreases with increase in pressure

5- Higher the temperature, higher will be the IFT of Brines

6- Density difference can be used to generalize the behavior of IFT to some extent, for CO_2/Brine and CO_2/Brine/Surfactant Systems

7- IFT decreases with time, so best time to measure IFT is when both fluids come to an equilibrium

8- Drop Volume (solubility) increases with pressure and decreases with temperature

9- Alfoterra (alkyl ether sulfate surfactant) is not stable at temperatures higher than 60^{o}C

10- Armovis (viscoelastic) gives quite low IFT values but fluorosurfactant give ultra-low IFTs

11- The lowest IFT out of "Armovis EHS, Alfoterra and FS-50" was shown by FS-50

12- For Oil-surfactant Systems, pressure behavior cannot be generalized.

13- Increase in temperature causes a delay of emulsification for Oil, BSS and CO_2 Systems

14- The best surfactant to be used with CO_2 is a fluorosurfactant based on the results that it provided ultra-low IFT and high contact angles.

15- At high temperature, emulsification is thermodynamically stable and the glass of the cell becomes completely blurred making it difficult to see.

16- Fluorosurfactant caused formation of micro-emulsions inside the cell.

17- Surfactant preference change with both temperature and pressure.

18- Minor error close to the critical point of CO_2 can give large errors.

19- IFT Experiments performed with Toluene, Pentadecane and Crude oil 2 were unsuccessful because they were very light and could not generate drop properly in CO_2.

20- It was tried to use 50% CO_2 and 50% BSS3 in the cell as Bulk fluid however the experiment was unsuccessful because CO_2 does not have high solubility and the oil drop could not be distinguished in presence of a layer of foam on the interface of CO_2 and BSS3.

21- Oil cannot be used as a Bulk fluid because it makes the whole cell black making it impossible to see the drop from the camera.

The results from contact angle experiments that were described in chapter 4 lead us to the following conclusions:

1- Fluorosurfactant plays a critical role in decreasing wettability of oil in the presence of CO_2 and brine.

2- At any point close to PIP (Phase inversion pressure) the rock becomes oil wet because of the alignment of surfactant atoms due to which surfactant changes preference.

3- Increase in pressure causes increase in gas-wettability of dolomite rock only until certain high pressure.

4- There is a transition zone for CA measurements where the rock becomes oil-wet from gas wet. This transition zone for each oil depends on temperature and pressure conditions and is close to phase inversion pressure (PIP).

5- This trend of static contact angle has been used to develop simple correlation based on the data given from these experiments. This correlation depends on IFT, pressure and density difference of fluids at 60^{o}C within the range of this experimental data. It can be used with CO_2, florosurfactant, Oil and dolomite systems.

6- The given correlation has an average error of 8.4% for matching the experimental data ANN model.

6.2 Recommendations

1. Further study of IFT with oils of different asphaltenes percentage and aromatics in the presence of CO_2 and FS-50 is needed.
2. More pressure and temperatures ranges need to be studied for the Oil/Brine/Surfactant/CO2/Dolomite system for both IFT and CA analysis.
3. Effect of change in surfactant concentration on micro-emulsions needs to be studied.
4. Playing with head and tail of surfactant can reveal valuable information.
5. Effect of change in pH on all experiments in this work needs to be studied.

7- Molecular simulation of contact angle experiments is required to study how the thin-film layer near the surface of the rock would look like at various conditions.

8- Fluorosurfactant needs to be used together with hydrocarbon surfactants and/or chelating agents to study behavior with crude oils in the presence of brine and CO_2.

9- The stability of micro emulsions needs to be quantified.

APPENDICES

APPENDIX A: DENSITIES OF FLUIDS

DENSITY OF CO_2

Table 11: Densities of CO_2

Component	Temperature °C	Pressure (psi)	Density (g/ml)
CO_2	**30**	1500	0.77667175
		2000	0.828729
		2500	0.866511
		3000	0.8949703
		3500	0.91696535
		4000	0.9357096
		4500	0.85251825
		5000	0.9673425
		5500	0.98053015
	60	1500	0.31150215
		2000	0.5279362
		2500	0.65755525
		3000	0.732431
		3500	0.7759695
		4000	0.8090912
		4500	0.8368226
		5000	0.859714
		5500	0.87903995
	90	1500	2170464
		2000	0.3372952
		2500	0.450093125
		3000	0.55102535
		3500	0.620354575
		4000	0.6720366
		4500	0.7140962
		5000	0.747468
		5500	0.774614875

DENSITIES OF BRINES

Table 12: Densities of Brine 1

Concentration	Temperature °C	Pressure (psi)	Density (g/ml)
67708 ppm in Deionized Water	**30**	1500	1.03875
		2000	1.04025
		2500	1.04168
		3000	1.0431
		3500	1.0444
		4000	1.04578
		4500	1.04709
		5000	1.04836
		5500	1.04959
	60	1500	1.02599
		2000	1.02801
		2500	1.02893
		3000	1.02985
		3500	1.0307
		4000	1.03155
		4500	1.03236
		5000	1.0332
		5500	1.03405
	90	1500	1.01091
		2000	1.01155
		2500	1.01211
		3000	1.01262
		3500	1.01316
		4000	1.01365
		4500	1.01413
		5000	1.01461
		5500	1.01503

Table 13: Densities of Brine 2

Concentration	Temperature °C	Pressure (psi)	Density (g/ml)
33854 ppm	**30**	1500	1.00779
		2000	1.00958
		2500	1.01125
		3000	1.01295
		3500	1.0146
		4000	1.01619
		4500	1.01778
		5000	1.01931
		5500	1.0208
	60	1500	0.99649
		2000	0.99776
		2500	0.99897
		3000	1.00013
		3500	1.00128
		4000	1.00239
		4500	1.00346
		5000	1.00453
		5500	1.00554
	90	1500	0.98033
		2000	0.98119
		2500	0.98202
		3000	0.98287
		3500	0.98362
		4000	0.98435
		4500	0.98508
		5000	0.98579
		5500	0.98644

Table 14: Densities of Brine 3

Concentration	Temperature °C	Pressure	Density (g/ml)
16927 ppm	**30**	1500	0.99449
		2000	0.99642
		2500	0.9983
		3000	1.00009
		3500	1.00183
		4000	1.003555
		4500	1.00525
		5000	1.00687
		5500	1.00846
	60	1500	0.98352
		2000	0.98491
		2500	0.98625
		3000	0.98748
		3500	0.98876
		4000	0.98998
		4500	0.99115
		5000	0.99232
		5500	0.99342
	90	1500	0.96713
		2000	0.96818
		2500	0.96918
		3000	0.97012
		3500	0.97092
		4000	0.97181
		4500	0.97266
		5000	0.97346
		5500	0.97433

Table 15: Densities of Brine 4

Concentration	Temperature °C	Pressure	Density (g/ml)
8464 ppm	**30**	1500	0.98755
		2000	0.98953
		2500	0.99147
		3000	0.99334
		3500	0.99519
		4000	0.99696
		4500	0.99869
		5000	1.00038
		5500	1.00205
	60	1500	0.97671
		2000	0.97818
		2500	0.97955
		3000	0.98093
		3500	0.98222
		4000	0.98347
		4500	0.98473
		5000	0.98594
		5500	0.9871
	90	1500	0.96041
		2000	0.96151
		2500	0.96252
		3000	0.96355
		3500	0.9644
		4000	0.96538
		4500	0.96623
		5000	0.96714
		5500	0.96799

DENSITIES OF BRINE-SURFACTANT SOLUTIONS

Table 16: Densities of BSS2

Component	Temperature °C	Pressure (psi)	Density (g/ml)
Armovis (0.1 % in Brine4)	**30**	1500	0.98817
		2000	0.99018
		2500	0.9921
		3000	0.99397
		3500	0.99579
		4000	0.99762
		4500	0.99932
		5000	1.001
		5500	1.00266
	60	1500	0.97732
		2000	0.97877
		2500	0.98016
		3000	0.98151
		3500	0.98281
		4000	0.98406
		4500	0.98533
		5000	0.98652
		5500	0.98769
	90	1500	0.96099
		2000	0.96208
		2500	0.96303
		3000	0.96401
		3500	0.96499
		4000	0.96596
		4500	0.96676
		5000	0.96759
		5500	0.96846

Table 17: Densities of BSS1

Component	Temperature °C	Pressure (psi)	Density (g/ml)
Alfoterra (0.1% Constant Concentration)	**30**	1500	0.9879
		2000	0.98991
		2500	0.99181
		3000	0.99369
		3500	0.99551
		4000	0.99732
		4500	0.99905
		5000	1.00073
		5500	1.00238
	60	1500	0.97694
		2000	0.97842
		2500	0.97978
		3000	0.9811
		3500	0.98246
		4000	0.98371
		4500	0.98494
		5000	0.98615
		5500	0.9873
	90	1500	0.96068
		2000	0.96175
		2500	0.9627
		3000	0.9637
		3500	0.96466
		4000	0.9656
		4500	0.96647
		5000	0.96736
		5500	0.96818

Table 18: Densities of BSS3

Component	Temperature °C	Pressure (psi)	Density (g/ml)
FS-50 (Concentration: 0.15%)	**30**	1500	0.98756
		2000	0.98963
		2500	0.99158
		3000	0.99345
		3500	0.9953
		4000	0.99708
		4500	0.9988
		5000	1.00049
		5500	1.00213
	60	1500	0.97674
		2000	0.97821
		2500	0.97968
		3000	0.98097
		3500	0.98227
		4000	0.98357
		4500	0.98479
		5000	0.98602
		5500	0.98719
	90	1500	0.96054
		2000	0.96154
		2500	0.96257
		3000	0.96359
		3500	0.96483
		4000	0.96569
		4500	0.96637
		5000	0.96724
		5500	0.96804

DENSITIES OF OILS

Table 19: Densities of Crude oil 1

Component	Temperature °C	Pressure	Density (g/ml)
Crude oil 1	**30**	1500	0.81813
		2000	0.82203
		2500	0.82592
		3000	0.82957
		3500	0.83313
		4000	0.83656
		4500	0.83988
		5000	0.84314
		5500	0.84615
	60	1500	0.79682
		2000	0.80081
		2500	0.80459
		3000	0.80828
		3500	0.81174
		4000	0.81507
		4500	0.81834
		5000	0.8214
		5500	0.82439
	90	1500	0.77748
		2000	0.78152
		2500	0.78528
		3000	0.78892
		3500	0.79239
		4000	0.79568
		4500	0.79876
		5000	0.80179
		5500	0.80464

Table 20: Densities of Squalane

Component	Temperature °C	Pressure	Density (g/ml)
Squalane	**30**	1500	0.72237
		2000	0.72737
		2500	0.73193
		3000	0.72628
		3500	0.74055
		4000	0.74461
		4500	0.74855
		5000	0.75239
		5500	0.75612
	60	1500	0.70305
		2000	0.70769
		2500	0.7121
		3000	0.71638
		3500	0.72053
		4000	0.72454
		4500	0.72838
		5000	0.73203
		5500	0.73564
	90	1500	0.6854
		2000	0.6899
		2500	0.6944
		3000	0.69868
		3500	0.70278
		4000	0.70665
		4500	0.7104
		5000	0.71399
		5500	0.71746

Table 21: Densities of Crude oil 2

Component	Temperature °C	Pressure	Density (g/ml)
Crude oil 2	30	1500	0.74234
		2000	0.74717
		2500	0.75188
		3000	0.75635
		3500	0.76071
		4000	0.76492
		4500	0.76896
		5000	0.77286
		5500	0.77664
	60	1500	0.71996
		2000	0.72481
		2500	0.72956
		3000	0.7341
		3500	0.73845
		4000	0.74263
		4500	0.74662
		5000	0.75046
		5500	0.75415
	90	1500	0.69933
		2000	0.70442
		2500	0.70924
		3000	0.71384
		3500	0.7183
		4000	0.72239
		4500	0.72637
		5000	0.73016
		5500	0.73386

Table 22: Densities of Toluene

Component	Temperature °C	Pressure	Density (g/ml)
Toluene	30	1500	0.79506
		2000	0.79998
		2500	0.8047
		3000	0.80922
		3500	0.81358
		4000	0.81778
		4500	0.82018
		5000	0.82571
		5500	0.82947
	60	1500	0.76467
		2000	0.77001
		2500	0.7749
		3000	0.77966
		3500	0.78428
		4000	0.78862
		4500	0.79282
		5000	0.79675
		5500	0.80062
	90	1500	0.73556
		2000	0.74129
		2500	0.74667
		3000	0.75184
		3500	0.75665
		4000	0.76125
		4500	0.76558
		5000	0.76979
		5500	0.77376

Table 23: Densities of Pentadecane

Component	Temperature °C	Pressure	Density (g/ml)
Pentadecane	**30**	1500	0.676724
		2000	0.68157
		2500	0.68661
		3000	0.69152
		3500	0.69628
		4000	0.70083
		4500	0.70527
		5000	0.70956
		5500	0.71399
	60	1500	0.65516
		2000	0.6604
		2500	0.66548
		3000	0.67036
		3500	0.67508
		4000	0.6796
		4500	0.68396
		5000	0.68805
		5500	0.69219
	90	1500	0.63613
		2000	0.64154
		2500	0.64666
		3000	0.65153
		3500	0.6562
		4000	0.66069
		4500	0.66503
		5000	0.66908
		5500	0.67296

APPENDIX B: INTERFACIAL TENSION VALUES

BRINES 1, 2, 3 AND 4

Table 24: Interfacial Tensions of Brine1

Concentration	Temperature °C	Pressures, Psi	IFT (mN/m)
67708 ppm in Deionized Water	**30**	1500	31
		2000	27
		2500	25.6
		3000	21.2
		3500	21.1
		4000	23.7
		4500	23.5
		5000	23
		5500	21.8
	60	1500	21
		2000	27.4
		2500	27.09
		3000	26.17
		3500	25.12
		4000	25.6
		4500	25.5
		5000	26.2
		5500	24.7
	90	1500	31.5
		2000	24.2
		2500	24.9
		3000	23.5
		3500	25.1
		4000	24.5
		4500	22.1
		5000	23.4
		5500	22.4

Table 25: Interfacial Tensions of Brine2

Concentration	Temperature °C	Pressures, Psi	IFT (mN/m)
33854 ppm	**30**	1500	28
		2000	26.55
		2500	25.45
		3000	24.09
		3500	22.6
		4000	21.26
		4500	20.29
		5000	17.93
		5500	15.03
	60	1500	21.44
		2000	23.21
		2500	25.2
		3000	25.2
		3500	24.29
		4000	23.83
		4500	22.2
		5000	21.96
		5500	20.96
	90	1500	23.4
		2000	23
		2500	22.5
		3000	22.1
		3500	22
		4000	20.76
		4500	20.5
		5000	21
		5500	20.46

Table 26: Interfacial Tensions of Brine3

Concentration	Temperature °C	Pressures, Psi	IFT (mN/m)
16927 ppm	**30**	1500	18.55
		2000	17.77
		2500	15.9
		3000	15.68
		3500	13.72
		4000	14.19
		4500	16.08
		5000	13.5
		5500	10.29
	60	1500	17.43
		2000	21.17
		2500	21.35
		3000	21.18
		3500	21.11
		4000	20.53
		4500	20.58
		5000	20.62
		5500	20.15
	90	1500	25.5
		2000	22.2
		2500	21.74
		3000	21.08
		3500	21.8
		4000	21
		4500	21
		5000	20
		5500	20.5

Table 27: Interfacial Tensions of Brine4

Concentration	Temperature °C	Pressures, Psi	IFT (mN/m)
8464 ppm	**30**	1500	15.9
		2000	15.46
		2500	15.16
		3000	14.33
		3500	13.66
		4000	12.62
		4500	12.45
		5000	12.02
		5500	7.77
	60	1500	20.9
		2000	19.89
		2500	21.15
		3000	20.29
		3500	20.47
		4000	18.85
		4500	17.63
		5000	16.5
		5500	16.09
	90	1500	24.3
		2000	21.47
		2500	21.29
		3000	21
		3500	21.45
		4000	21.32
		4500	21.06
		5000	20.94
		5500	18.88

INTERFACIAL TENSIONS OF BRINE-SURFACTANT SOLUTIONS

Table 28: Interfacial Tensions of BSS 2

Surf-Soln	Temperature °C	Pressures, Psi	IFT
Armovis (0.1 % Constant Concentration)	**30**	1500	3.38
		2000	2.97
		2500	2.73
		3000	2.46
		3500	2.22
		4000	2.05
		4500	1.76
		5000	1.52
		5500	1.23
	60	1500	5.34
		2000	3.62
		2500	2.88
		3000	2.66
		3500	2.54
		4000	2.33
		4500	2.21
		5000	2.06
		5500	1.93
	90	1500	7.02
		2000	5
		2500	3.41
		3000	2.76
		3500	2.73
		4000	2.65
		4500	2.42
		5000	2.12
		5500	1.98

Table 29: Interfacial Tensions of BSS 1

Surf-Soln	Temperature °C	Pressures, Psi	IFT (mN/m)
Alfotera (0.1% Constant Concentration)	**30**	1500	2.7
		2000	2.64
		2500	2.59
		3000	2.55
		3500	2.46
		4000	2.25
		4500	2.02
		5000	1.81
		5500	1.43
	60	1500	5.15
		2000	3.51
		2500	2.86
		3000	2.75
		3500	2.45
		4000	2.42
		4500	2.45
		5000	2.45
		5500	2.35
	90	1500	7.45
		2000	5.17
		2500	3.76
		3000	3.2
		3500	3.2
		4000	4.8
		4500	5.15
		5000	6.3
		5500	7.1

Table 30: Interfacial Tensions of BSS 3

Surf-Soln	Temperature °C	Pressures, Psi	IFT (mN/m)
FS-50 (Concentration: 0.15%)	**30**	1500	0.5
		2000	0.34
		2500	0.28
		3000	0.18
		3500	0.16
		4000	0.27
		4500	0.25
		5000	0.25
		5500	0.25
	60	1500	Unstable drop
		2000	1.1
		2500	0.75
		3000	0.66
		3500	0.48
		4000	0.39
		4500	0.33
		5000	0.24
		5500	0.24
	90	1500	Unstable drop
		2000	Unstable drop
		2500	1.51
		3000	1.22
		3500	1.02
		4000	0.72
		4500	0.53
		5000	0.32
		5500	0.17

INTERFACIAL TENSIONS OF OILS IN PRESENCE OF CO_2-BSS3

Table 31: Interfacial Tensions of Crude oil 1

Oil	Temperature °C	Pressures, Psi	IFT
Crude oil 1	**30**	1500	0.62
		2000	0.07
		2500	0.48
		3000	2
		3500	3.22
		4000	4.92
		4500	8.03
		5000	10.72
		5500	12
	60	1500	3.77
		2000	2.6
		2500	2.4
		3000	1.65
		3500	0.86
		4000	0.16
		4500	0.63
		5000	1.34
		5500	2.03

Table 32: Interfacial Tensions of Squalane

Oil	Temperature °C	Pressures, Psi	IFT
Squalane	**30**	1500	2.32
		2000	21.7
		2500	5.91
		3000	3.58
		3500	2.47
		4000	2.47
		4500	2.12
		5000	2
		5500	1.94
	60	1500	5.28
		2000	2.47
		2500	0.76
		3000	0.25
		3500	1.29
		4000	4.18
		4500	10.3
		5000	2.2
		5500	1.04

APPENDIX C: CONTACT ANGLE VALUES

CONTACT ANGLES OF OILS IN THE PRESENCE OF CO_2-BSS3

Table 33: Contact Angles of Crude oil 1

Oil Type	Temperature °C	Pressure (psi)	Contact Angle (degrees)
Crude oil 1	60	1500	11.7
		2000	25.2
		2500	39.6
		3000	97.2
		3500	26.8
		4000	105.9
		4500	100.6
		5000	107.5
		5500	56.7

Table 34: Contact Angles of Squalane

Oil Type	Temperature °C	Pressure (psi)	Contact Angle (degrees)
Squalane	60	1500	39.5
		2000	96
		2500	140
		3000	152
		3500	137
		4000	105.9
		4500	122.1
		5000	122.3
		5500	81.4

Table 35: Contact Angles of Crude oil 2

Oil Type	Temperature °C	Pressure (psi)	Contact Angle (degrees)
Crude oil 2	60	1500	13
		2000	49.5
		2500	58.5
		3000	98
		3500	101
		4000	18
		4500	96
		5000	127
		5500	98

APPENDIX D: INTERFACIAL TENSIONS AS FUNCTION OF TIME AT DIFFERENT PRESSURES AND CONSTANT TEMPERATURES

At 30°C

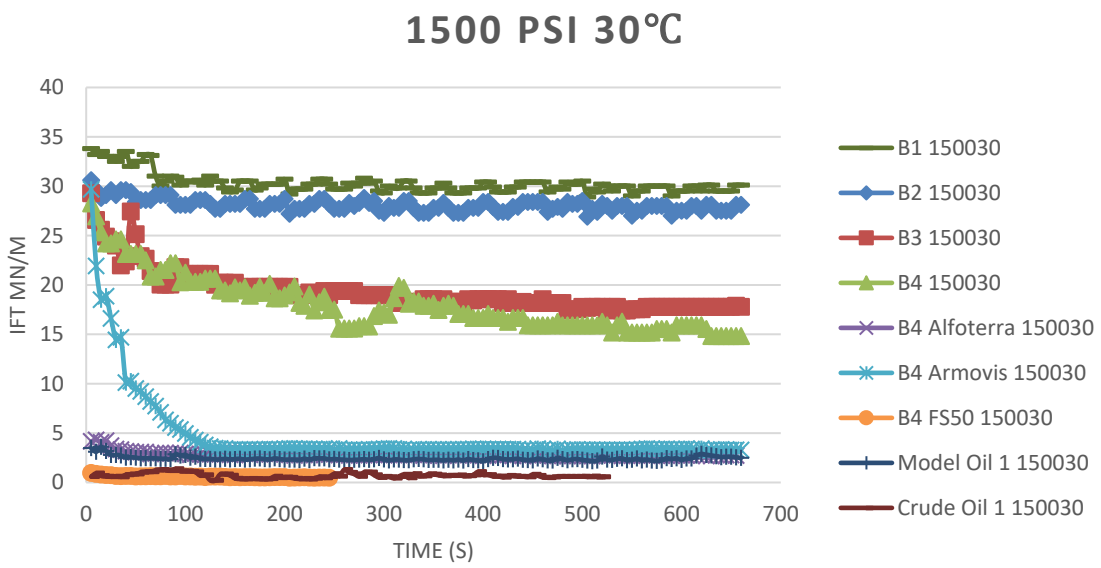

Figure 69: Interfacial Tensions as function of time at 30°C and 1500 Psi

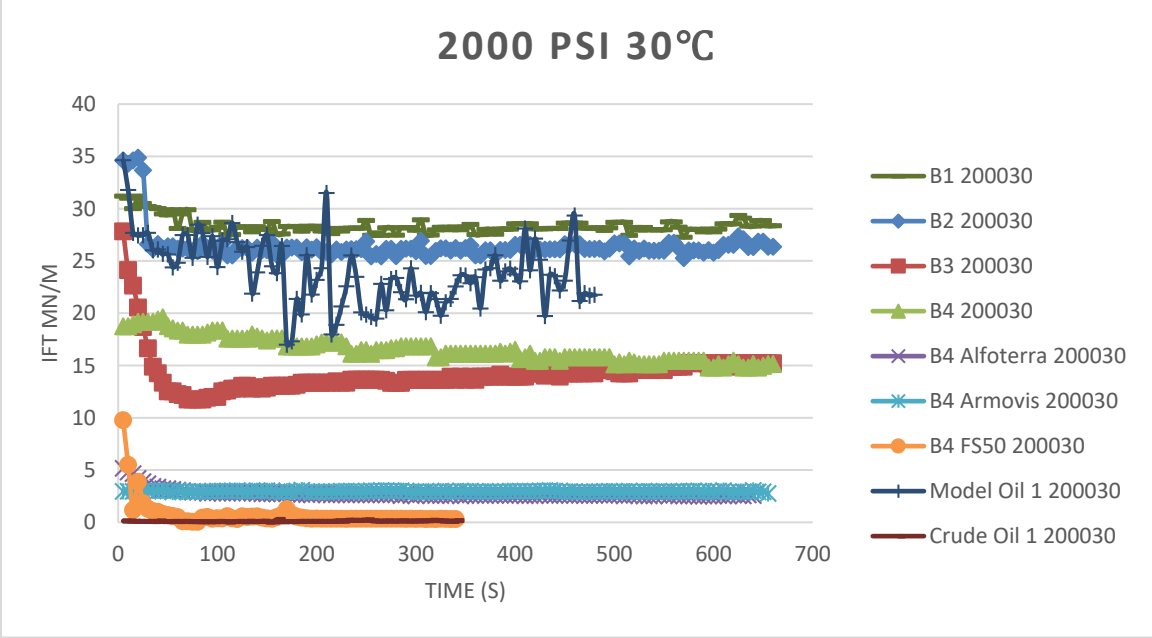

Figure 70: Interfacial Tensions as function of time at 30°C and 2000psi

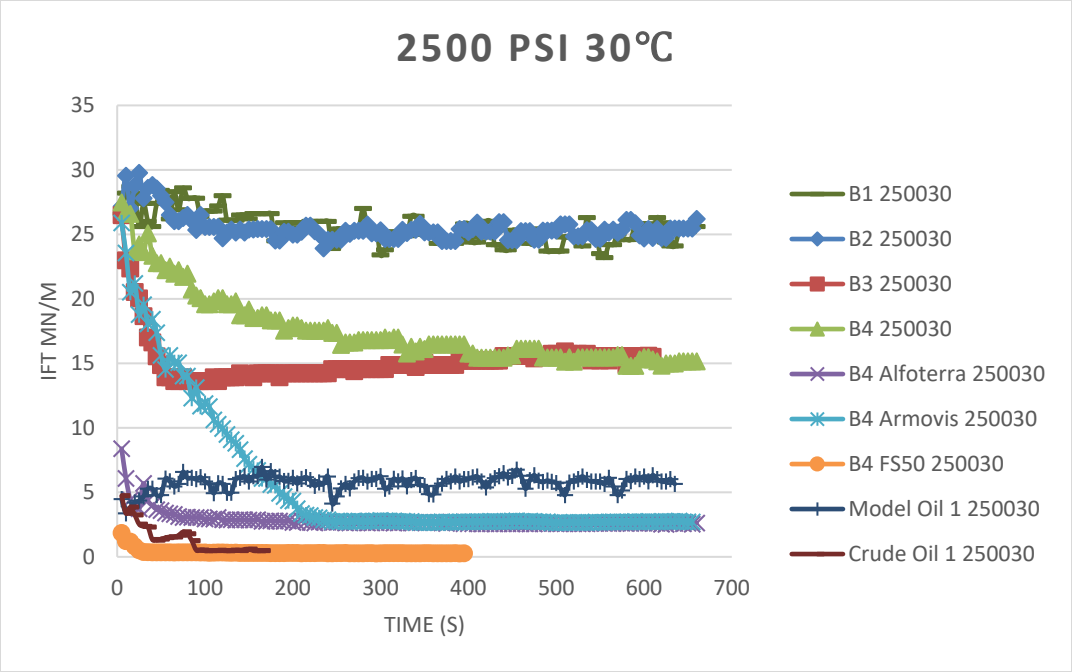

Figure 71: Interfacial Tension as function of time at 30°C and 2500psi

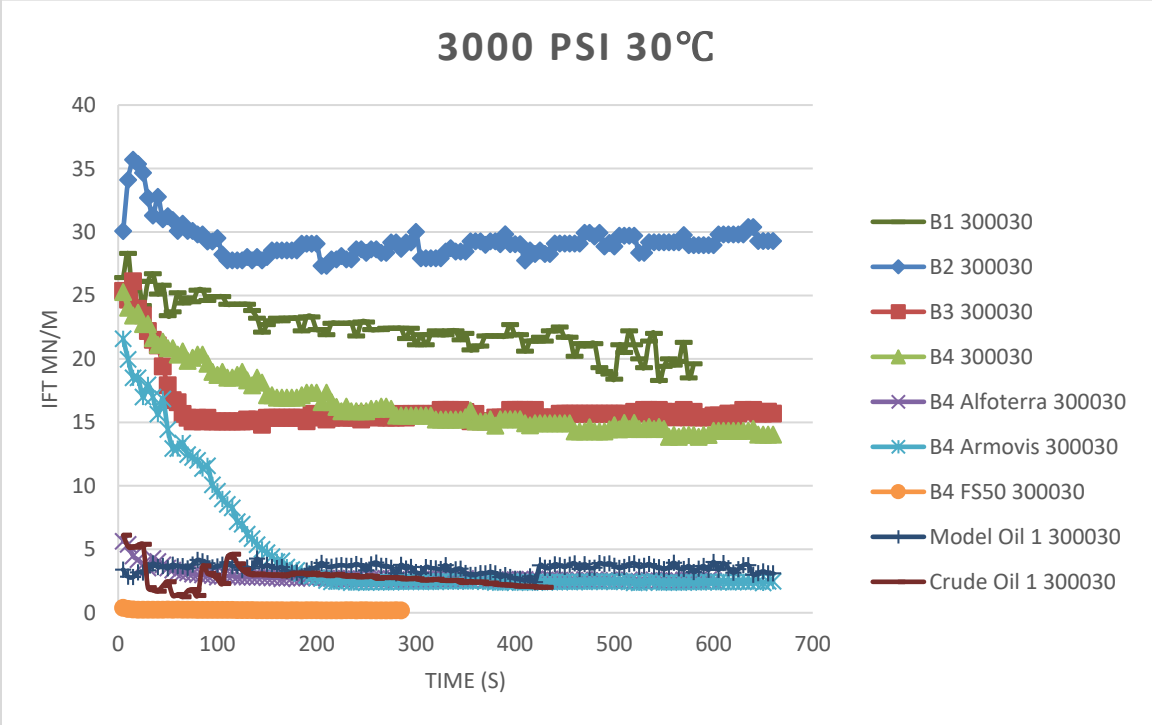

Figure 72: Interfacial Tension as function of time at 30°C and 3000psi

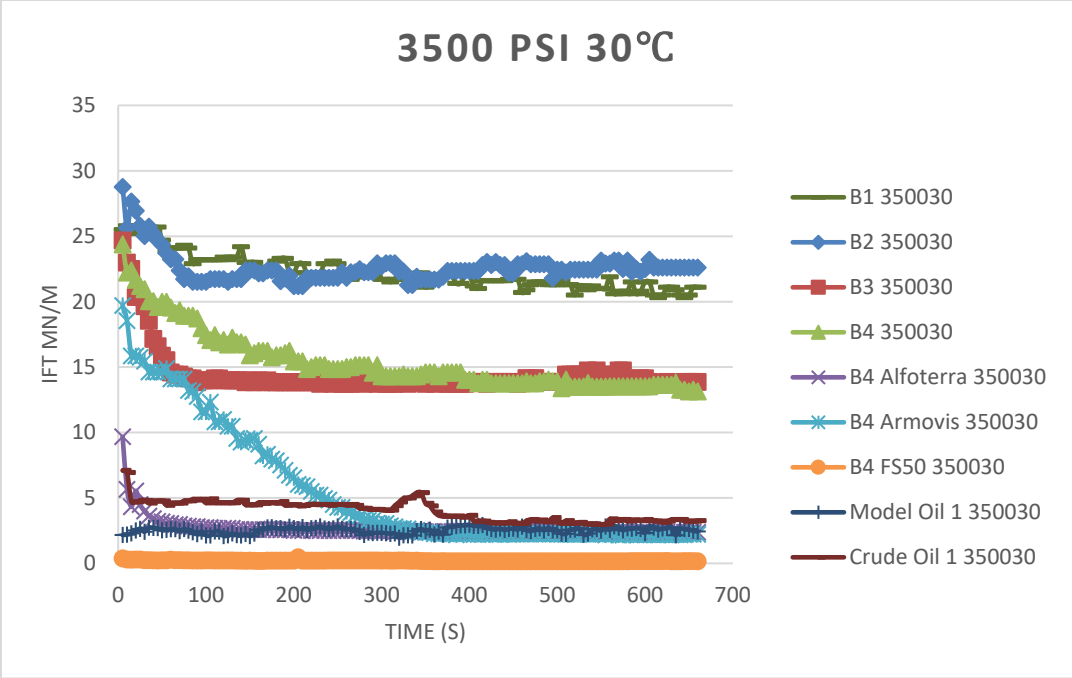

Figure 73: Interfacial Tension as function of time at 30ºC and 3500 psi

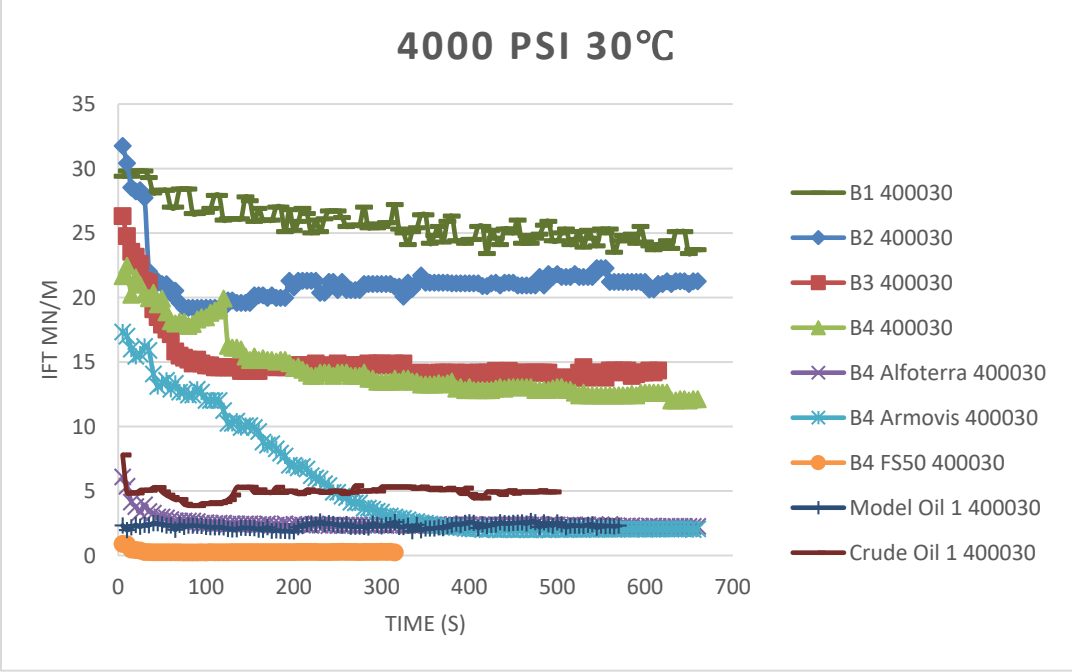

Figure 74: Interfacial Tension as function of time at 30ºC and 4000 psi

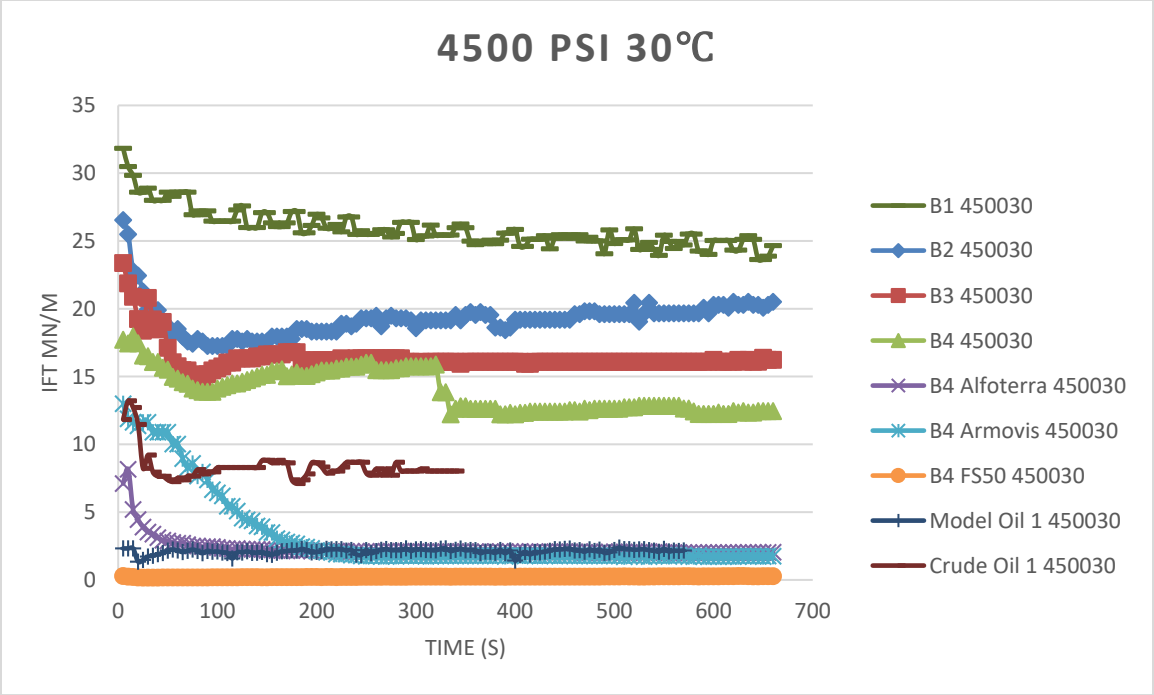

Figure 75: Interfacial tension as function of time at 30ºC and 4500 psi

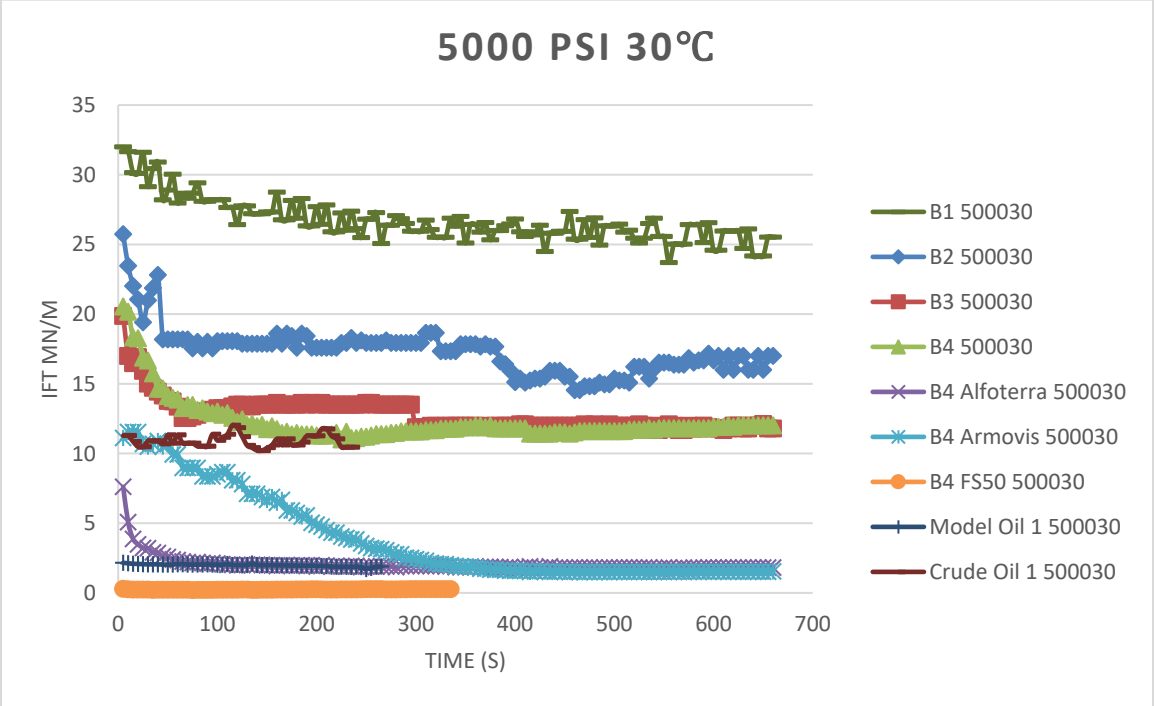

Figure 76: Interfacial tension as function of time at 30ºC and 5000 psi

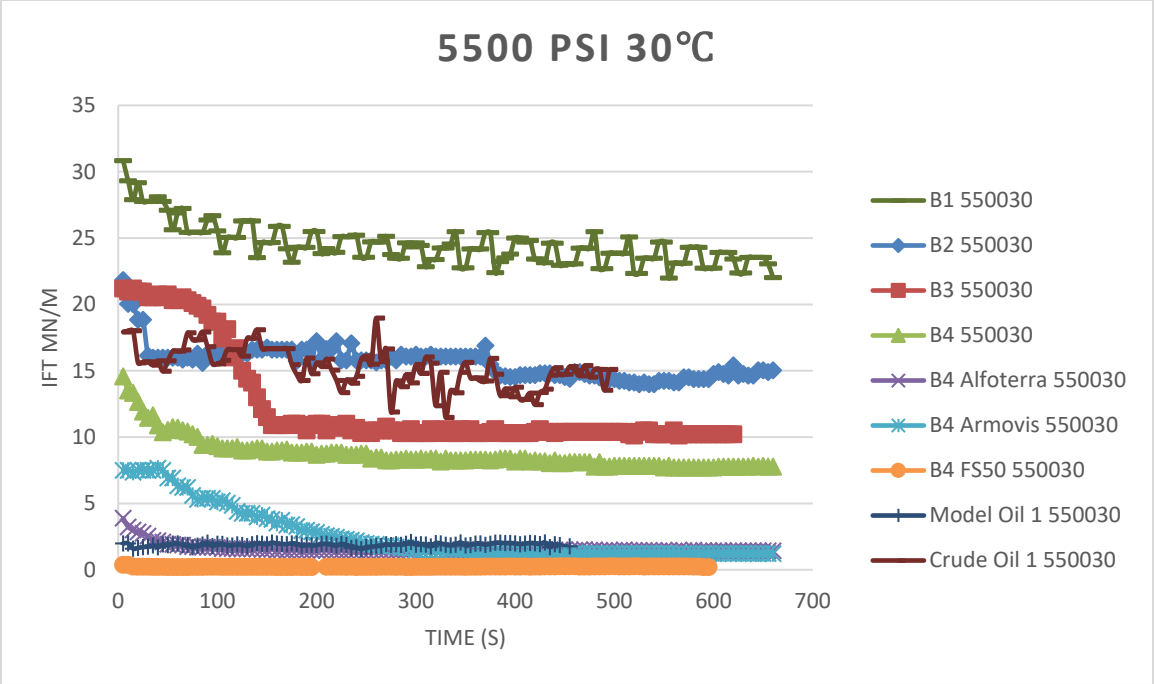

Figure 77: Interfacial tension as function of time at 30ºC and 5500 psi

At 60ºC

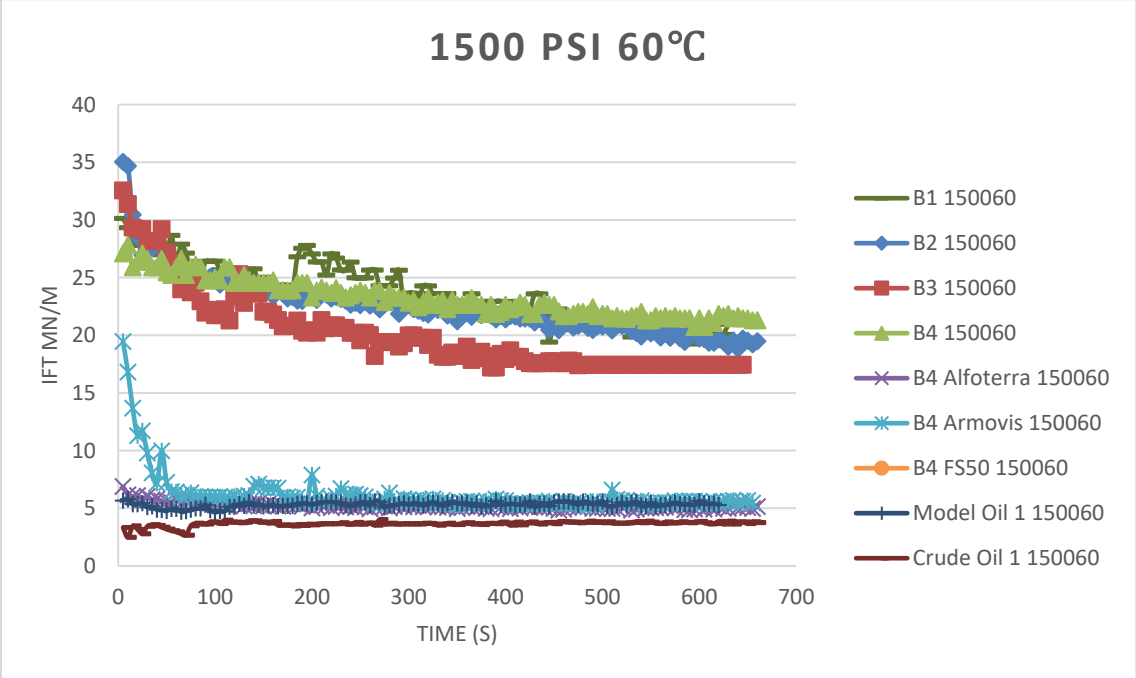

Figure 78: Interfacial tensions as function of time at 60ºC and 1500 psi

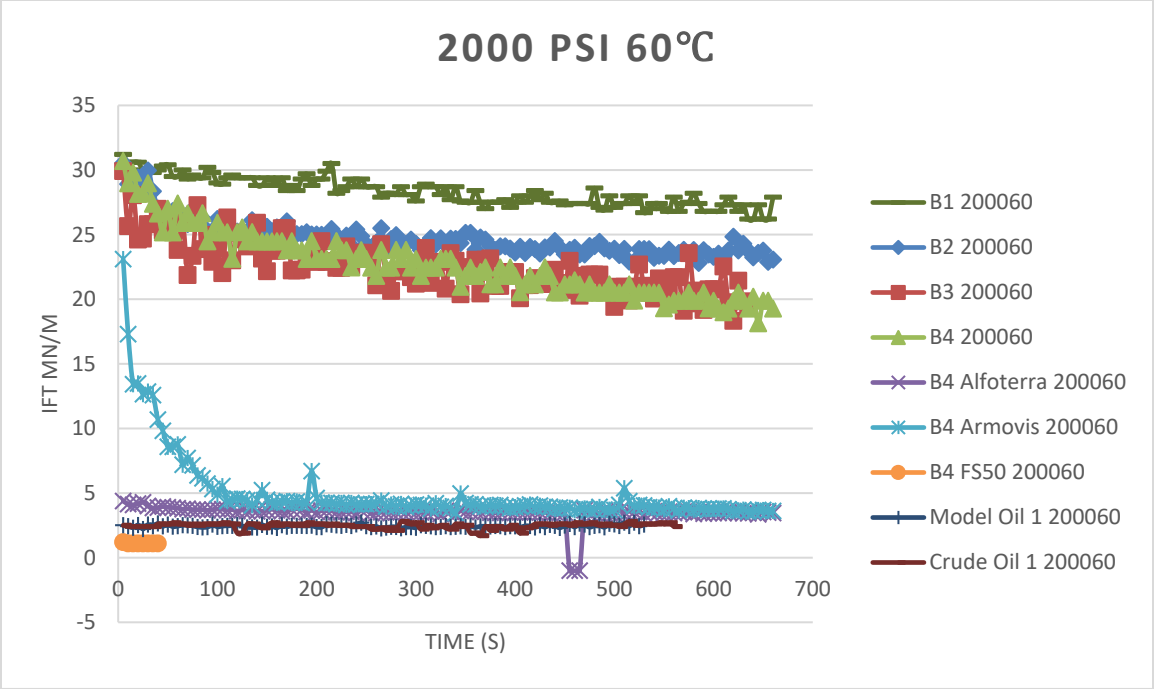

Figure 79: Interfacial Tensions as function of time at 60°C and 2000 psi

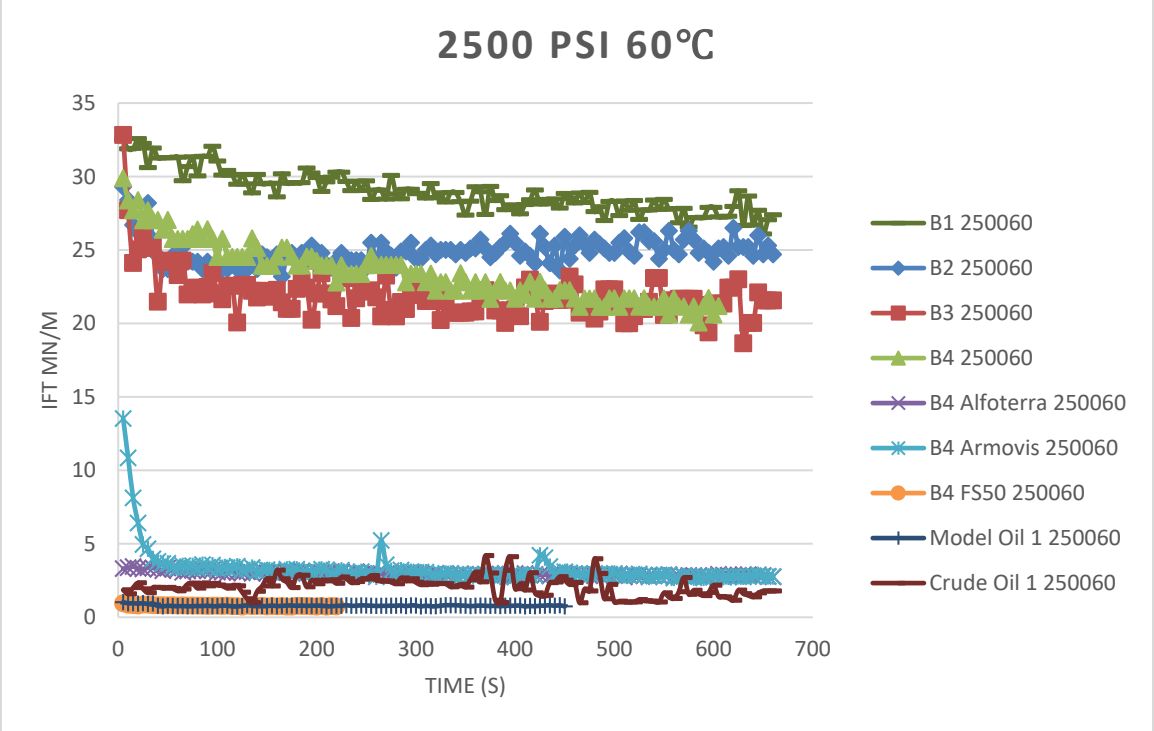

Figure 80: Interfacial Tension as function of time at 60°C and 2500 psi

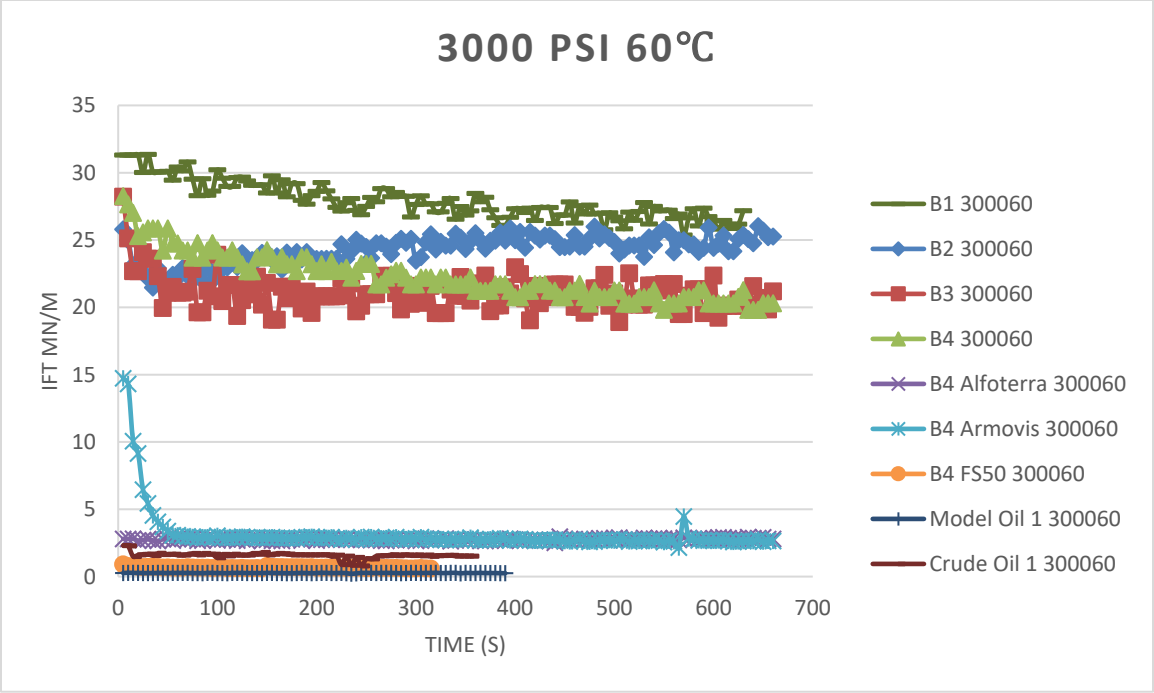

Figure 81: Interfacial Tension as a function of time at 60ºC and 3000 psi

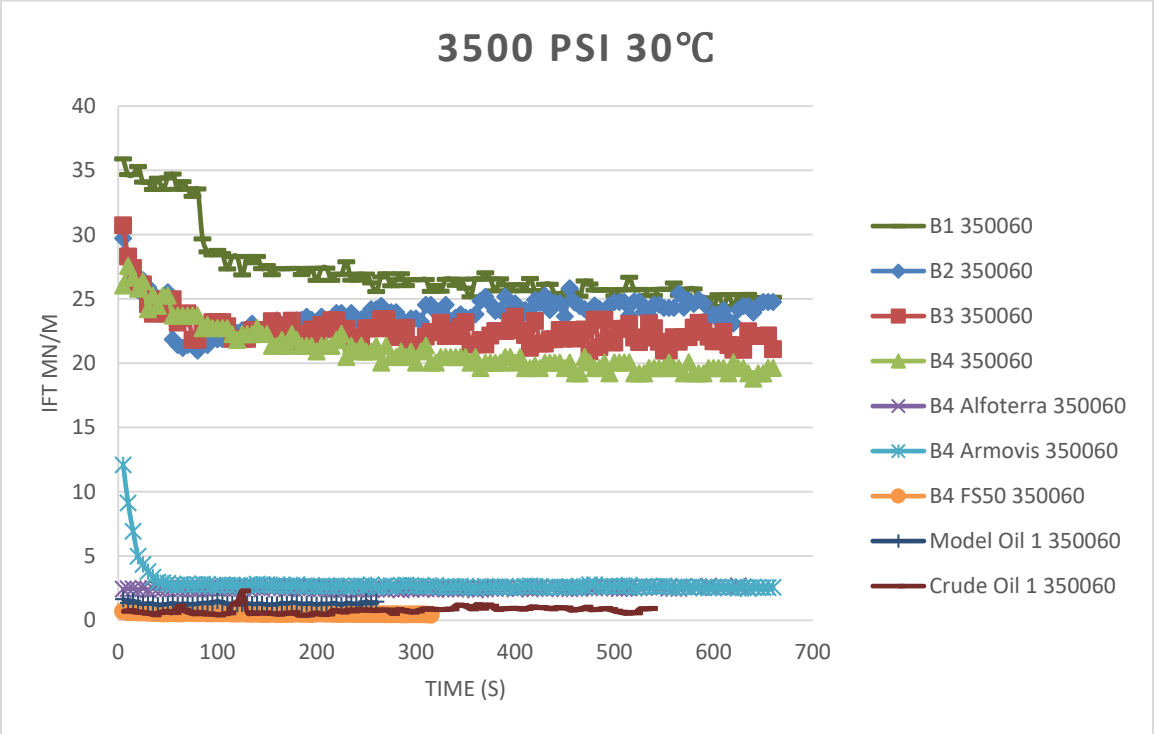

Figure 82: Interfacial Tension as a function of time at 60ºC and 3500 psi

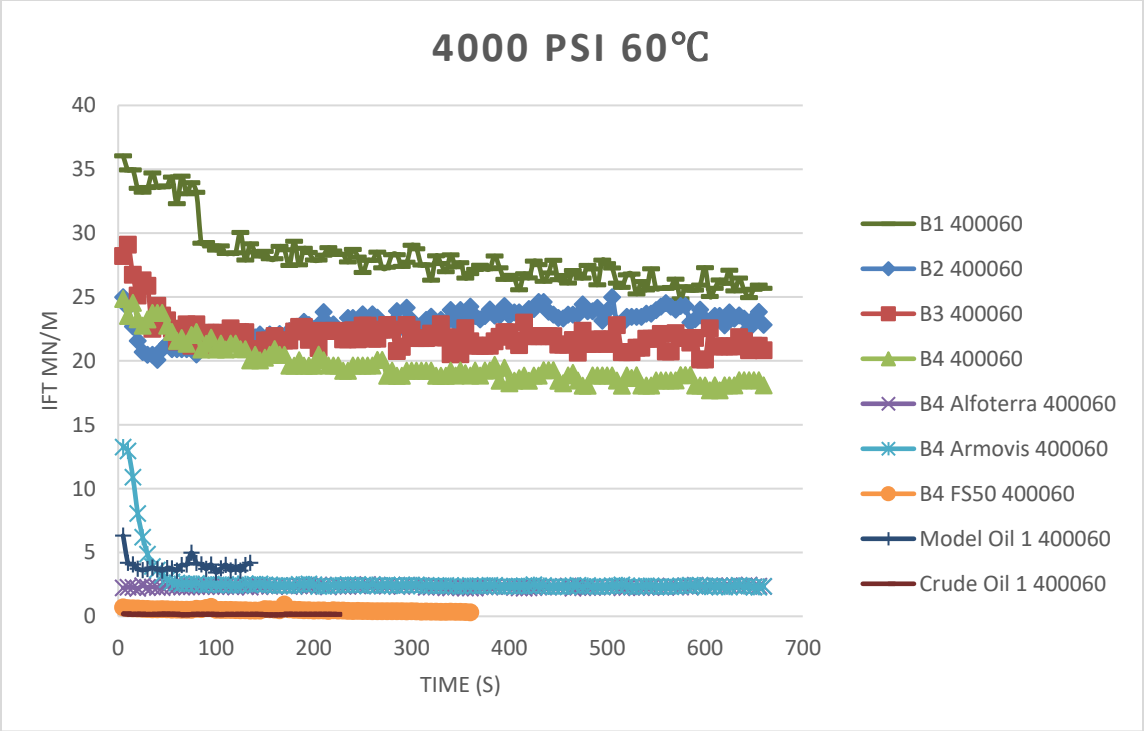

Figure 83: Interfacial Tension as function of time at 60ºC and 4000 psi

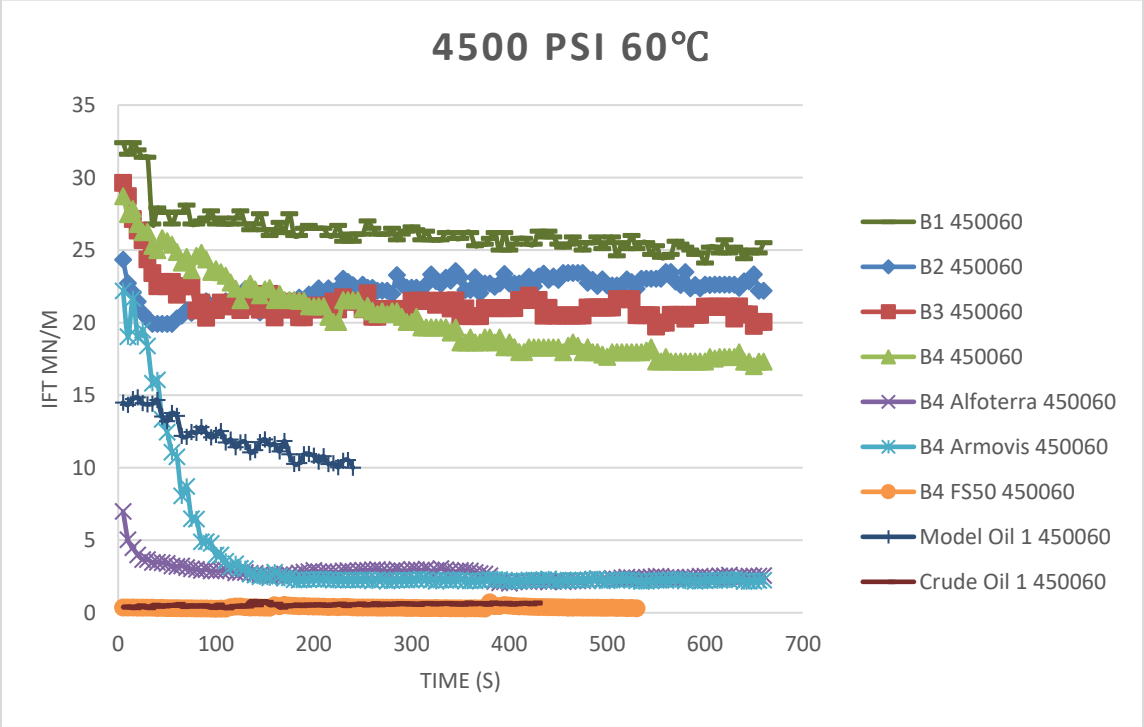

Figure 84: Interfacial Tension as function of time at 60ºC and 4500 psi

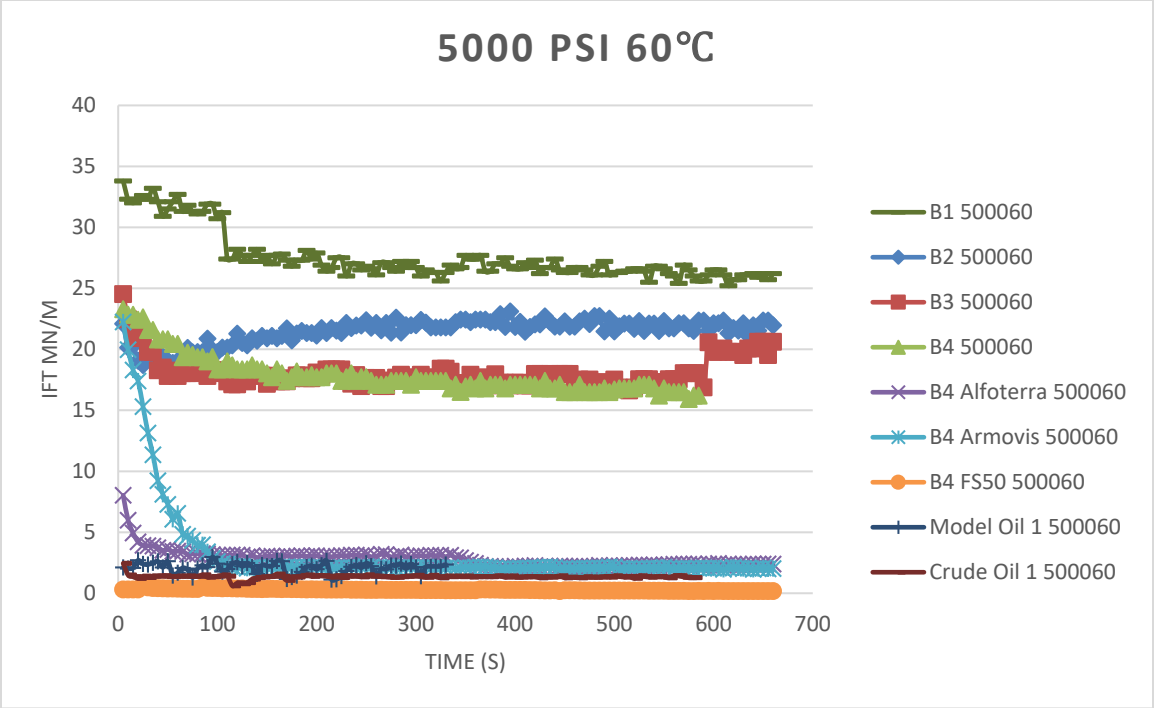

Figure 85: Interfacial Tension as function of time at 60ºC and 5000 psi

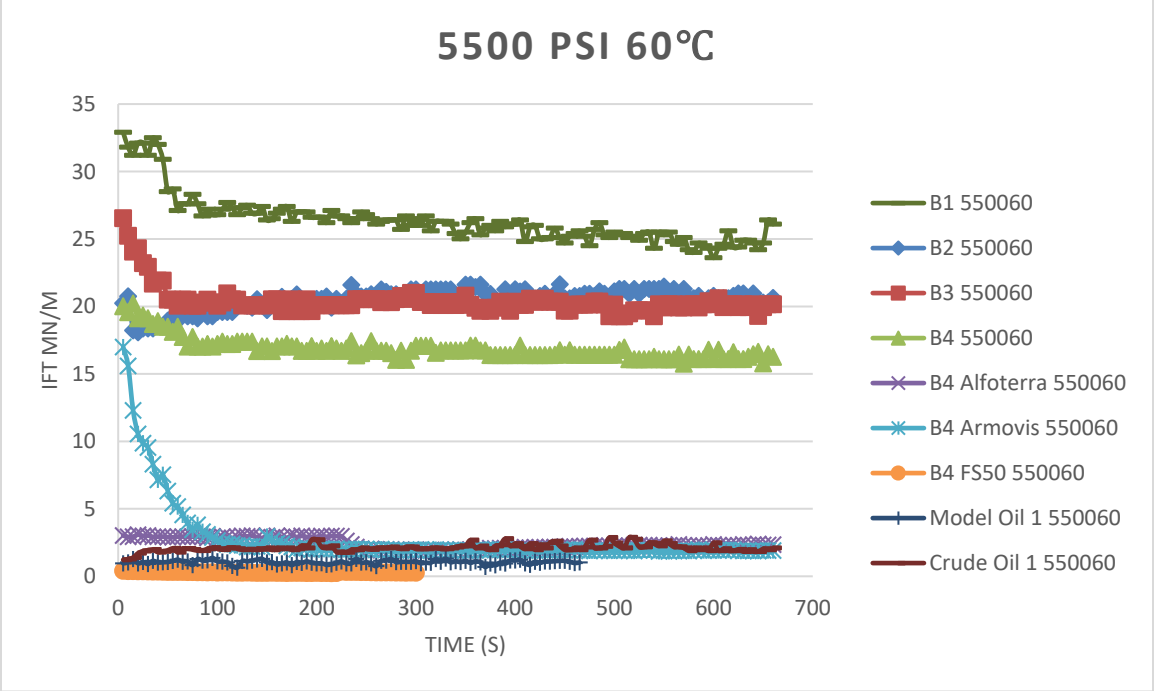

Figure 86: Interfacial tension as function of time at 60ºC and 5500 psi

At 90ºC:

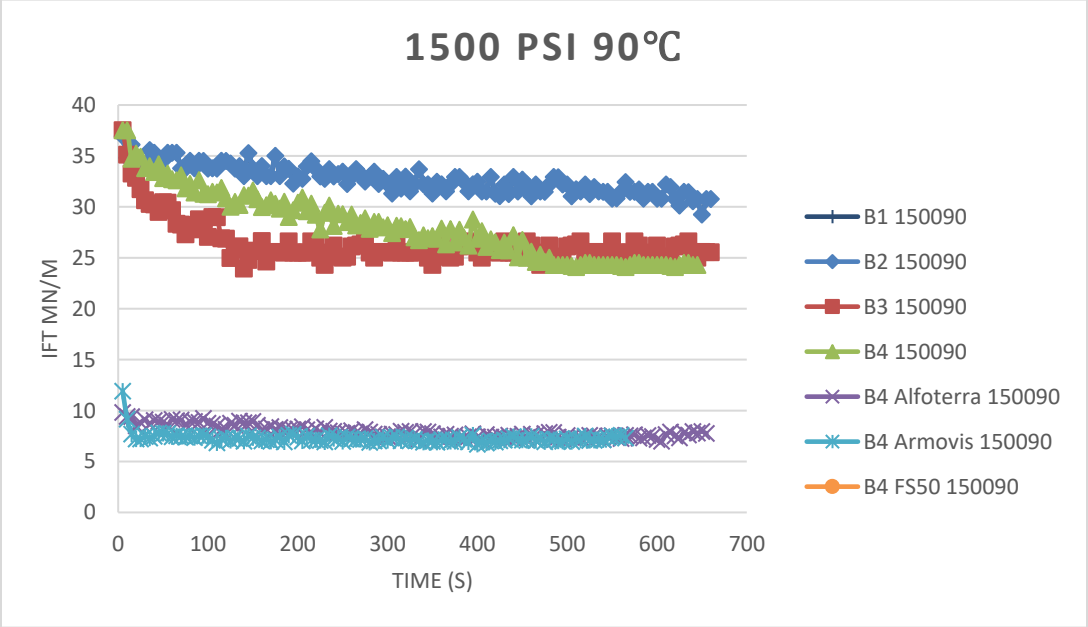

Figure 87: Interfacial tension as a function of time at 90ºC and 1500psi

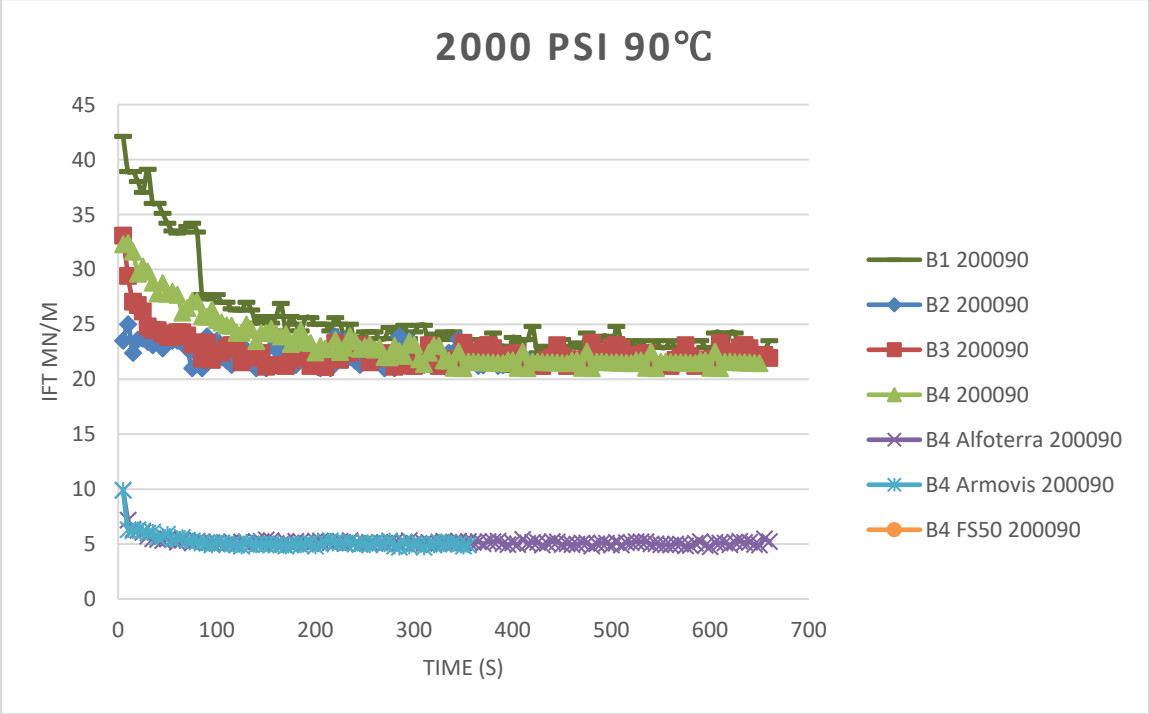

Figure 88: Interfacial tension as a function of time at 90ºC and 2000 psi

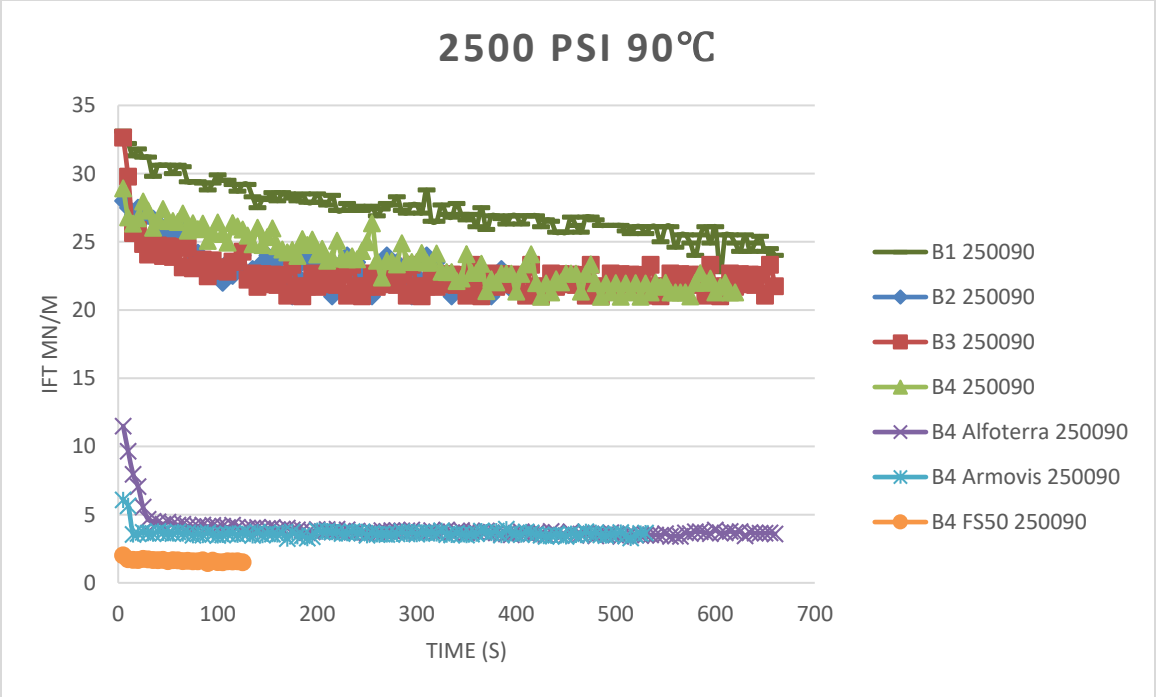

Figure 89: Interfacial tension as a function of time at 90ºC and 2500psi

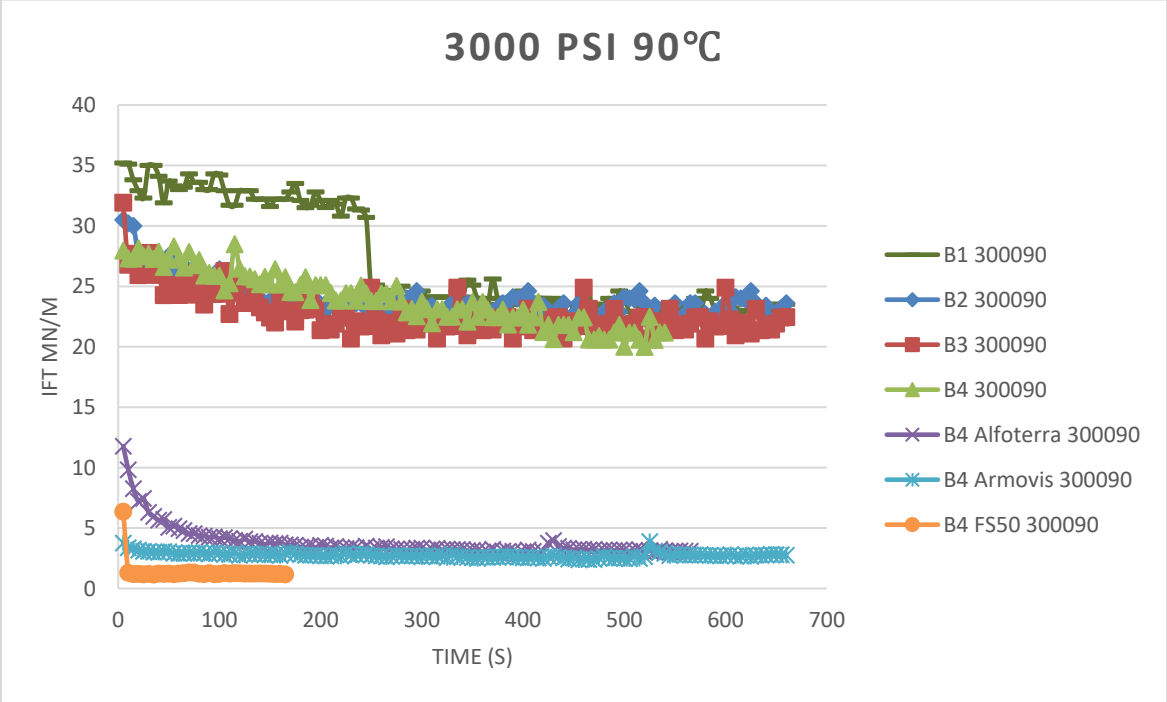

Figure 90: Interfacila tension as a function of time at 90ºC and 3000 psi

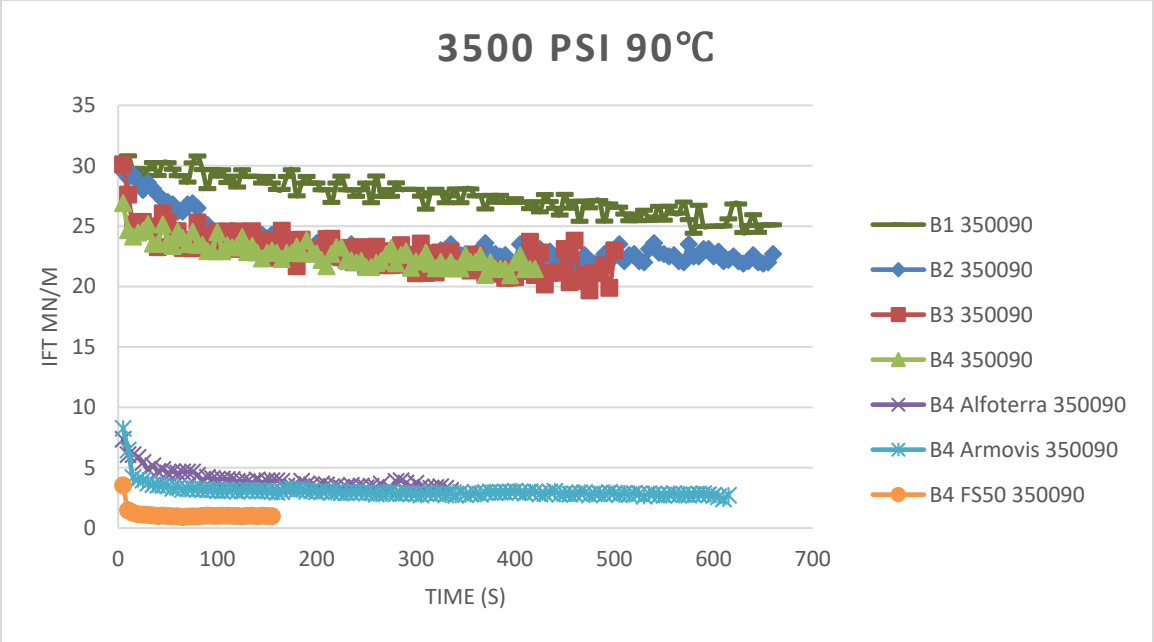

Figure 91: Interfacial tension as a function of time at 90ºC and 3500 psi

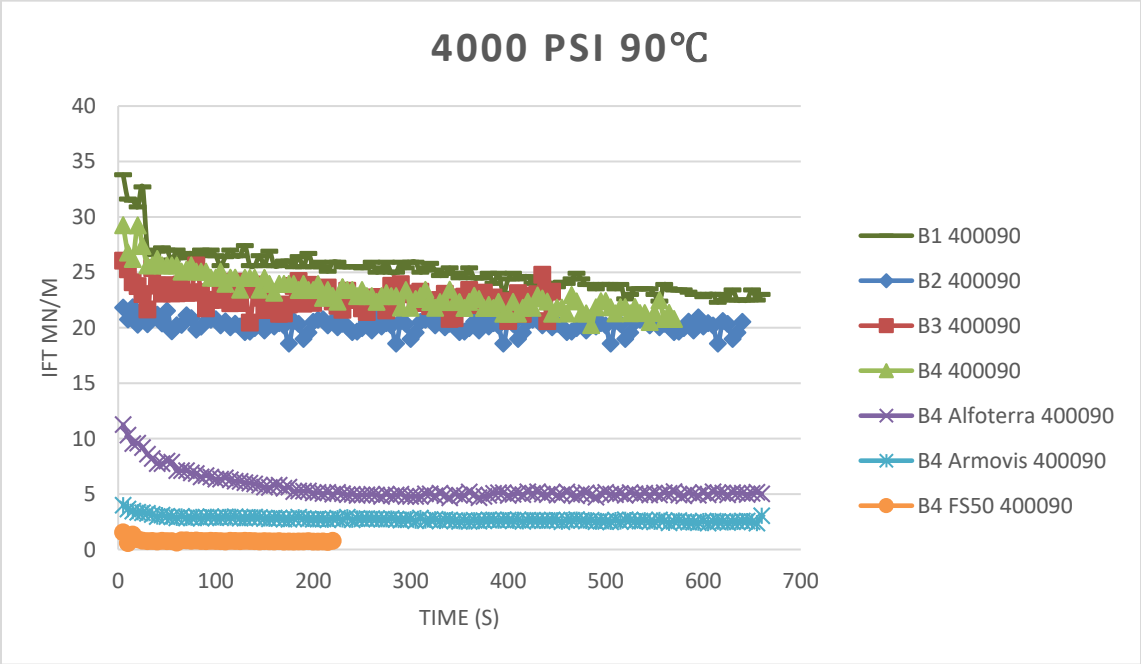

Figure 92: Interfacial tension as a function of time at 90ºC and 4000 psi

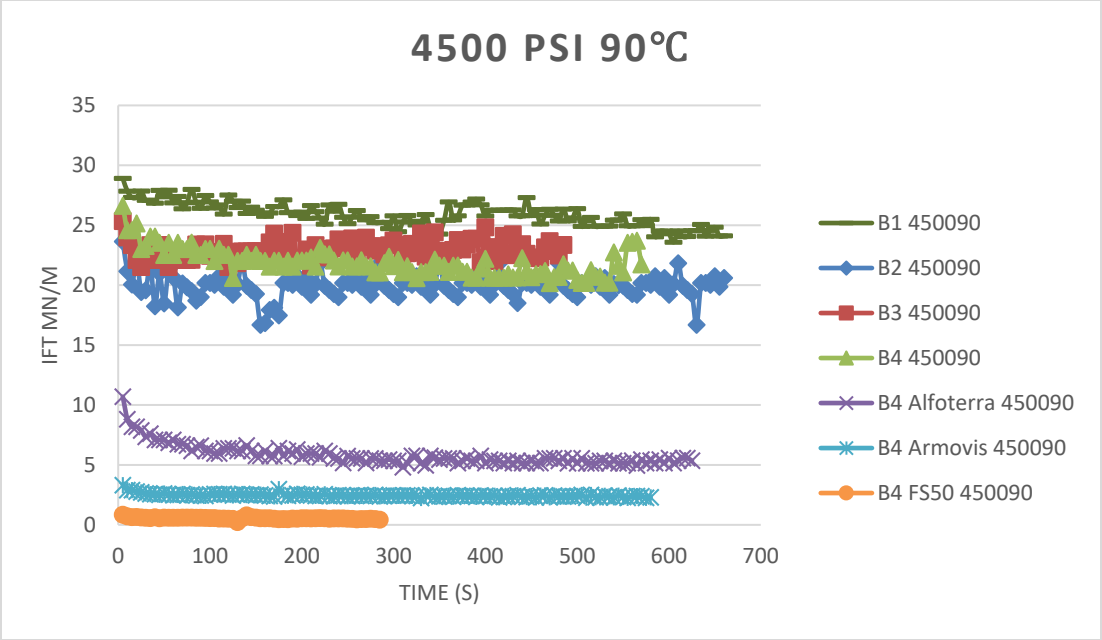

Figure 93: Interfacial tension as a function of time at 90°C and 4500 psi

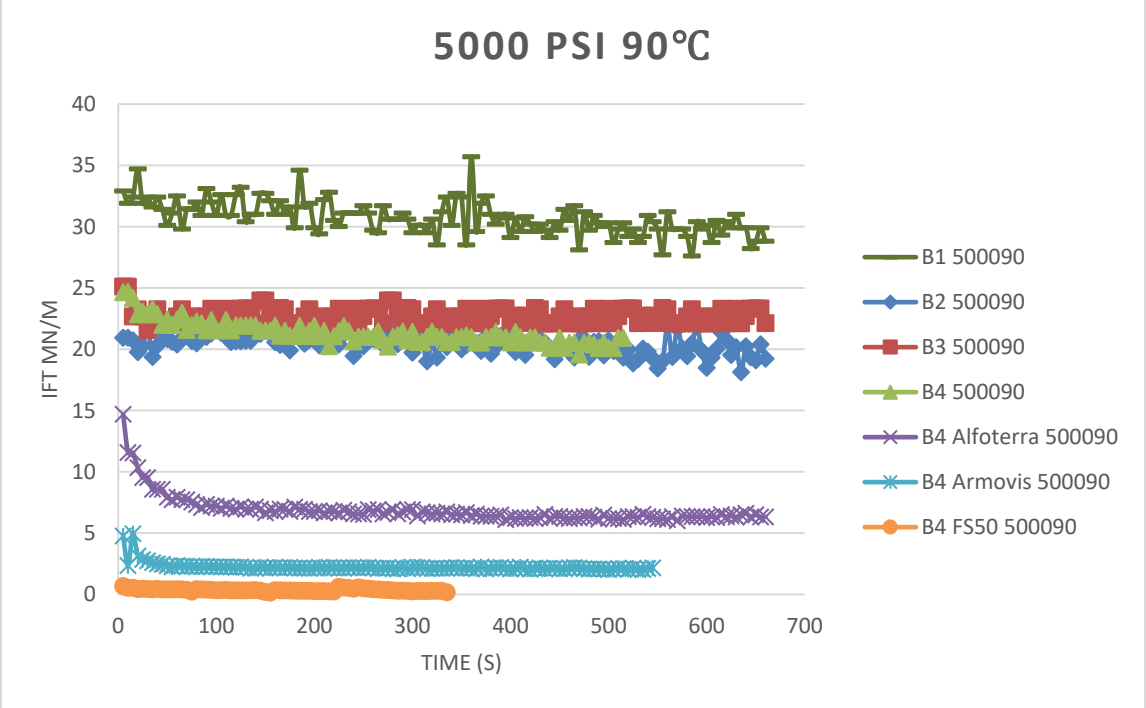

Figure 94: Interfacial tension as a function of time at 90°C and 5000 psi

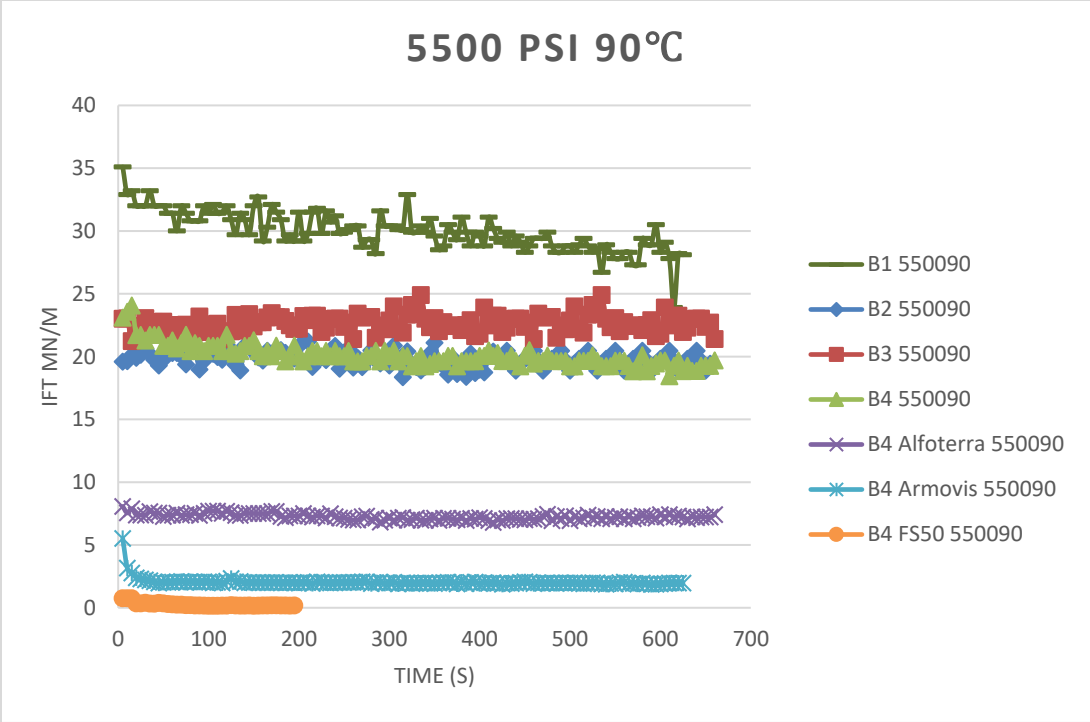

Figure 95: Interfacial tension as function of time at 90ºC and 5500 psi

APPENDIX E: DROP PROFILES

Brines

At 30ºC

Figure 96: Drop profile- Brine1 at pressures (left to right) 1500 to 5500 psi and 30ºC

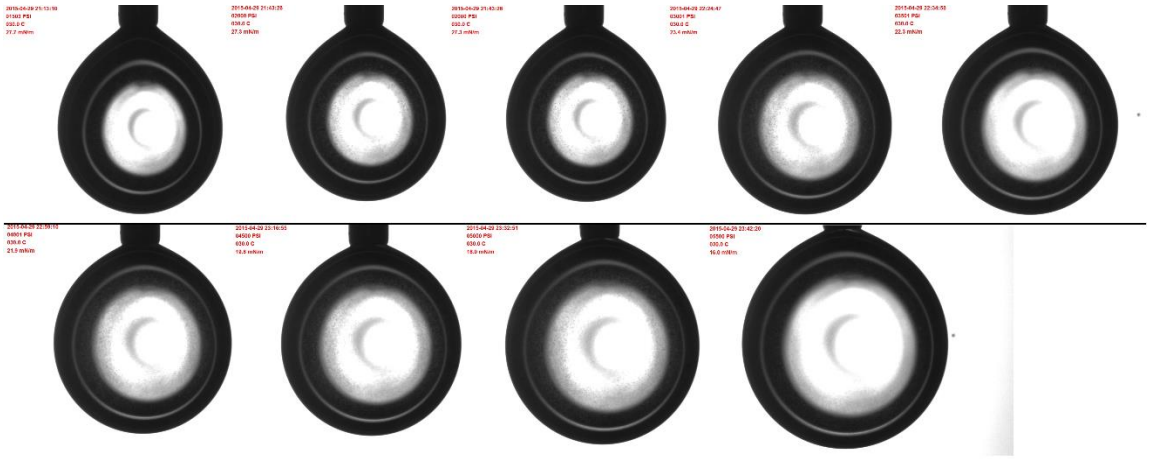

Figure 97: Drop profile- Brine2 at pressures (left to right) 1500 to 5500 psi and 30ºC

Figure 98: Drop profile- Brine3 at pressures (left to right) 1500 to 5500 psi and 30ºC

Figure 99: Drop profile- Brine4 at pressures (left to right) 1500 to 5500 psi and 30ºC

At 60ºC

Figure 100: Drop profile- Brine1 at pressures (left to right) 1500 to 5500 psi and 60ºC

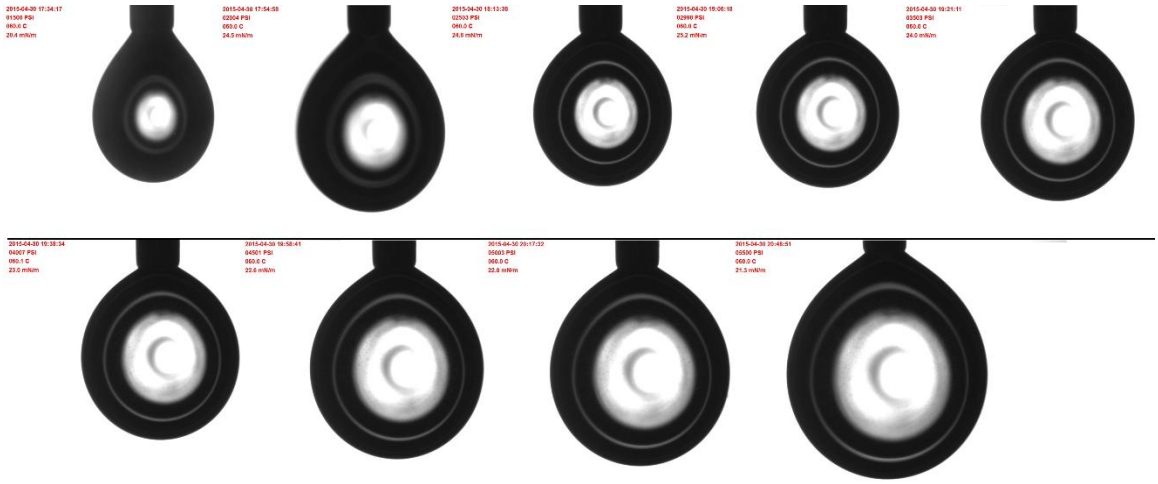

Figure 101: Drop profile- Brine2 at pressures (left to right) 1500 to 5500 psi and 60ºC

Figure 102: Drop profile- Brine3 at pressures (left to right) 1500 to 5500 psi and 60ºC

Figure 103: Drop profile- Brine4 at pressures (left to right) 1500 to 5500 psi and 60ºC

At 90ºC

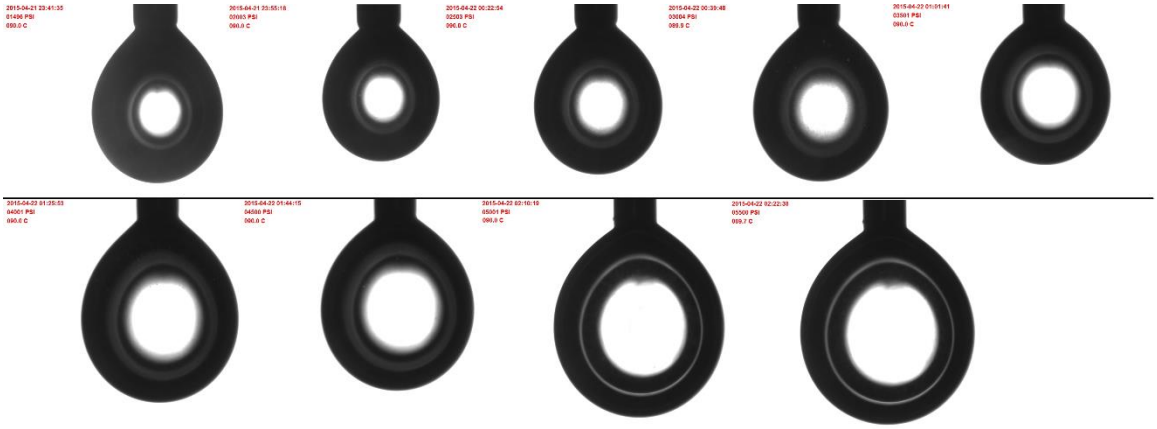

Figure 104: Drop profile- Brine1 at pressures (left to right) 1500 to 5500 psi and 90ºC

Figure 105: Drop profile- Brine2 at pressures (left to right) 1500 to 5500 psi and 90ºC

Figure 106: Drop profile- Brine3 at pressures (left to right) 1500 to 5500 psi and 90ºC

Figure 107: Drop profile- Brine4 at pressures (left to right) 1500 to 5500 psi and 90ºC

Brine-Surfactant Solutions

At 30ºC

Figure 108: Drop profile- BSS1 at pressures (left to right) 1500 to 5500 psi and 30ºC

Figure 109: Drop profile- BSS2 at pressures (left to right) 1500 to 5500 psi and 30ºC

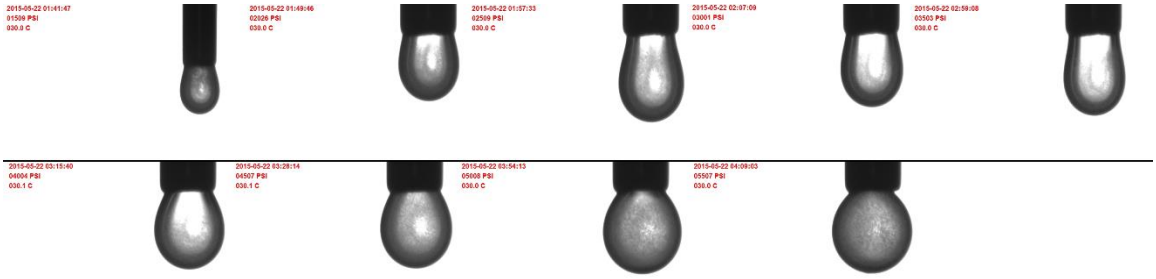

Figure 110: Drop profile- BSS3 at pressures (left to right) 1500 to 5500 psi and 30ºC

At 60ºC

Figure 111: Drop profile- BSS1 at pressures (left to right) 1500 to 5500 psi and 60ºC

Figure 112: Drop profile- BSS2 at pressures (left to right) 1500 to 5500 psi and 60ºC

Figure 113: Drop profile- BSS3 at pressures (left to right) 1500 to 5500 psi and 60ºC

At 90ºC

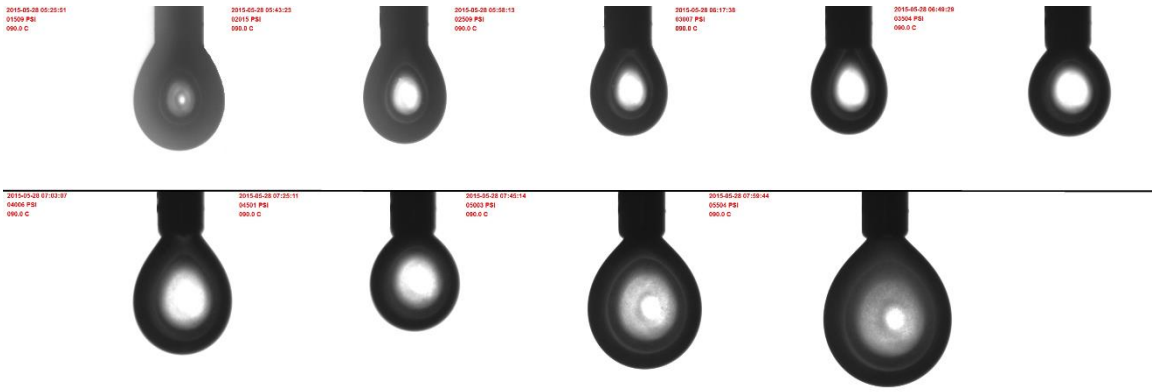

Figure 114: Drop profile- BSS1 at pressures (left to right) 1500 to 5500 psi and 90ºC

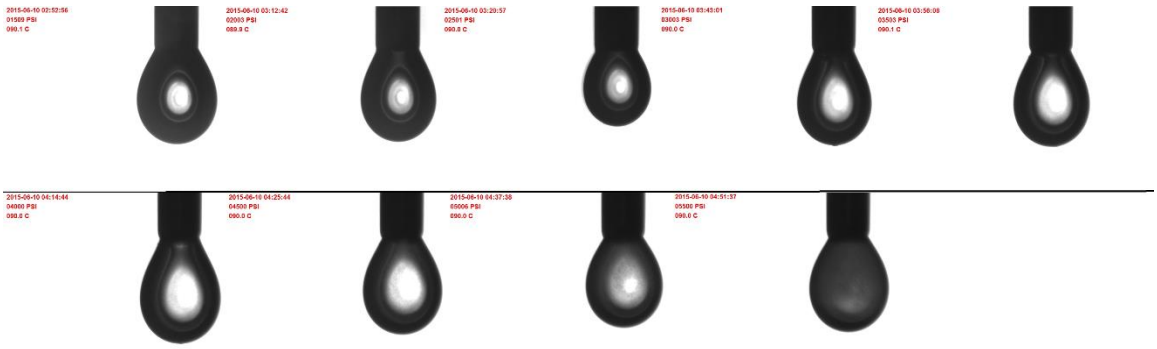

Figure 115: Drop profile- BSS2 at pressures (left to right) 1500 to 5500 psi and 90ºC

Figure 116: Drop profile- BSS1 at pressures (left to right) 1500 to 5500 psi and 90ºC

Oils

At 30ºC

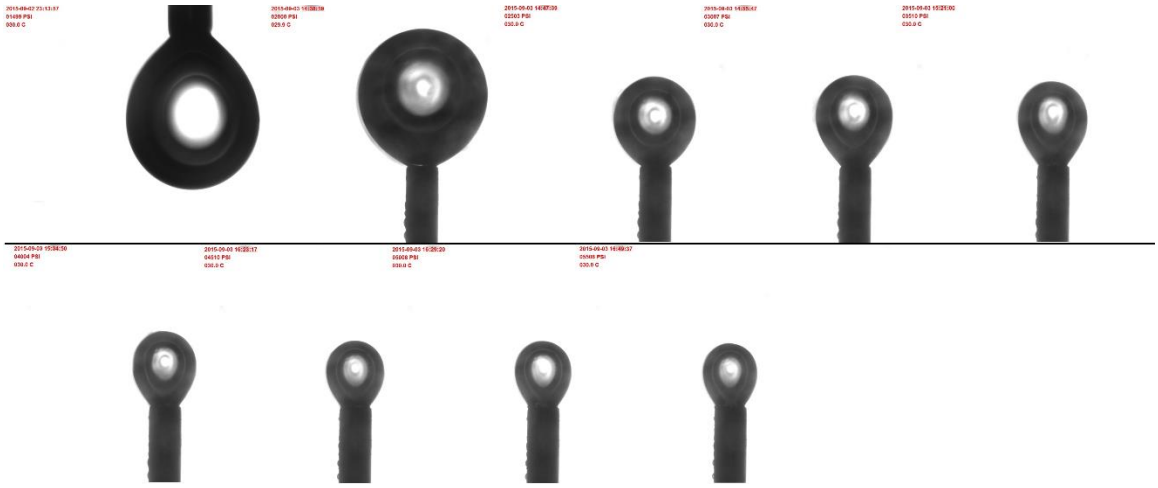

Figure 117: Drop profile- Squalane at pressures 1500 to 5500 psi and 30ºC

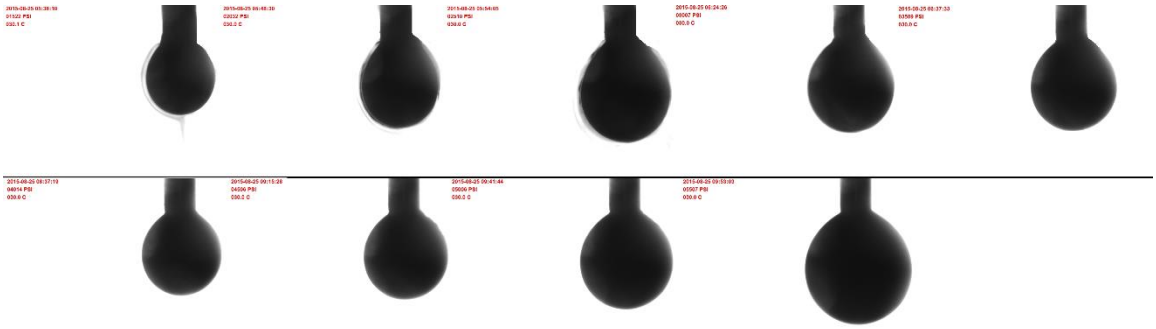

Figure 118: Drop profile- Crude1 at pressures 1500 to 5500 psi and 30ºC

At 60ºC

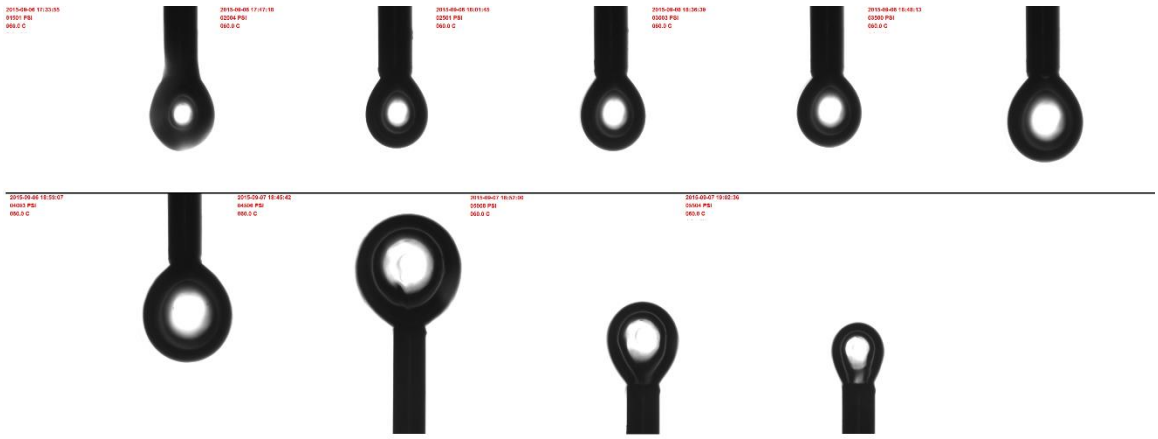

Figure 119: Drop profile- Squalane at pressures 1500 to 5500 psi and 60ºC

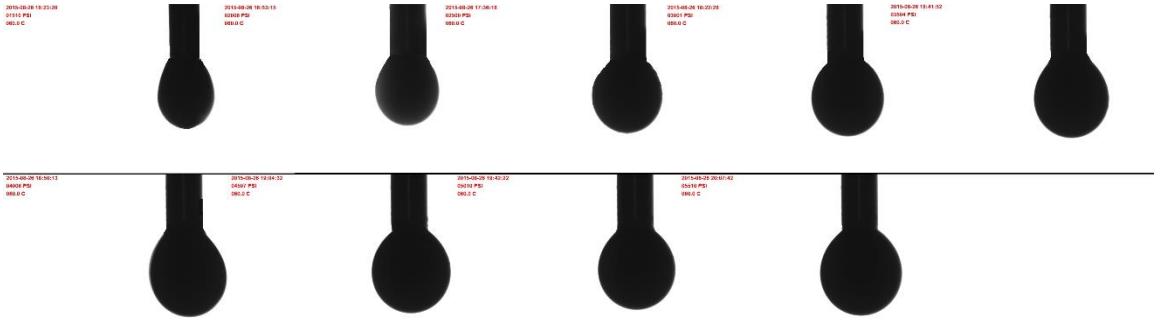

Figure 120: Drop profile- Crude1 at pressures 1500 to 5500 psi and 60ºC

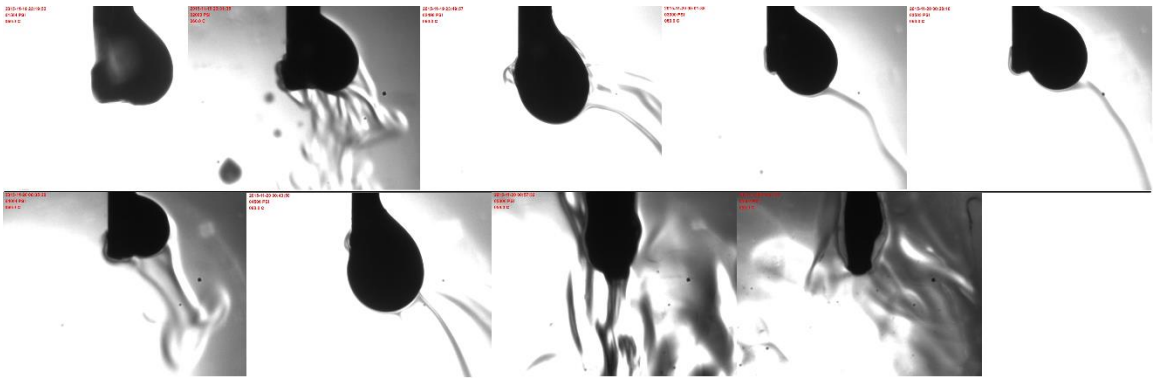

Figure 121: Drop profile- Crude2 at pressures 1500 to 5500 psi and 60ºC

Contact Angle Experiments

Crude oil 1 at 60ºC

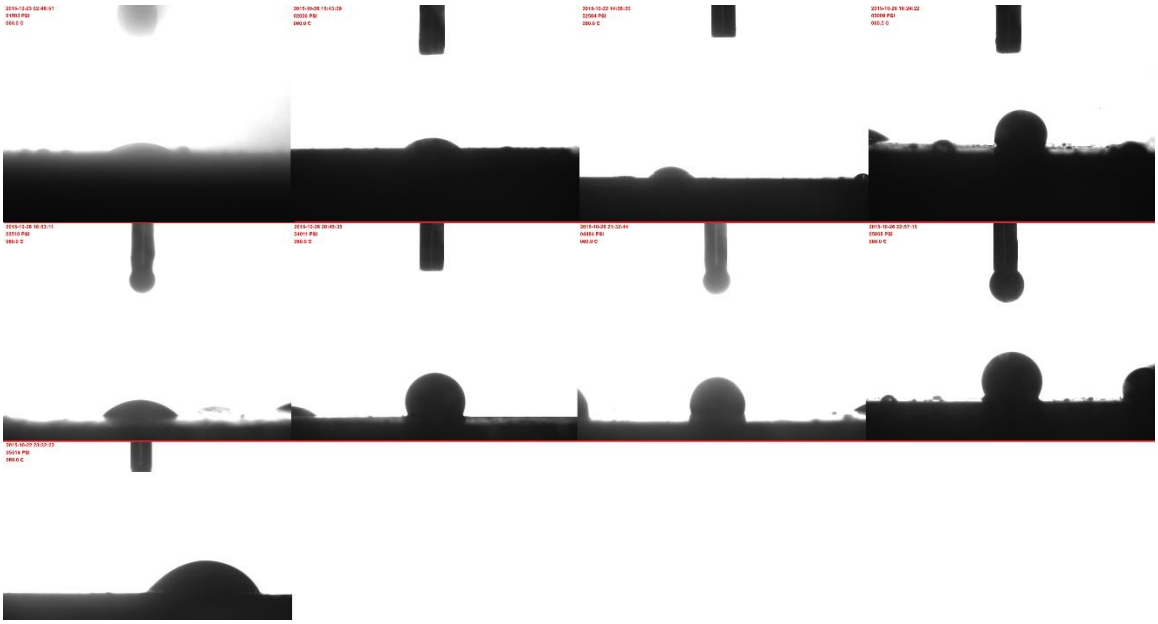

Figure 122: CA Drop profile- Crude1 at pressures 1500 to 5500 psi and 60ºC

Squalane at 60ºC

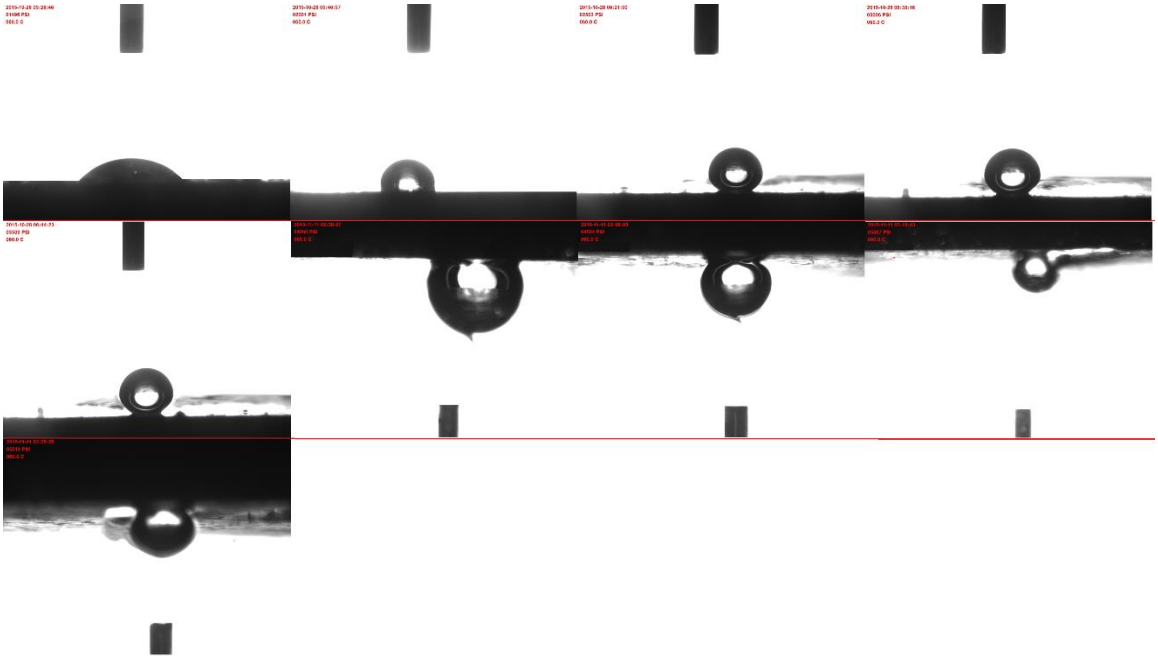

Figure 123: CA Drop profile- Squalane at pressures 1500 to 5500 psi and 60ºC

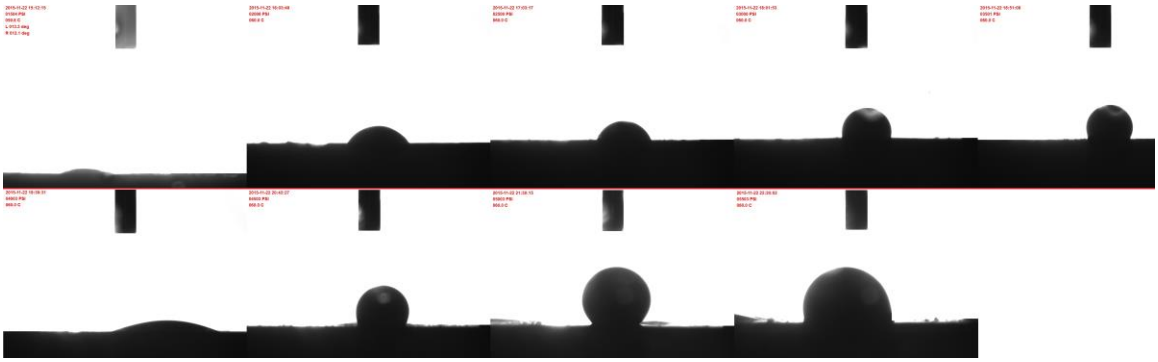

Figure 124: CA Drop profile- Crude2 at pressures 1500 to 5500 psi and 60^{o}C

APPENDIX F

Correlation Parameters

Table 36: Parameters of CA Correlation

$w1_{i,1}$	$w1_{i,2}$	$w1_{i,3}$	$w_{2,i}$	$b_{1,i}$	b_2
2.461168	0.961075	-2.05418	-1.1217	-2.57961	-0.63986
0.415262	2.552612	-1.53557	0.649854	-2.34526	
1.806469	-1.91561	2.040436	-1.41558	-1.51262	
1.306621	-2.44383	1.631914	2.313308	-0.91655	
2.14467	-2.34128	1.3602	1.207241	-0.279	
-5.13255	1.220157	-0.90888	2.776423	0.304125	
-3.70864	1.545599	-3.12364	3.088561	-1.51209	
7.414321	3.083599	2.944771	4.518283	4.724991	
-3.03451	0.606316	0.549544	0.517334	-2.16638	
1.809452	-2.40584	-1.08831	0.939483	2.823868	

Normalization:

Input parameters should be normalized for the new correlation and then the output must be de-normalized between -1 and +1 using traditional two-point formula given below:

$$\frac{Y - Y_{min}}{Y_{max} - Y_{min}} = \frac{X - X_{min}}{X_{max} - X_{min}}$$

$$Y = \frac{X - X_{min}}{X_{max} - X_{min}} (Y_{max} - Y_{min}) + Y_{min}$$

Where

Y = Input Parameter in normalized form

Y_{max} = 1

Y_{min} = -1

X_{min} = Input Data maximum value.

X_{max} = Input Data minimum Value

X = Input Parameter normalized form

$$Y = \frac{X - Xmin}{Xmax - Xmin} * 2 - 1$$

Therefore, the output obtained by using the correlation will be in normalized form that must be de-normalized using the following equation

$$\mathrm{CA} = \frac{(152 - 11.7)(\mathrm{CA_n} + 1)}{2} + 11.7$$

REFERENCES

[1] B. Bennion, H. Energy, S. Bachu, A. Energy, and U. Board, "SPE 99325 The Impact of Interfacial Tension and Pore - Size Distribution / Capillary Pressure Character on CO 2 Relative Permeability at Reservoir Conditions in CO 2 -Brine Systems," 2006.

[2] A. Syahputra, J.-S. Tsau, and R. B.Grigg, "Laboratory Evaluation of Using Lignosulfonate and Surfactant Mixture in CO2 Flooding," *Proc. SPE/DOE Improv. Oil Recover. Symp.*, 2000.

[3] W. Xu, S. C. Ayirala, and D. N. Rao, "Measurement of Surfactant-Induced Interfacial Interactions at Reservoir Conditions," *SPE Annu. Tech. Conf. Exhib.*, Apr. 2005.

[4] R. A. Albrecht and S. S. Marsden, "Foams as Blocking Agents in Porous Media," *Soc. Pet. Eng. J.*, vol. 10, no. 1, pp. 51–55, Mar. 1970.

[5] H. Yaghoobi, J. S. Tsau, and R. B. Grigg, "Effect of Foam on CO Breakthrough: Is This Favorable to Oil Recovery?," in *SPE Permian Basin Oil and Gas Recovery Conference*, 1998.

[6] J.-S. Tsau and J. P. Heller, "Evaluation of Surfactants for CO2-Foam Mobility Control," in *Permian Basin Oil and Gas Recovery Conference*, 1992.

[7] S. H. Yang and R. L. Reed, "Mobility Control Using CO2 Forms," in *SPE Annual Technical Conference and Exhibition*, 1989.

[8] G. C. Bernard, L. W. Holm, and C. P. Harvey, "Use of Surfactant to Reduce CO2 Mobility in Oil Displacement," *Soc. Pet. Eng. J.*, vol. 20, no. 4, pp. 281–292, Aug. 1980.

[9] J.-S. Tsau and R. B. Grigg, "Assessment of Foam Properties and Effectiveness in Mobility Reduction for CO2-Foam Floods," in *International Symposium on Oilfield Chemistry*, 1997.

[10] K. K. Mohanty, "Dilute Surfactant Methods for Carbonate Formations," Houston, 2003.

[11] E. A. Spinler, D. R. Zornes, D. P. Tobola, and A. Moradi-Araghi, "Enhancement of Oil Recovery Using a Low Concentration of Surfactant to Improve Spontaneous and Forced Imbibition in Chalk." Society of Petroleum Engineers.

[12] J. R. Bragg, W. W. Gale, W. A. McElhannon Jr., O. W. Davenport, M. D. Petrichuk, and T. L. Ashcraft, "Loudon Surfactant Flood Pilot Test." Society of Petroleum Engineers.

[13] A. Skauge, E. I. Dale, and C. Centre, "SPE 111435 Progress in Immiscible WAG Modelling," 2007.

[14] Y.-P. Sun, Ed., *Supercritical Fluid Technology in Materials Science and Engineering: Synthesis, Properties and Applications*. Marcel Dekker, 2002.

[15] M. P. Andersson, M. V. Bennetzen, A. Klamt, and S. L. S. Stipp, “First-Principles Prediction of Liquid/Liquid Interfacial Tension,” *J. Chem. Theory Comput.*, vol. 10, no. 8, pp. 3401–3408, Aug. 2014.

[16] A. Alidad, “Drop dependence,” *PhD Thesis, Dep. Mech. Ind. Eng. Univ. Toronto*, 2001.

[17] S. Kumar, G. Abbas, and P. Engineering, “OTC-24738-MS Wettability Alteration by New Acid-Alkali-Surfactant-Polymer Formulation in High Salinity Carbonate Reservoirs,” 2014.

[18] S. Bachu and D. B. Bennion, “Interfacial tension between CO2, freshwater, and brine in the range of pressure from (2 to 27) MPa, temperature from (20 to 125) ° C, and water salinity from (0to334 000)mg · L-1,” *J. Chem. Eng. Data*, vol. 54, no. 3, pp. 765–775, 2009.

[19] S. Saraji, M. Piri, and L. Goual, “The effects of SO2 contamination, brine salinity, pressure, and temperature on dynamic contact angles and interfacial tension of supercritical CO2/brine/quartz systems,” *Int. J. Greenh. Gas Control*, vol. 28, pp. 147–155, Sep. 2014.

[20] S. Kim and J. C. Santamarina, “Engineered CO2 injection: The use of surfactants for enhanced sweep efficiency,” *Int. J. Greenh. Gas Control*, vol. 20, pp. 324–332, Jan. 2014.

[21] S. Iglauer, A. Salamah, M. Sarmadivaleh, K. Liu, and C. Phan, “Contamination of silica surfaces: Impact on water–CO2–quartz and glass contact angle measurements,” *Int. J. Greenh. Gas Control*, vol. 22, pp. 325–328, Mar. 2014.

[22] C. Chalbaud, M. Robin, J.-M. Lombard, H. Bertin, and P. Egermann, “Brine/CO 2 Interfacial Properties and Effects on CO 2 Storage in Deep Saline Aquifers,” *Oil Gas Sci. Technol. – Rev. l’Institut Français du Pétrole*, vol. 65, no. 4, pp. 541–555, Jul. 2010.

[23] Z. Lun, H. Fan, H. Wang, M. Luo, W. Pan, and R. Wang, “Interfacial tensions between reservoir brine and CO 2 at high pressures for different salinity,” in *Energy and Fuels*, 2012, vol. 26, no. 6, pp. 3958–3962.

[24] A. Shariat, R. G. Moore, S. A. Mehta, K. C. Van Fraassen, K. E. Newsham, and J. A. Rushing, “CMTC 150010 Laboratory Measurements of CO 2 -H 2 O Interfacial Tension at HP / HT Conditions : Implications for CO 2 Sequestration in Deep Aquifers,” no. February, pp. 7–9, 2012.

[25] A. Georgiadis, G. Maitland, J. P. M. Trusler, and A. Bismarck, “Interfacial Tension Measurements of the (H2O + n-Decane + CO2) Ternary System at Elevated Pressures and Temperatures,” *J. Chem. Eng. Data*, vol. 56, no. 12, pp. 4900–4908, 2011.

[26] C. Sun and G. Chen, “Measurement of Interfacial Tension for the CO 2 Injected Crude Oil + Reservoir Water System,” *J. Chem. Eng. Data*, vol. 50, no. 3, pp. 936–938, May 2005.

[27] D. Yang, P. Tontiwachwuthikul, and Y. Gu, “Interfacial Tensions of the Crude Oil + Reservoir Brine + CO 2 Systems at Pressures up to 31 MPa and Temperatures of 27 °C and 58 °C,” *J. Chem. Eng. Data*, vol. 50, no. 4, pp. 1242–1249, Jul. 2005.

[28] W. Xing, Y. Song, Y. Zhang, M. Nishio, Y. Zhan, W. Jian, and Y. Shen, “Research Progress of the Interfacial Tension in Supercritical CO2-water/oil System,” *Energy Procedia*, vol. 37, pp. 6928–6935, 2013.

[29] D. L. F. T. H. L. E. J. P. Gibeau, D. L. Flock, T. H. Le, and J. P. Gibeau, “THE EFFECT OF TEMPERATURE ON THE INTERFACIAL TENSION OF HEAVY CRUDE OILS USING THE PENDENT DROP APPARATUS The eJffect of temperature on the interfacial tension of heavy crude oils using the Pendent Drop apparatus University of Alberta,” vol. 3.

[30] S. H. Talebian, I. M. Tan, R. Masoudi, and M. Onur, “Fluid–fluid interactions in a system of CO2, oil, surfactant solution, and brine at high pressures and temperatures – A Malaysian reservoir case,” *J. Pet. Sci. Eng.*, vol. 124, pp. 313–322, Dec. 2014.

[31] X. Li, E. Boek, G. C. Maitland, and J. P. M. Trusler, “Xuesong Li, Edo Boek, Geoffrey C. Maitland, and J. P. Martin Trusler *,” 2012.

[32] X. Li, E. S. Boek, G. C. Maitland, and J. P. M. Trusler, “Interfacial Tension of (Brines + CO 2): CaCl 2 (aq), MgCl 2 (aq), and Na 2 SO 4 (aq) at Temperatures between (343 and 423) K, Pressures between (2 and 50) MPa, and Molalities of (0.5 to 5) mol·kg –1,” *J. Chem. Eng. Data*, vol. 57, no. 5, pp. 1369–1375, May 2012.

[33] K. Kashefi, “Measurement and Modelling of Interfacial Tension and Viscosity of Reservoir Fluids,” Heriot-Watt University, 2012.

[34] M. Cao and Y. Gu, “Oil recovery mechanisms and asphaltene precipitation phenomenon in immiscible and miscible CO2 flooding processes,” *Fuel*, vol. 109, pp. 157–166, 2013.

[35] Z. Yang, X. Liu, Z. Hua, Y. Ling, M. Li, M. Lin, and Z. Dong, “Interfacial tension of CO2 and crude oils under high pressure and temperature,” *Colloids Surfaces A Physicochem. Eng. Asp.*, vol. 482, pp. 611–616, Oct. 2015.

[36] I. O. Awari-yusuf, “Measurement of crude oil interfacial tension to determine minimum miscibility in carbon dioxide and nitrogen,” Dalhousie University, 2013.

[37] T. Akutsu, Y. Yamaji, H. Yamaguchi, M. Watanabe, R. L. Smith, and H. Inomata, “Interfacial tension between water and high pressure CO2 in the presence of hydrocarbon surfactants,” *Fluid Phase Equilib.*, vol. 257, no. 2, pp. 163–168, 2007.

[38] D. Yang, P. Tontiwachwuthikul, and Y. Gu, “Interfacial interactions between reservoir brine and CO2 at high pressures and elevated temperatures,” *Energy and Fuels*, vol. 19, no. 1, pp. 216–223, 2005.

[39] S. R. P. da Rocha, K. L. Harrison, and K. P. Johnston, “Effect of Surfactants on the

Interfacial Tension and Emulsion Formation between Water and Carbon Dioxide," *Langmuir*, vol. 15, no. 2, pp. 419–428, Jan. 1999.

[40] E. Ruckenstein, "Microemulsions, Macroemulsions, and the Bancroft Rule," *Langmuir*, vol. 12, no. 26, pp. 6351–6353, 1996.

[41] B. P. Binks, "Relationship between microemulsion phase behavior and macroemulsion type in systems containing nonionic surfactant," *Langmuir*, vol. 9, no. 1, pp. 25–28, Jan. 1993.

[42] a. Ameri, N. S. Kaveh, E. S. J. Rudolph, K. Wolf, R. Farajzadeh, and J. Bruining, "Investigation on Interfacial Interactions among Crude Oil–Brine–Sandstone Rock–CO 2 by Contact Angle Measurements," *Energy & Fuels*, vol. 27, no. 2, pp. 1015–1025, Feb. 2013.

[43] A. A. Hamouda, K. A. R. Gomari, and U. Stavanger, "SPE 99848 Influence of Temperature on Wettability Alteration of Carbonate Reservoirs," 2006.

[44] R. Gupta and K. K. Mohanty, "SPE 113407 Wettability Alteration of Fractured Carbonate Reservoirs," no. April, pp. 19–23, 2008.

[45] M. B. Alotaibi, R. A. Nasralla, and A. Texas, "SPE 129972 Wettability Challenges in Carbonate Reservoirs," no. April, pp. 24–28, 2010.

[46] C. Shelf and P. Technology, "Experimental Investigation of the Effects of Temperature , Pressure , and Crude Oil Composition on Interfacial Properties," no. July, pp. 321–328, 1986.

[47] P. M. Lichaa, H. Alpustun, J. H. Abdul, W. A. Nofal, and A. B. Fuseni, "WETTABILITY EVALUATION OF A CARBONATE."

[48] R. a. Almehaideb, M. T. Ghannam, and A. Y. Zekri, "Experimental Investigation of Contact Angles Under Oil-Microbial Solution on Carbonate Rocks," *Pet. Sci. Technol.*, vol. 22, no. 3–4, pp. 423–438, Jan. 2004.

[49] D. Yang, Y. Gu, and P. Tontiwachwuthikul, "Wettability Determination of the Crude Oil−Reservoir Brine−Reservoir Rock System with Dissolution of CO 2 at High Pressures and Elevated Temperatures," *Energy & Fuels*, vol. 22, no. 4, pp. 2362–2371, Jul. 2008.

[50] N. Shojai kaveh, C. Berentsen, S. E. J. Rudolph-Floter, K. H. Wolf, and W. R. Rossen, "Wettability Determination by Equilibrium Contact Angle Measurements: Reservoir Rock- Connate Water System With Injection of CO2," in *SPE Europec/EAGE Annual Conference*, 2012.

[51] C. Martavaltzi, A. Dakik, S. Agrawal, and A. Gupta, "Wettability alteration of carbonates by optimizing brine and surfactant composition," in *Kuwait international petroleum conference and exhibition*, 2012, p. SPE 163348.

[52] V. Mirchi, S. Saraji, L. Goual, and M. Piri, "Dynamic Interfacial Tensions and Contact Angles of Surfactant-in-Brine/Oil/Shale Systems: Implications to Enhanced Oil Recovery in Shale Oil Reservoirs," *SPE Improv. Oil Recover. Symp.*, Apr. 2014.

[53] Alshaikh and Mahadevan, “SPE-172187-MS Impact of Brine Composition on Carbonate Wettability : A Sensitivity Study,” no. April, pp. 21–24, 2014.

[54] P. et. al. Jaeger, “Influence of Compressed Carbon Dioxide on the Capillarity of the Gas− Crude Oil− Reservoir Water System,” *J. Chem. ...*, pp. 5246–5251, 2010.

[55] D. Y. Kwok and a. W. Neumann, *Contact angle measurement and contact angle interpretation*, vol. 81, no. 3. 1999.

[56] Y. Yuan and T. R. Lee, *Surface Science Techniques*, vol. 51. 2013.

[57] Woodward Roger P., “Surface Tension Measurements Using the Drop Shape Method,” *First Ten Angstroms Inc Tech. Inf.*, pp. 1–6, 2008.

[58] Kruss GmbH, “Contact angle measurement in practice (1) With care to accuracy : preparations and general conditions for contact angle measurements,” *Pract. Contact Angle Meas. Man.*, vol. 49, no. 1, pp. 98–100, 2007.

[59] A. W. Adamson and A. P. Gast, *Physical Chemistry of Surfaces*. John Wiley & Sons, 1997.

[60] A. S. Michaels and E. A. Hauser, “Interfacial Tension at Elevated Pressure and Temperature. II. Interfacial Properties of Hydrocarbon–Water Systems.,” *J. Phys. Chem.*, vol. 55, no. 3, pp. 408–421, Mar. 1951.

[61] J. P. Millette, D. S. Scott, I. G. Reilly, P. Majerski, J. Piskorz, D. Radlein, and T. J. W. Debruijn, “An apparatus for the measurement of surface tensions at high pressures and temperatures,” *Can. J. Chem. Eng.*, vol. 80, no. 1, pp. 126–134, 2002.

[62] Vinci Technologies, “T 700 c,” *IFT 700 Oper. Man.*, no. 6, p. 1000.

[63] Y. Wu, S. Iglauer, P. Shuler, Y. Tang, and W. a. Goddard, “Branched alkyl alcohol propoxylated sulfate surfactants for improved oil recovery,” *Tenside, Surfactants, Deterg.*, vol. 47, no. 3, pp. 152–161, 2010.

[64] S. Kefi, J. Lee, T. Pope, and P. Sullivan, “Expanding applications for viscoelastic surfactants,” *Oilf. Rev*, vol. 16, no. 4, pp. 10–23, 2004.

[65] I. Lakatos, J. Toth, T. Bodi, J. Lakatos-szabo, U. Miskolc, P. D. Berger, and L. Christie, “Application of Viscoelastic Surfactants as Mobility-Control Agents in Low-Tension Surfactant Floods,” *Spe 106005*, pp. 1–14, 2007.

[66] Y. Chen, T. L. Pope, and J. C. Lee, “Novel CO2 -Emulsified Viscoelastic Surfactant Fracturing Fluid System,” *SPE Eur. Form. Damage Conf.*, p. 94603, 2005.

[67] X. Sun, X. Liang, S. Wang, and Y. Lu, “Experimental study on the rheology of CO2 viscoelastic surfactant foam fracturing fluid,” *J. Pet. Sci. Eng.*, vol. 119, pp. 104–111, 2014.

[68] L.-B. Ouyang, “New Correlations for Predicting the Density and Viscosity of Supercritical Carbon Dioxide,” *Open Pet. Eng. J.*, vol. 4, pp. 13–21, 2011.

[69] P. Chiquet, J. L. Daridon, D. Broseta, and S. Thibeau, “CO2/water interfacial tensions under pressure and temperature conditions of CO2 geological storage,” *Energy Convers. Manag.*, vol. 48, no. 3, pp. 736–744, 2007.

[70] P. K. Bikkina, O. Shoham, and R. Uppaluri, “Equilibrated interfacial tension data of the CO2-water system at high pressures and moderate temperatures,” *J. Chem. Eng. Data*, vol. 56, no. 10, pp. 3725–3733, 2011.

[71] B. Chun, “Interfacial tension in high-pressure carbon dioxide mixtures,” *Ind. & Eng. Chem.*, pp. 4371–4377, 1995.

[72] A. Hebach, A. Oberhof, N. Dahmen, A. Kögel, H. Ederer, and E. Dinjus, “Interfacial tension at elevated pressures-measurements and correlations in the water + carbon dioxide system,” *J. Chem. Eng. Data*, vol. 47, no. Figure 2, pp. 1540–1546, 2002.

[73] C. Chalbaud, M. Robin, J.-M. Lombard, F. Martin, P. Egermann, and H. Bertin, “Interfacial tension measurements and wettability evaluation for geological CO2 storage,” *Adv. Water Resour.*, vol. 32, no. 1, pp. 98–109, 2009.

[74] N. Spycher, K. Pruess, and J. Ennis-King, “CO2-H2O mixtures in the geological sequestration of CO2. I. Assessment and calculation of mutual solubilities from 12 to 100°C and up to 600 bar,” *Geochim. Cosmochim. Acta*, vol. 67, no. 16, pp. 3015–3031, 2003.

[75] N. Spycher and K. Pruess, “CO2-H2O mixtures in the geological sequestration of CO2. II. Partitioning in chloride brines at 12–100°C and up to 600 bar,” *Geochim. Cosmochim. Acta*, vol. 69, no. 13, pp. 3309–3320, 2005.

[76] H. Teng, “Mass transfer of CO 1 through liquid CO 1 Đwater interface,” *Int. J. Heat Mass Transf.*, vol. 41, pp. 3204–3214, 1998.

[77] B. Kvamme, T. Kuznetsova, A. Hebach, A. Oberhof, and E. Lunde, “Measurements and modelling of interfacial tension for water+carbon dioxide systems at elevated pressures,” *Comput. Mater. Sci.*, vol. 38, no. 3, pp. 506–513, 2005.

[78] Z. Yang, M. Li, B. Peng, M. Lin, and Z. Dong, “Dispersion property of CO 2 in oil. 2: Volume expansion of CO 2 + organic liquid at near-critical and supercritical conditions of CO 2,” *J. Chem. Eng. Data*, vol. 57, no. 4, pp. 1305–1311, 2012.

[79] S. Adkins, P. Liyanage, G. W. P. Pinnawala Arachchilage, T. Mudiyanselage, U. Weerasooriya, and G. Pope, “A New Process for Manufacturing and Stabilizing High-Performance EOR Surfactants at Low Cost for High-Temperature, High-Salinity Oil Reservoirs,” *Proc. SPE Improv. Oil Recover. Symp.*, 2010.

[80] S. Adkins, G. W. P. Pinnawala Arachchilage, S. Solairaj, J. Lu, U. Weerasooriya, and G. A. Pope, “Development of Thermally and Chemically Stable Large-Hydrophobe Alkoxy Carboxylate Surfactants,” *SPE Improv. Oil Recover. Symp.*, pp. 1–10, 2013.

[81] H. Yang, C. Britton, P. J. Liyanage, S. Solairaj, D. H. Kim, Q. Nguyen, U.

Weerasooriya, and G. a Pope, “Low-Cost , High-Performance Chemicals for Enhanced Oil Recovery,” *Spe 129978*, no. 1998, 2010.

[82] K. E. Oshea, K. M. Kirmse, M. A. Fox, and K. P. Johnston, “Polar and Hydrogen-Bonding Interactions in Supercritical Fluids - Effects on the Tautomeric Equilibrium of 4-(Phenylazo)-1-Naphthol,” *J. Phys. Chem.*, vol. 95, no. 20, pp. 7863–7867, 1991.

[83] M. O’neill, Q. Cao, and M. Fang, “Solubility of homopolymers and copolymers in carbon dioxide,” *Ind. Eng. Chem. Res.*, vol. 5885, no. 98, pp. 3067–3079, 1998.

[84] K. a. Consan and R. D. Smith, “Observations on the solubility of surfactants and related molecules in carbon dioxide at 50°C,” *J. Supercrit. Fluids*, vol. 3, no. 2, pp. 51–65, Jun. 1990.

[85] F. P. D. I. Aveyard R., Binks B.P., Clark S., “Cloud points, solubilisation and interfacial tensions in systems containing nonionic surfactants,” *J. Chem. Technol. Biotechnol.*, vol. 48, no. 1988, pp. 161–171, 1990.

[86] G. J. McFann and K. P. Johnston, “Phase Behavior of Nonionic Surfactant/Oil/Water Systems Containing Light Alkanes,” *Langmuir*, vol. 9, no. May, pp. 2942–2948, 1993.

[87] P. Walstra, “Principles of Emulsion Formation,” *Chem. Eng. Sci.*, vol. 48, no. 2, pp. 333–349, 1993.

[88] K. Li and A. Firoozabadi, “Experimental Study of Wettability Alteration to Preferential Gas-Wetting in Porous Media and Its Effects,” *SPE Reserv. Eval. Eng.*, vol. 3, no. 2, pp. 139–149, 2000.

[89] L. You, W. Zhang, Y. Kang, Z. Chen, and X. Liu, “Stability of Fluorosurfactant Adsorption on Mineral Surface for Water Removal in Tight Gas Reservoirs,” vol. 2015, 2015.

[90] Y. Wang, L. Ma, B. Bai, G. Jiang, J. Jin, and Z. Wang, “Wettability Alteration of Sandstone by Chemical Treatments,” vol. 2013, 2013.

VITAE

Name	: Ahmad Mahboob
Nationality	: Pakistani
Date of Birth	:8/11/1990
Email	: ahmadz@live.co.uk
Address	: KFUPM Graduate Housing, Building # 813, Room # 220
Academic Background	: **MS (Petroleum Engineering)**
	December, 2016
	King Fahd University of Petroleum and Minerals
	Dhahran, Saudi Arabia
	B.Sc. (Petroleum Engineering)
	December, 2011
	University of Engineering and Technology (UET)
	Lahore, Pakistan

Publications

1- Poster presentation “An Experimental Study of Interfacial tension and Contact Angles of CO2/Brines/Surfactants/Oil Systems with Dolomite Rock” at AICHE Meeting 2015, paper number 431445, ISBN: 978-0-8169-1094-6

2- Winner of 2016 SPE-KSA YP&SO Paper Contest

3- Presented “An Experimental Study of Interfacial tension and Contact Angles of CO2/Brines/Surfactants/Oil Systems with Dolomite Rock” at YPTS 2016

10- Conference Paper “An Experimental Study of Interfacial tension and Contact Angles of CO2/Brines/Surfactants/Oil Systems with Dolomite Rock” 182839-MS SPE 2016

11- Conference Paper “A Rigorous Correlation for Quantitative Prediction of Water Cresting in Multi-Fractured Horizontal Wells” 182778-MS SPE 2016